



Dalhousie University

Department of Earth Sciences

Halifax, Nova Scotia

Canada B3H 3J5

(902) 494-2358

FAX (902) 494-6889

DATE April 28, 2000

AUTHOR Robert W. Cuthbert

TITLE Structure and Strain of the Burwash Formation,

Slave Province, Northwest Territories

Degree B.Sc. Earth Science Convocation: May Year 2000

Permission is herewith granted to Dalhousie University to circulate and to have copied for non-commercial purposes, at its discretion, the above title upon the request of individuals or institutions.

THE AUTHOR RESERVES OTHER PUBLICATION RIGHTS, AND NEITHER THE THESIS NOR EXTENSIVE EXTRACTS FROM IT MAY BE PRINTED OR OTHERWISE REPRODUCED WITHOUT THE AUTHOR'S WRITTEN PERMISSION.

THE AUTHOR ATTESTS THAT PERMISSION HAS BEEN OBTAINED FOR THE USE OF ANY COPYRIGHTED MATERIAL APPEARING IN THIS THESIS (OTHER THAN BRIEF EXCERPTS REQUIRING ONLY PROPER ACKNOWLEDGEMENT IN SCHOLARLY WRITING) AND THAT ALL SUCH USE IS CLEARLY ACKNOWLEDGED.

Acknowledgments

This thesis was completed under the supervision of Dr. John Waldron, Saint Mary's University. He provided me with excellent advice, guidance and support. Without those Excel Spreadsheets, I would still be making calculations today.

Thanks to Mark Ferguson for being great to work with in the field, and turning my summer job into an adventure. Working in the Northwest Territories is an experience I will never forget.

Thanks to all those who contributed to this project, either helping in the field, donating data, butter tarts, or providing entertainment near Hearne Lake.

Most of all, thanks to my Family for always being there, for the support, and helping me understand the most important things in life.

Abstract

The Burwash Formation is an extensive package of Archean volcanic-turbidite sedimentary units in the Slave Province, Northwest Territories. The turbidites are metamorphosed to greenschist facies, and have undergone two episodes of deformation. The F_1 generation folds were refolded forming a fold interference pattern, intermediate between dome, and mushroom shape. Cleavage is axial planar to F_2 fold hinges. Rare volcanic tuff sequences provide good markers for stratigraphic correlation and strain analysis. Bulk strain was determined by two different methods, the Fry, and Rf/Phi . In both cases a prolate ellipsoid is found, with the long axis steeply plunging. The prolate shape is consistent with two episodes of plane strain.

Table of Contents

Acknowledgments	I
Abstract	II
Table of Contents	III
Table of Figures	V
Table of Tables	VII
Chapter 1 Introduction	1
1.1 Thesis Statement	
1.2 Introduction to the Slave Province	
1.2.1 Basement Rocks	
1.2.2 Volcanic Rocks of the YKSG	
1.2.3 Sedimentary Rocks of the YKSG	
1.2.4 Younger Plutonic Rocks	
1.2.5 Jackson Lake Formation	
1.2.6 Structure	
1.2.7 Tectonic Models	
Chapter 2 Sediments of the Burwash Formation	11
2.1 Introduction to the Burwash Formation	
2.2 Sediments and Felsic Tuff Layers	
Chapter 3 Field Based Results	19
3.1 Structural Field Mapping Area	
3.2 Methodology	
3.3 Bedding	
3.4 Veins	
3.5 Folds	
3.6 Cleavage	
3.7 Overprinting and Structural Interpretations	
Chapter 4 Strain Analysis	32
4.1 Uses for Strain Analysis	
4.2 Samples	
4.3 Theoretical Basis of the Fry Method	
4.4 Methods using the Fry Plot	
4.5 Discussion of Fry Plots	
4.6 Theoretical Basis of the Rf/Phi Method	
4.7 Methods using Rf/Phi	

Table of Figures

Figure 01	Map of Slave Province in Canadian Shield	2
Figure 02	General map of Slave Province	3
Figure 03	Map of Yellowknife Supergroup	4
Figure 04	Airphoto with fold interference pattern	6
Figure 05	Ripple marks with S_1 flattening	9
Figure 06	Photo: thin section, metasediment	13
Figure 07	Photo: thin section, metasilstone	14
Figure 08	Photo Watta Lake Tuff, Type locality	15
Figure 09	Photo: thin section, coarse layer, WLT (ek007)	16
Figure 10	Photo: thin section, coarse layer, WLT (eD076)	18
Figure 11	Map of Hearne and Watta Lake	20
Figure 12	Structural map	see map in folder
Figure 13	Schematic cross-section through structural map	24
Figure 14	Stereoplot of bedding in northeast of map area	25
Figure 15	Stereoplot of bedding in central east of map area	26
Figure 16	Stereoplot of bedding across F_2 fold	27
Figure 17	Ramsay(1967) fold interference classification	29
Figure 18	Stereoplot of cleavage	30
Figure 19	Fry plot, sample eK007, section a	A3-16
Figure 20	Fry plot, sample eK007, section b	A3-17
Figure 21	Fry plot, sample eK007, section c	A3-18
Figure 22	Sample Standard Marker Deformation Grid	37
Figure 23	DePaor(1988) orientation net	38
Figure 24	Rf/Phi plot(Ramsey): sample eK007 section a	A3-19
Figure 25	Rf/Phi plot(Ramsey): sample eK007 section b	A3-20
Figure 26	Rf/Phi plot(Ramsey): sample eK007 section c	A3-21
Figure 27	Rf/Phi plot(DePaor): sample eK007 section a	A3-22
Figure 28	Rf/Phi plot(DePaor): sample eK007 section b	A3-23
Figure 29	Rf/Phi plot(DePaor): sample eK007 section c	A3-24
Figure 30	Rf/Phi plot(DePaor): sample eD076 section a	A3-25
Figure 31	Rf/Phi plot(DePaor): sample eD076 section b	A3-26
Figure 32	Rf/Phi plot(DePaor): sample eD076 section c	A3-27
Figure 33	Scan: Sample eK007, section a	41
Figure 34	Scan: Sample eK007, section b	42
Figure 35	Scan: Sample eK007, section c	43
Figure 36	Scan: Sample eD076, section a	44
Figure 37	Scan: Sample eD076, section b	45
Figure 38	Scan: Sample eD076, section c	46
Figure 39	E2E3 results: Sample eK007(Fry)	A3-28

Figure 40	E2E3 results: Sample eK007(Rf/Phi)	A3-29
Figure 41	E2E3 results: Sample eD076(Rf/Phi)	A3-30
Figure 42	Stereoplot, principal axes of ellipsoid eK007	49
Figure 43	Stereoplot, principal axes of ellipsoid eD076	50
Figure 44	Stratigraphic section dY052	52
Figure 45	Stratigraphic section eD076	53

Table of tables

Table 01	Field Data	A1
Table 02	Results of Fry and Rf/Phi plot	35
Table 03	Rf/Phi data: sample eK007, section a	A3-02
Table 04	Rf/Phi data: sample eK007, section b	A3-04
Table 05	Rf/Phi data: sample eK007, section c	A3-06
Table 06	Rf/Phi data: sample eD076, section a	A3-10
Table 07	Rf/Phi data: sample eD076, section b	A3-12
Table 08	Rf/Phi data: sample eD076, section c	A3-14
Table 09	Excel calculations: Sample eK007, Fry data	A3-31
Table 10	Excel calculations: Sample eK007, Rf/Phi data	A3-32
Table 11	Excel calculations: Sample eD076, Rf/Phi data	A3-33
Table 12	Summary of Excel calculations	48

Chapter 1: Introduction

1.1 Thesis Statement

This thesis records an investigation to assess the structures produced by multiple deformation events in an extensive unit of turbidites in the Slave Province, Northwest Territories. A small but typical section of the Burwash Formation was chosen for analysis. The first objective was to map the structure, including a fold interference pattern. The second objective was to determine the bulk strain produced from deformation events through the evaluation of a coarse grained volcanic tuff layer.

1.2 Introduction to the Slave Province

The Slave Province (Figure 01) is located in the Northwest corner of the Canadian Shield. The basement craton of the Slave Structural Province (Figure 02) is composed of gneisses and other basement granitoid plutons assembled prior to 2.92 Ga (Bleeker et al. 1999a).

Extensive volcanic sequences and turbidite sedimentary rocks accumulated between 2.71 and 2.65 Ga. The supercrustal rocks of Archean age are termed Yellowknife Supergroup (YKSG) (Henderson 1985). The YKSG (Figure 03) covers approximately 35% of the Slave Structural Province. Syn to late granitoid plutons intruded the YKSG between 2.73 to 2.58 Ga.

1.2.1 Basement Rocks

The basement complex (Figure 03) is composed of older dioritic to tonalitic gneisses including the 4.05 Ga Acasta gneiss, and younger granitoid complexes.

Figure 01: Location of the Slave Province in the Canadian Shield.
(modified after Bleeker 1995)

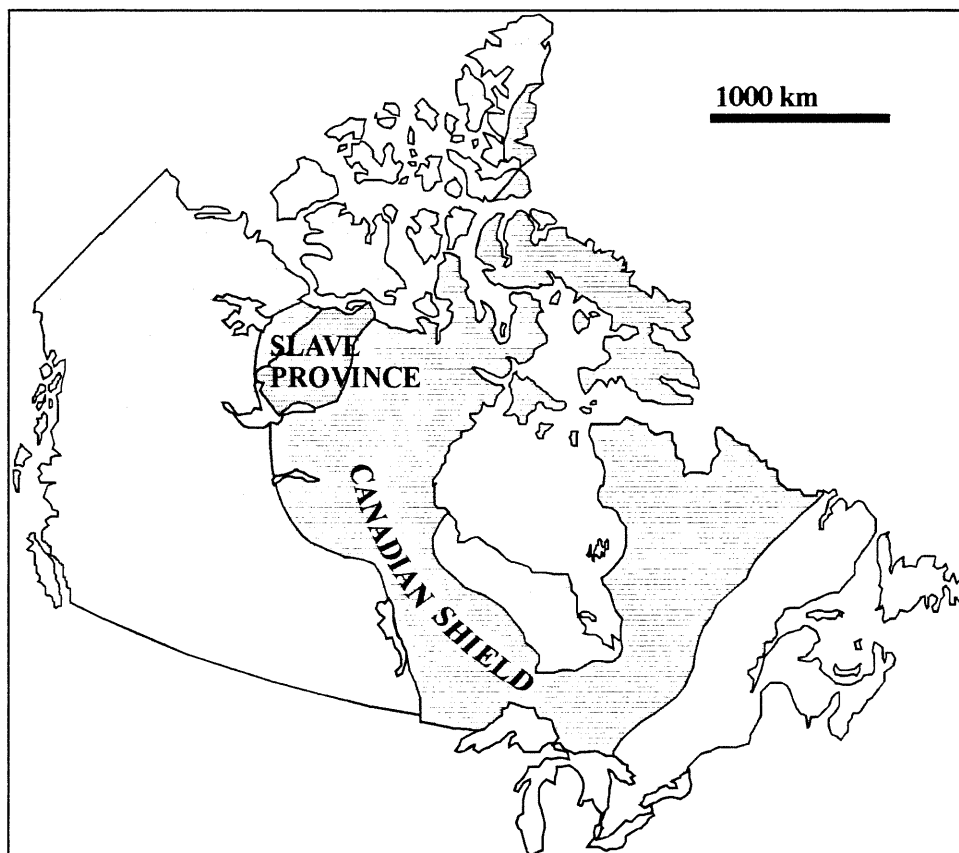


Figure 02: Geologic map of the Slave Craton. (Modified after Bleeker 1995)

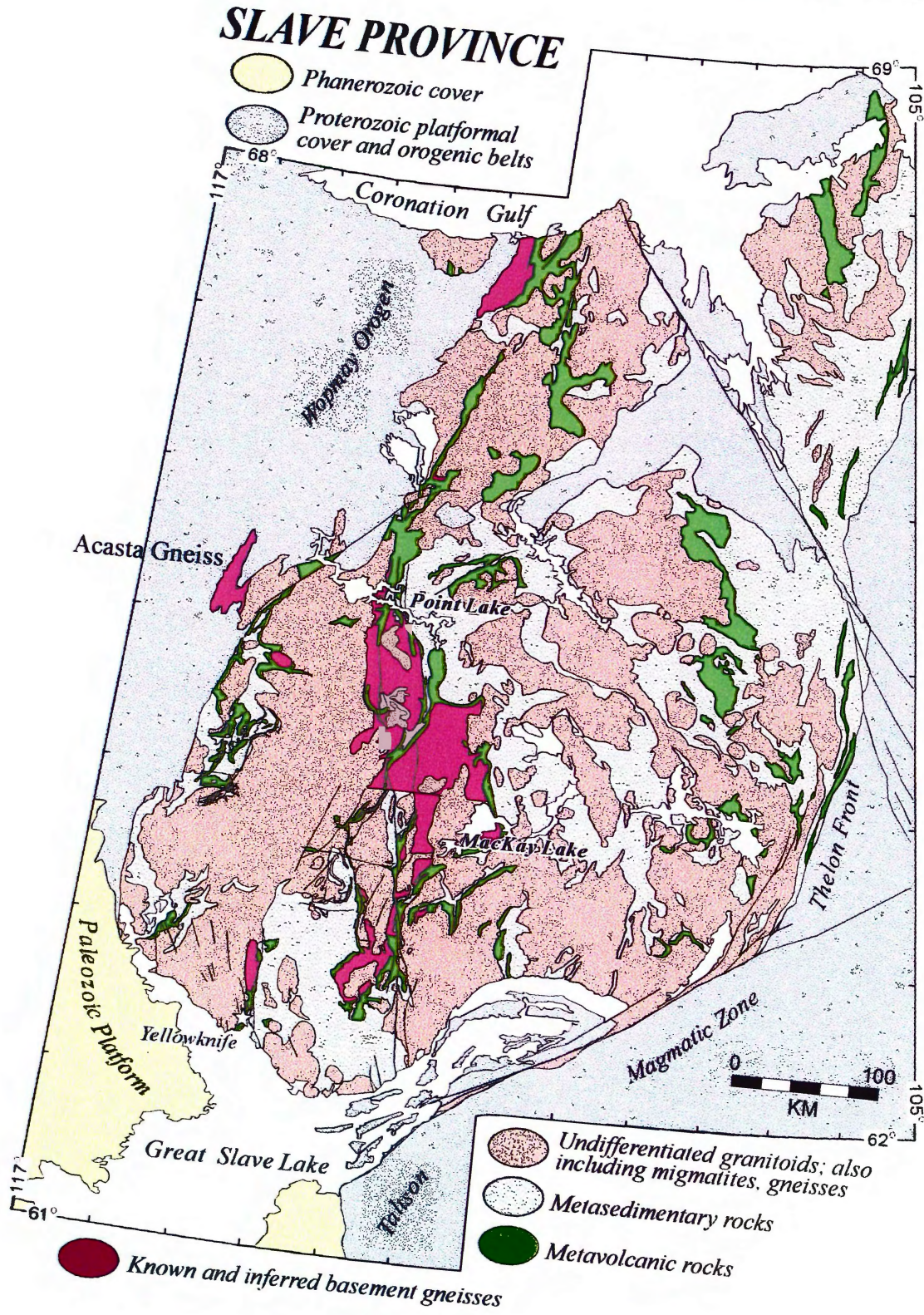
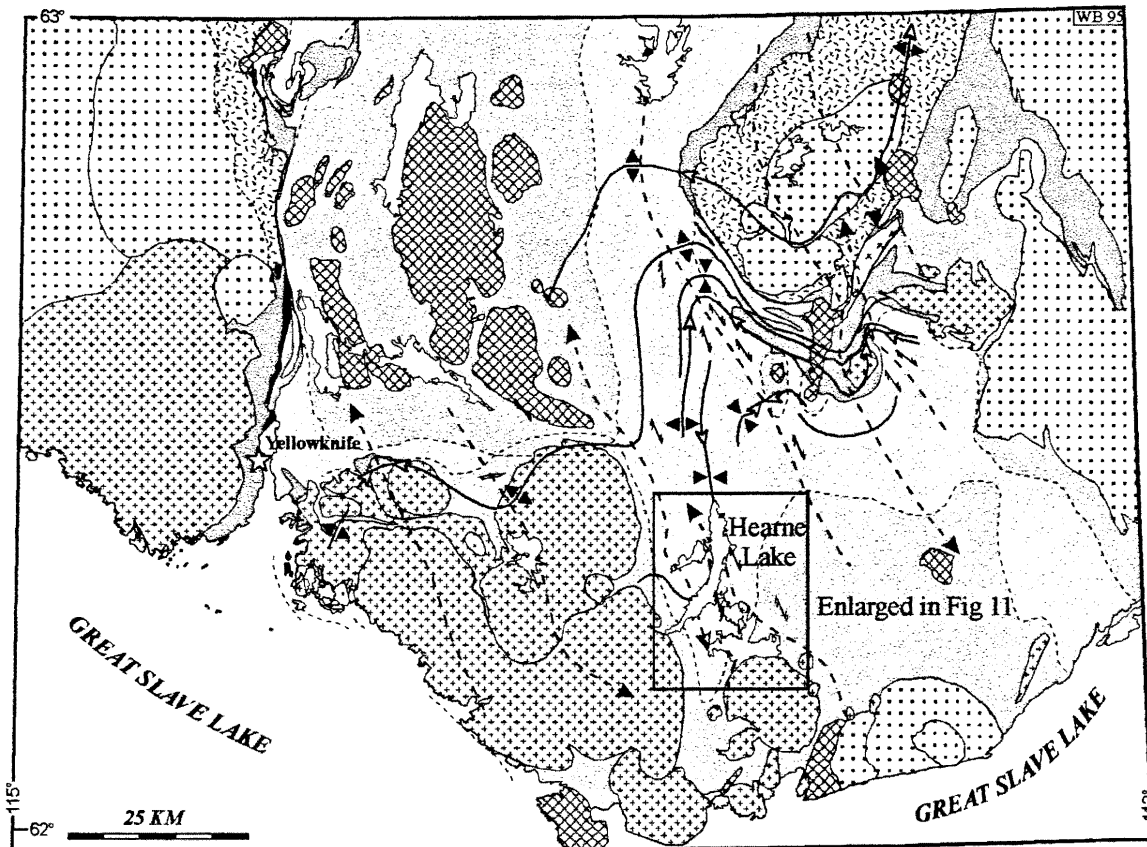





Figure 03: Map of the Yellowknife Supergroup. (Modified after Bleeker 1995)







 Traces of upright, periclinal F_1 folds, syn- and anticlinoria, refolded by F_2 ; F_1 fold belt affects Burwash Formation, volcanic rocks, and basement complexes, but is cut by Defeat Suite




 Regional S_2 cleavage, axial planar to F_2 folds, transects F_1 periclinal

 Traces of steeply plunging northwest-trending F_2 folds; arrow heads indicate direction of fold closure trends locally extended to indicate S_2 trajectories

Supracrustal Rocks of the Yellowknife Supergroup

Post-Burwash Formation Granitoid Rocks

-  *Jackson Lake Formation*: ca 2.60 Ga coarse clastic rocks, including cross-bedded sandstones and polymict conglomerates
-  *Burwash Formation*: ca. 2.66 Ga metaturbidites greenschist (light grey) to amphibolite facies (medium grey)
-  2.73-2.66 Ga mafic to intermediate and felsic metavolcanic rocks
-  *Sleepy Dragon and Anton basement complexes*; including abundant 2.70-2.66 Ga and younger plutonic rocks (undifferentiated)

-  *Prosperous Suite*: white to pink two-mica granite to granodiorite, mostly within Burwash Formation host rocks
- Defeat Suite*:
-  Biotite±hornblende tonalite to granodiorite Hornblende diorite
-  Other Granitoid Rocks

The Anton Complex is dated at 2.945 Ga, and is located to the north of Yellowknife. The 2.93 to 2.95 Ga Sleepy Dragon Complex borders the Yellowknife supracrustal basin to the east. The Anton and Sleepy Dragon Complex are composed of tonalites, granodiorites, and minor granites. Due to the similarities in age, composition, cover stratigraphy and geophysical data, Bleeker et al. (1999a) propose to combine these complexes under the title Central Slave Basement Complex (CSBC). This CSBC has been deformed, and intruded by younger plutonic rocks.

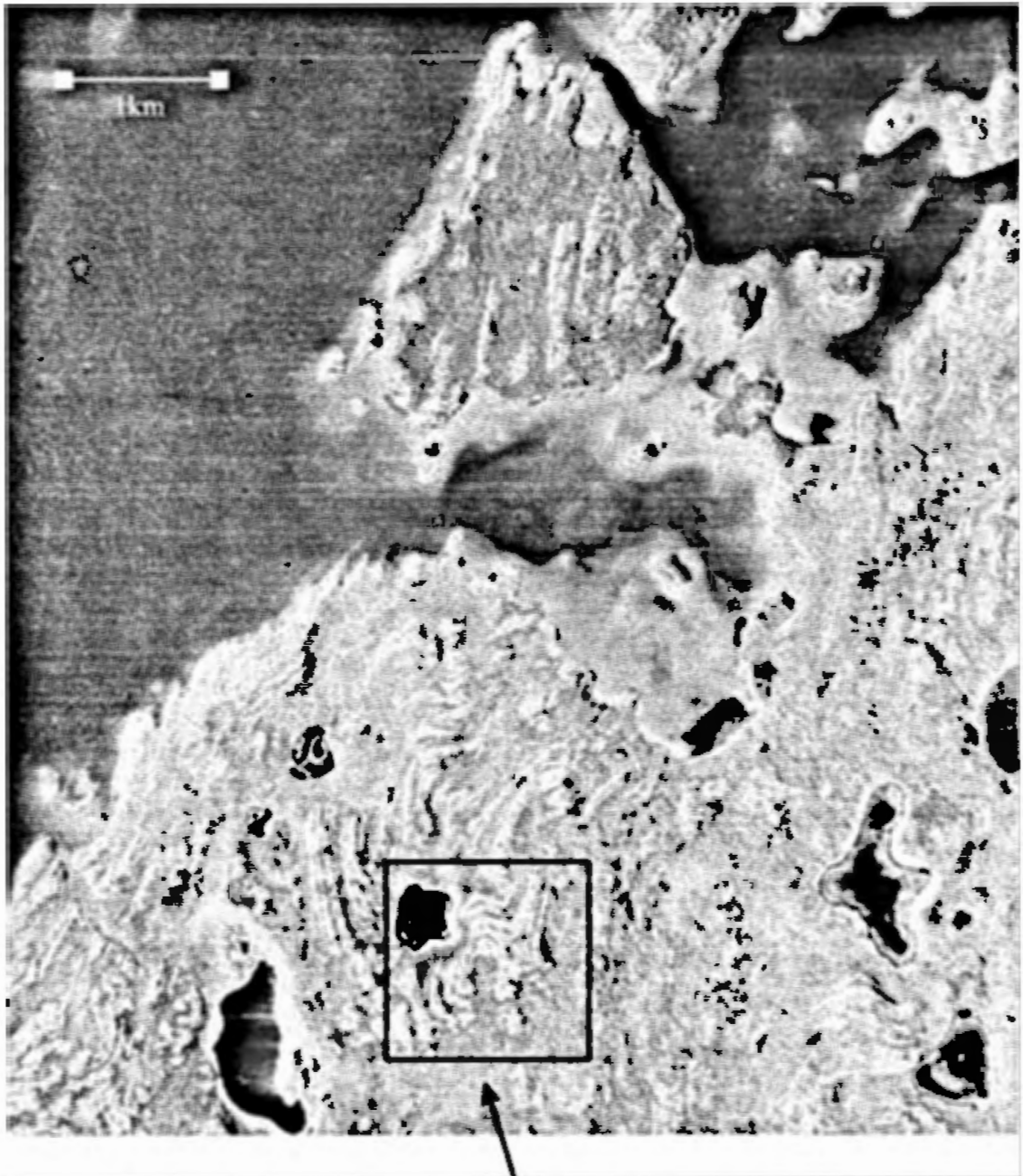
1.2.2 Volcanic Rocks of the YKSG

Sequences of volcanic rocks overlie the Central Slave Basement Complex. The volcanics on the west side of the YKSG are composed of the basaltic Kam Group and the intermediate-felsic Banting Group. The volcanics on the east side of the YKSG include the basaltic Cameron, and Beaulieu River volcanics. The mafic volcanic rocks form thick successions of massive, and pillowed flows, composed mainly of basalt with minor andesite (Henderson 1985). The mafic volcanics are overlain by the felsic, dacitic to rhyolitic flows interbedded with thin bedded sediments.

1.2.3 Sedimentary Rocks of the YKSG

The volcanic rocks are locally contemporaneous with the sedimentary rocks. The Burwash Formation (Figure 03) forms 80% of the Yellowknife Supergroup. The Burwash Formation turbidite successions (Figure 04) are difficult to map and interpret not only because of their structural complexity but because they consist of innumerable repetitions of metagreywacke and metasilstone of varying thickness (Padgham 1990). Research during the summers of 1998-99 conducted by Mark Ferguson used structure and sequences of tuffaceous beds to develop a local stratigraphy. A more complete description of the Burwash Formation will be covered in Chapter 2.

Figure 04: Airphoto including part of the mapping area, which displays the fold interference pattern. (Property of Canadian Government)



Fold interference pattern

1.2.4 Younger Plutonic Rocks

A large portion of the Slave province consists of Archean granitoid rocks. Henderson (1985) distinguished twelve different suites, based on textural and mineralogical characteristics. The most extensive plutonic rocks in the YKSG are the Defeat and Prosperous Suite Granitoids. The Defeat Suite plutons are located to the east and west of Yellowknife, in the southern region of the YKSG. Henderson (1985) claims the plutons are generally concordant with the supracrustal rocks. The Prosperous Suite Granite is centrally located in the YKSG. The Prosperous granite contains two micas and abundant pegmatite; it is highly discordant with the supracrustal rocks (Henderson 1985).

1.2.5 Jackson Lake Formation

The Jackson Lake Formation has been described by Henderson (1985) as a local basal conglomerate, overlain by cross-bedded sandstone interbedded with thin layers of conglomerate. The Jackson Lake Formation lies unconformably over the Kam Group, from which the basal conglomerates were derived.

1.2.6 Structure

Structure in the Burwash has been described by Fyson (1975), Henderson (1985), and recently by Bleeker (1995). Bleeker (1995) has mapped the Burwash at a scale of 1:50,000 (Figure 03) and discovered high amplitude upright F_1 folds with doubly plunging axes. Contrary to Fyson (1975), Bleeker and Beaumont-Smith (1995) believe the doubly plunging nature of the F_1 folds was produced during F_1 development, rather than from an F_0 event. Prominent quartz saddle reef and en echelon vein arrays typically accompany F_1 hinges. Concretions, loadcasts, flames, ripples and shale casts are strongly flattened parallel to S_1 (Figure 05). F_1 folds developed under low-grade (burial) metamorphic conditions that predated all granitoid intrusions.

In most areas S_2 cleavage has developed and obliterated S_1 . Bleeker and Beaumont-Smith (1995) have determined that F_2 related strain, associated with the S_2 cleavage, may have produced 25 per cent horizontal shortening across this section. The F_2 event tightened the F_1 folds, rotated their axes and increased the attitudes of their double plunges. Bleeker and Beaumont-Smith (1995) describe the F_2 folds as steeply plunging, forming as a result of transpression during emplacement of the Defeat and Prosperous Suite granitoids. The F_2 event produced mushroom interference patterns by refolding F_1 folds, that can be observed throughout the Yellowknife Domain (Figure 04).

1.2.7 Tectonic Models

Previous tectonic models have been reviewed by Padgham (1990) and Bleeker et al. (1999b) and are summarized in the following section.

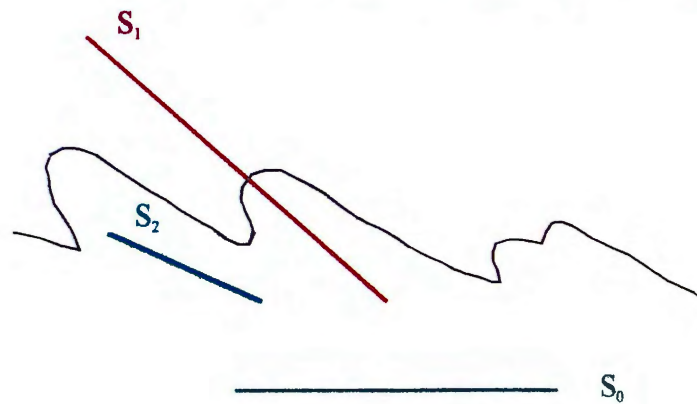
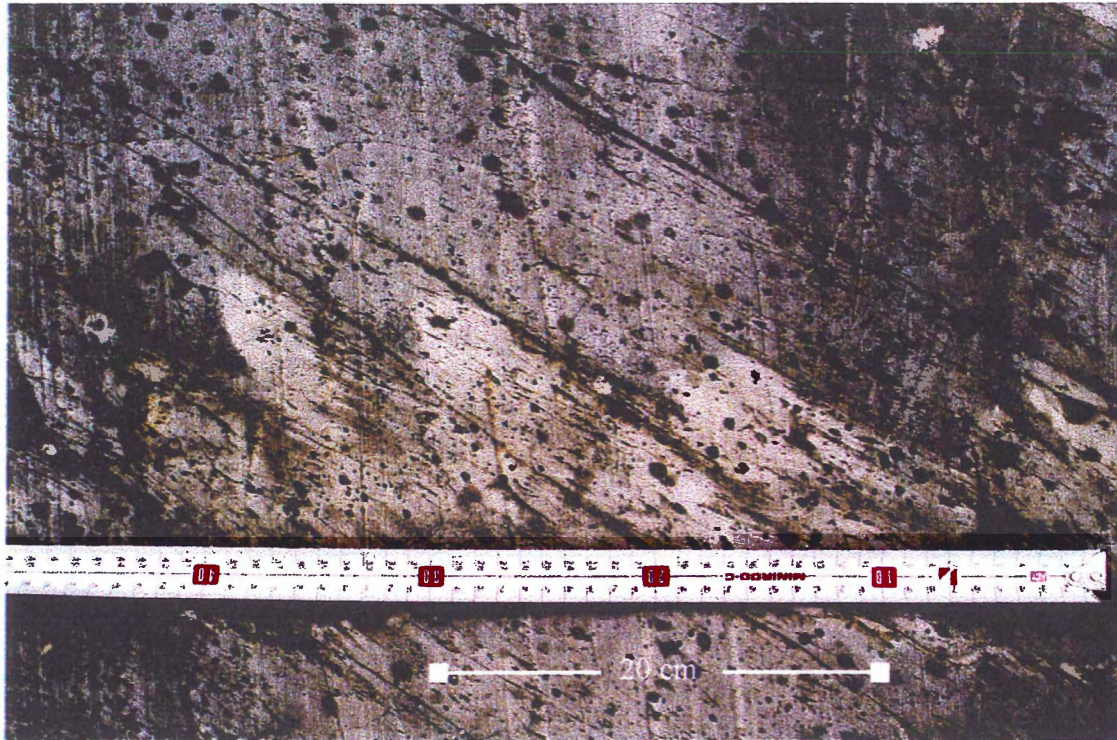
McGlynn and Henderson (1970, 1972) and Henderson (1981, 1985) thought that the YKSG sediments were deposited in ensialic rift basins, with volcanism mainly along basin-margin faults. Helmstaedt et al. (1985) contended Archean sea floor spreading produced the YKSG mafic volcanic sequences. Fyson (1988) added to this model with Helmstaedt, suggesting that mafic volcanics were produced during a rifting event before a 3 Ga salic crust rifting event.

Kusky (1989) suggested that arc-continent collision occurred and he divided the Slave into four separate terranes, which were interpreted to be a magmatic arc, accretionary prism, and microcontinental fragments and equivalents. The Slave Structural Province is considered by Padgham (1990) to have evolved as a west facing subduction complex, that collided with the Anton microcontinent. Hoffman (1986) claims the Slave Structural Province was a prograding arc-trench system which formed a collage of arc volcanic and plutonic rocks, fore-arc basin deposits, and exotic blocks, including seamounts, and ophiolite scraped from the subducting plate (Padgham 1990).

Bleeker et al. (1999b) propose a model which is based on an arc type environment.

Extensional faulting associated with rifting affected a thin succession of 2.93 Ga sediments, predominantly quartzite and banded iron formation. This thin succession is

Figure 05: Picture shows ripple marks(light features) which have been flattened in the orientation of F_1 orientation of cleavage and bedding are displayed in the schematic diagram.



Schematic showing relationship of bedding and two generations of cleavage to ripple marks.

stratigraphically between the Central Slave Basement Complex and the Yellowknife Supergroup and has been termed the Central Slave Cover Group. This model incorporates a regional decollement which developed at low angles during extension. The extension eventually led to subsidence and formation of structurally controlled basins. The basins are associated with voluminous sequences of tholeiitic lava flows. Sedimentary sequences were deposited in the basins before regional deformation. Bleeker's model is backed up by recent dating of three differently timed dyke swarms.

Chapter 2:

Sediments of the Burwash Formation

2.1 Introduction to the Burwash Formation

Henderson (1985) identified the Burwash Formation (Figure 03) as about 5000 m of interbedded massive to graded greywackes and thin siltstones. The rocks are metamorphosed from greenschist to amphibolite facies. These rocks show characteristics of deposition by turbidity currents. Most beds are graded, and many show one or more of the Bouma (1962) sequence of sedimentary structures. In areas of low metamorphic grade, erosive, depositional and soft sediment deformation structures are preserved. The sediments are proposed to have been deposited on a submarine fan complex near the margin of a large Archean sedimentary basin (Henderson 1985).

Sediment modal and chemical compositions indicate there must have been an extensive source area with mixed provenance involving volcanic and granitic terrains, with a major contribution of felsic volcanics (Henderson 1972). This denotes the presence of sialic crust prior to deposition. The sediments are texturally and chemically immature; petrographically, one quarter of the sediment is composed of quartz; the remainder is volcanic and plutonic grains. Although the turbidites are superficially very much the same throughout, some areas are dominated by coarse phases, which include polymictic conglomerates and thick beds of coarse lithic sandstone (Padgham 1990).

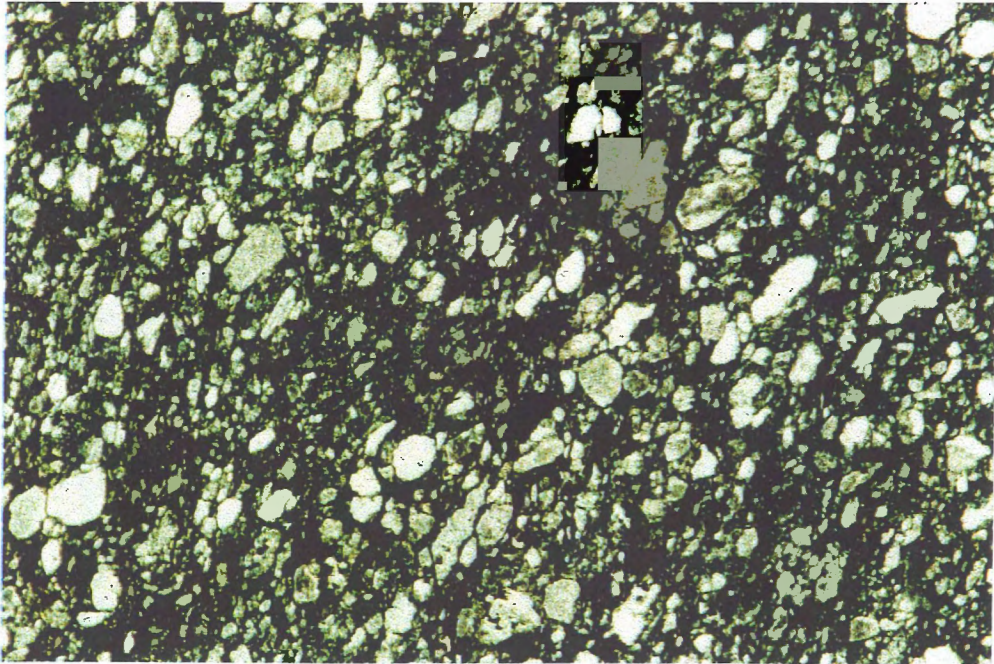
2.2 Sediments and Felsic Tuff layers

Representative samples of metagreywacke and metasilstone were examined petrographically. The metasandstone (Figure 06) is composed of abundant quartz, biotite, and chlorite; opaque minerals are present; and feldspar is rare. The quartz grains form sub-angular shapes several millimeters in length. Chlorite forms elongated inequant shaped crystals, which display a weak alignment. In hand sample, individual grain boundaries cannot be determined, and there is a poorly defined spaced S_2 cleavage.

The metasilstone (Figure 07) is much finer grained than the metasandstone. The metasilstone contains very fine grains of quartz, and abundant biotite crystals elongated in a common direction. Chlorite forms fine grained elongated crystals. There is an abundant fine grained matrix in which minerals are difficult to identify. Cleavage is observed in the field and hand sample. In thin section, the platy minerals are aligned defining the cleavage fabric. According to classification in Yardley (1989) the mineral assemblage indicate that these rocks are metamorphosed to the biotite zone in the greenschist facies.

Throughout the Burwash Formation there are rare complex rhythmic beds of felsic tuff interbedded in the turbidite stratigraphy. These felsic layers range from single millimeter thick bands to sequences several metres thick. The felsic layers typically alternate with black shale layers. The Watta Lake Tuff (WLT) (Figure 08) is an excellent example of one of these felsic tuff layers. The WLT is approximately 25 cm thick and has a characteristic sequence of thick and thin beds of alternating light coloured tuff and black shale. There is a 5 cm coarse grained layer that is unique when compared with all other tuff sequences known to the area. The WLT and a second tuff (named the RC tuff by M.E. Ferguson, personal communication 1999) have been identified at several localities, kilometres apart. Part of the research work being performed by Mark Ferguson is to develop a local stratigraphy, using the WLT and RC tuff layers to correlate stratigraphic columns.

Figure 07: Photo of a representative sample of metasiltstone from the Burwash Formation. Abundant biotite grains are aligned, defining the cleavage in the sample. Sample was cut near perpendicular to cleavage.



— 2mm —

Figure 07: Photo of a representative sample of metasilstone from the Burwash Formation. Abundant biotite grains are aligned, defining the cleavage in the sample. Sample was cut near perpendicular to cleavage.



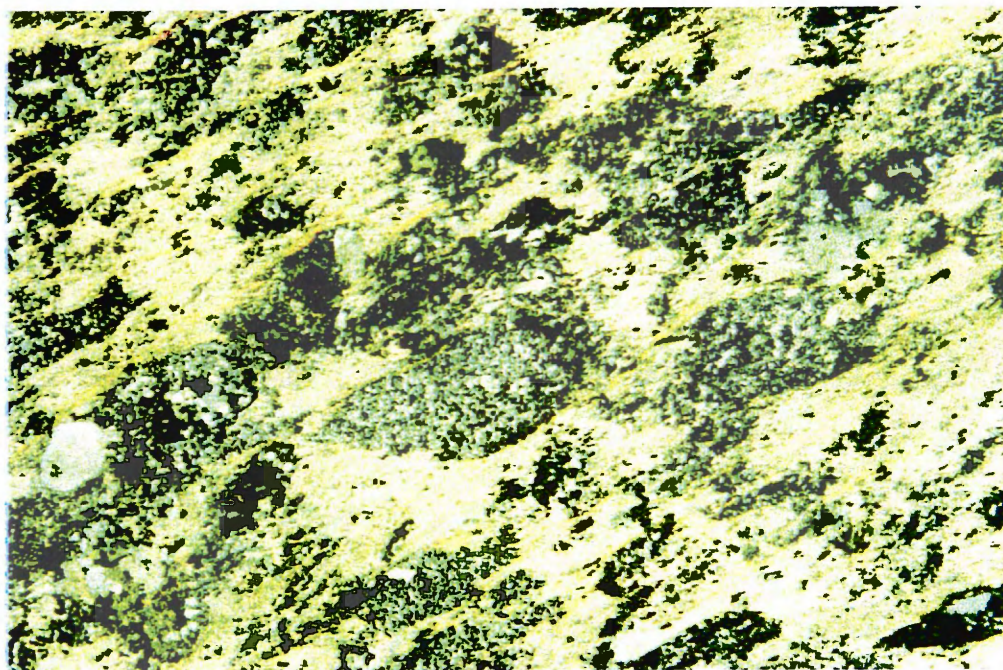
— 2mm —

Figure 08: Photo of the Watta Lake Tuff, taken at the Type locality on Watta Lake. The WLT contains the characteristic coarse grained tuff layer, used for strain analysis.



Coarse grained tuff bed

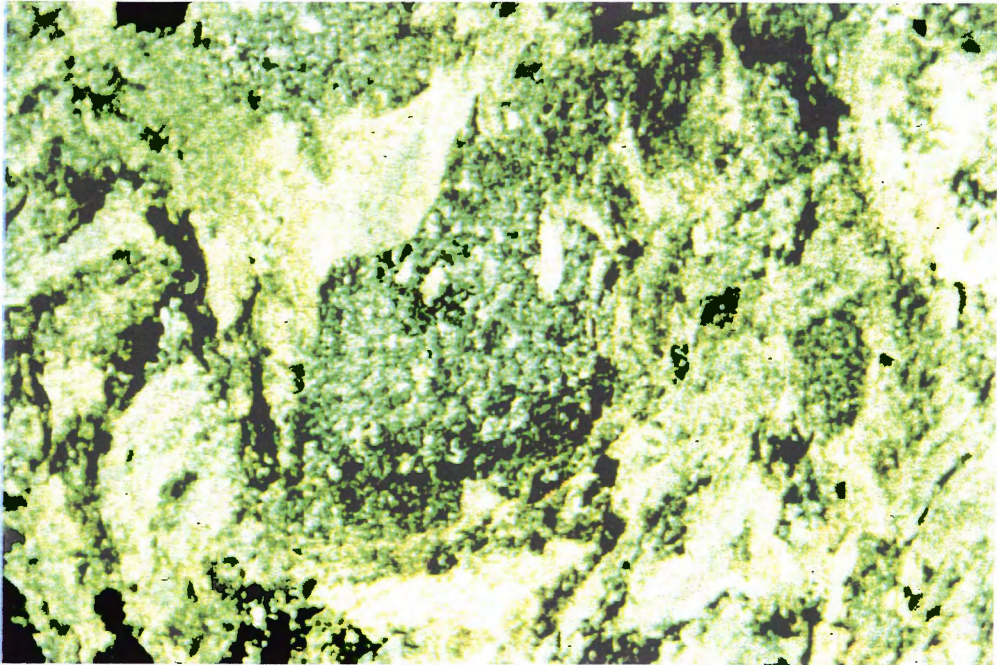
Figure 09: Photo of a thin section of sample eK007. Volcanic clasts are elongate, and oriented in a common direction NE. The platy matrix is deflected around the clasts.



6mm

The coarse layer of the WLT was analyzed under microscope. Sample eK007 (Figure 09) is composed dominantly of quartz clasts and volcanic fragments with a granoblastic texture and angular to sub-angular grain boundaries. Clasts range in size from 1 to 6 mm in length, and are elongated in a common direction. The matrix is composed of elongated platy minerals, aligned defining a fabric in the rock. Cleavage can be seen in hand sample. The cleavage defined by platy minerals is deflected around clast boundaries. Sample eD076 (Figure 10) contains volcanic clasts ranging in size from 2 mm to 8 mm. The clasts contain a matrix of plagioclase laths, which are oriented oblique to the matrix of the rock. Within the clasts, elliptical quartz grains with poikiloblastic centers are surrounded by new grain growth, and elongated in the same direction as the rock's matrix.

Figure 10: Photo of a thin section of sample eD076. The matrix of sample defines a fabric, oriented N-S. Central clast contains elliptical quartz grains which are oriented N-S. plagioclase lath matrix in the clast are elongated and oriented NE-SW.



6mm

Chapter 3

Field Based Results

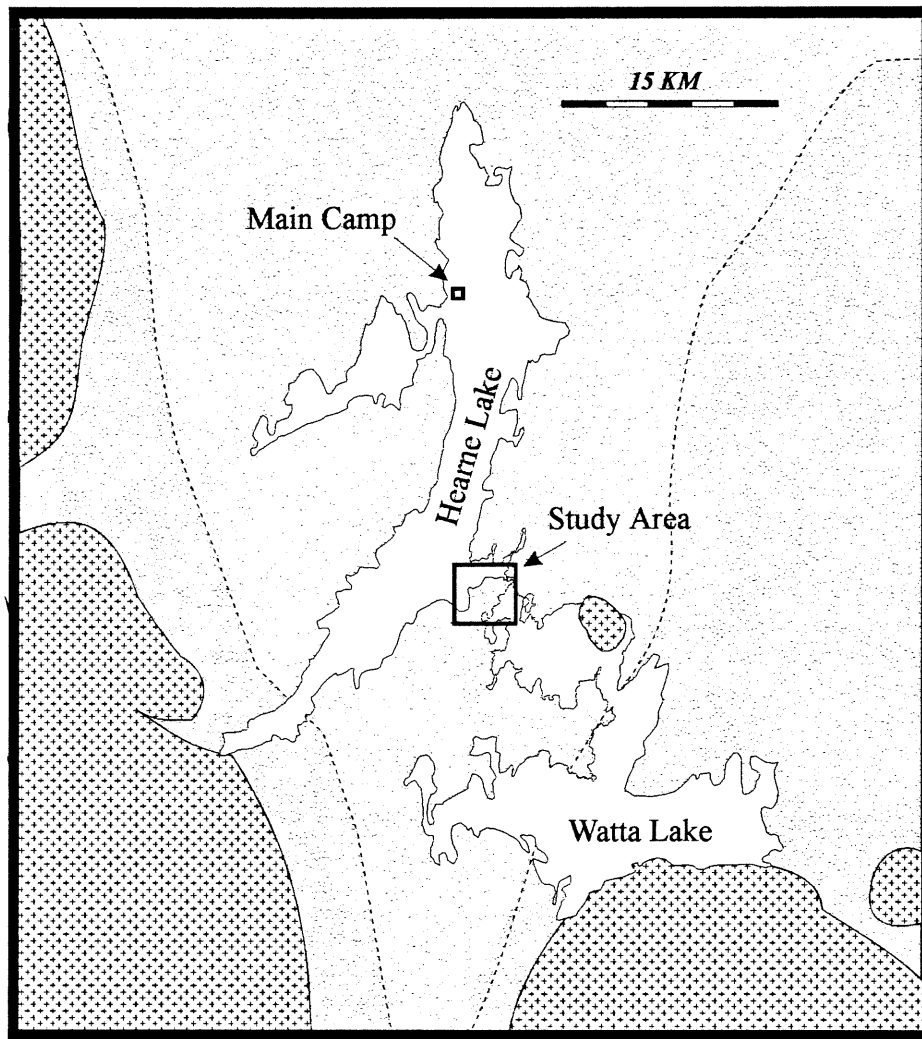
3.1 Structural Field Mapping area


The structural field mapping area (Figure 11) encompasses approximately six square kilometers between Hearne and Watta Lake. This area was mapped for structure, and samples of the Watta Lake Tuff were collected for bulk strain analysis.


3.2 Methodology

Before entering the field, 1:20,000 scale air photos were interpreted. The trace of bedding was generally easy to follow, and was transferred onto mylar. There are several areas with complex fold patterns (Figure 04) which could not be resolved. Mapping of the area was accomplished over a one week period during the summer field season of 1999. The field mapping was conducted by myself, with the assistance of Steve Green, Mark Ferguson and Wouter Bleeker. The area was accessed by Zodiac from a main camp which was located on Hearne lake (Figure 11). Observations, including bedding and cleavage measurements, were taken approximately every one hundred meters along the shoreline in areas of abundant outcrop, otherwise where outcrop and features were available. Several traverses were made inland, generally along prominent ridges. Mapping was done using 1:20,000 air photos. Locations, bedding and cleavage were plotted on mylar overlays, with observations and data collected in a field book. Bedding was measured from exposed bedding planes typically where lithology changed, between metasandstone and metasilstone. The metasilstone was strongly cleaved in areas, and cleavage measurements were taken where available. Way-up was determined from scour features, grading, and soft sediment deformation structures. Additional field data were made available by W. Bleeker. Field data are recorded in Table 01 in Appendix I.

Figure 11: Map including Hearne and Watta Lake (Refer to Figure 03 for location), indicates location of main camp, and study area for this project. (Modified after Bleeker 1995).



 *Burwash Formation:* ca. 2.66 Ga metaturbidites
greenschist (light grey) to amphibolite facies (medium grey)

 *Defeat Suite:*
Biotite+hornblende tonalite to granodiorite

3.3 Bedding

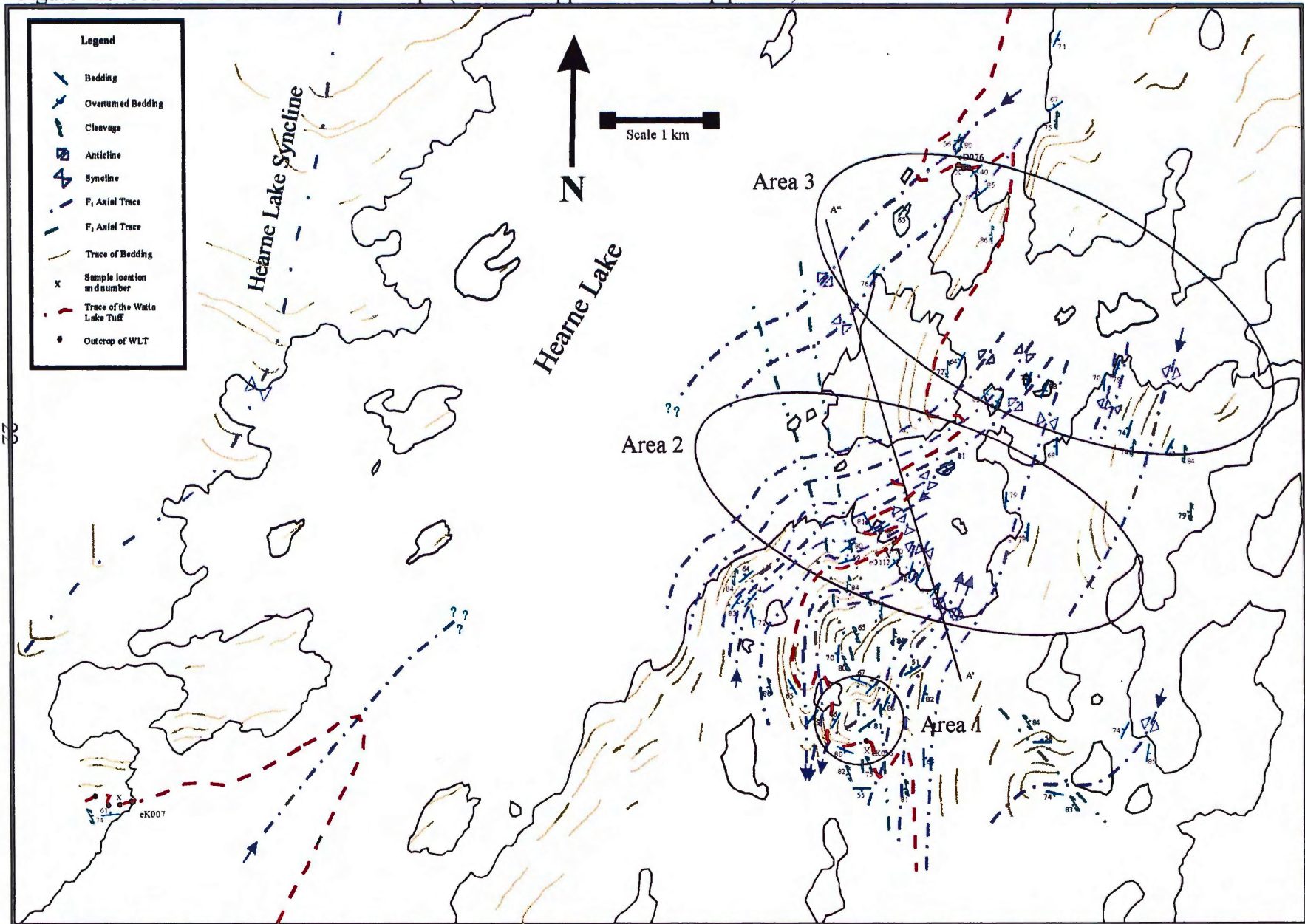
The main lithologies in the outcrop are alternating layers of metamorphosed sandstone and siltstone. The rocks have been metamorphosed to greenschist facies in the study area. The metasandstone is fine to coarse grained, tan to light grey, generally massive, and cleavage is rare in outcrop. The metasiltstone is very fine grained, light to dark grey, and highly cleaved in most areas.

There are some sedimentary features preserved in both facies. Bedding is preserved in most areas and can be determined from grading, lithology changes, and sedimentary features. The majority of sedimentary features observed were soft sediment deformation structures including flames and loads. Some of the other features included scour and fill marks, ripple marks, and silt rip-up clasts. There are areas where bedding and sedimentary features are obscured by cleavage, metamorphism, weathering and growth of lichens. The bedding is steeply dipping throughout the whole map area (Figure 12).

3.4 Veins

There are several different generations of veins noted in the area. The most common veins were observed as being concordant with bedding. These veins are generally several centimetres thick and can be traced for tens of metres. Thin quartz veins, several millimetres thick, observed in some metasiltstone and tuff layers, are usually ptymatically folded and die out over distances of less than one meter parallel to their length. In one area, several parallel veins at approximately 1m spacing cross-cut bedding. These veins are approximately 3 cm thick and could be traced across the outcrop for several meters.

Figure 12: Scaled version of structural map. (Refer to Appendix II in map pocket)



3.5 Folds

Two different scales of folding can be seen in the air photos. The kilometer scale folds are termed by Bleeker and Beaumont-Smith (1985) Hearne Lake syncline, and Hearne Lake Anticlinorium, as they are of regional scale (Figure 12).

From the airphoto, the trace of bedding of competent metasandstone beds can be followed, fairly continuously. Individual beds generally strike northeast, and curve forming "V" shaped fold closure patterns. Some of the beds are discontinuous and exposure is poor in marsh areas. The beds form what appears to be a nearly closed, dome shape, fold interference pattern (Figure 04) in Area 1 of figure 12.

A cartoon cross-section (Figure 13) was constructed along A'-A''. This section runs approximately parallel with the F₂ fold axial trace, and cuts the F₁ axial trace at a high angle. The cross-section, and field data plotted on the structural map (Figure 12) enabled the F₁ folds to be characterized. The amplitude of the folds through the cross-section is determined to be approximately 200 m. In the classification of Ramsay and Huber (1983) the F₁ folds are upright, with fold closures to the north and south, indicating some are double plunging. The F₁ folds have interlimb angles between 110 and 50 degrees, and are classified as open to close according to Fleuty (1964).

Bedding was plotted on stereonet covering two areas of the structural map to aid with the interpretation of F₁ folds. The best-fit great circle was plotted through the poles to bedding, to approximate the profile plane. The pole to this great circle was then plotted, which approximates the hinge line. The hinges of F₁ folds in Area 3 (Figure 14) have an average attitude of 22-219; according to the classification in McClay (1987) these are gently plunging folds. The hinges of the folds in the Area 2 (Figure 15) have a mean attitude of 61-196. These folds are classified as steeply plunging folds.

The F₁ axial traces (Figure 12) show significant curvature in Area 2 of the map, compared with F₁ axial traces to the east and northeast, which have a more linear northeast trend. North dipping bedding measurements across Area 2 are plotted on a stereonet (Figure 16) The F₂ is inferred to have caused the change of attitude of the F₁ axial trace. The poles to bedding across this interference provide an approximation of the

Figure 13: Schematic cross-section through F_1 fold trace, and approximately parallel to the F_2 fold axial trace.

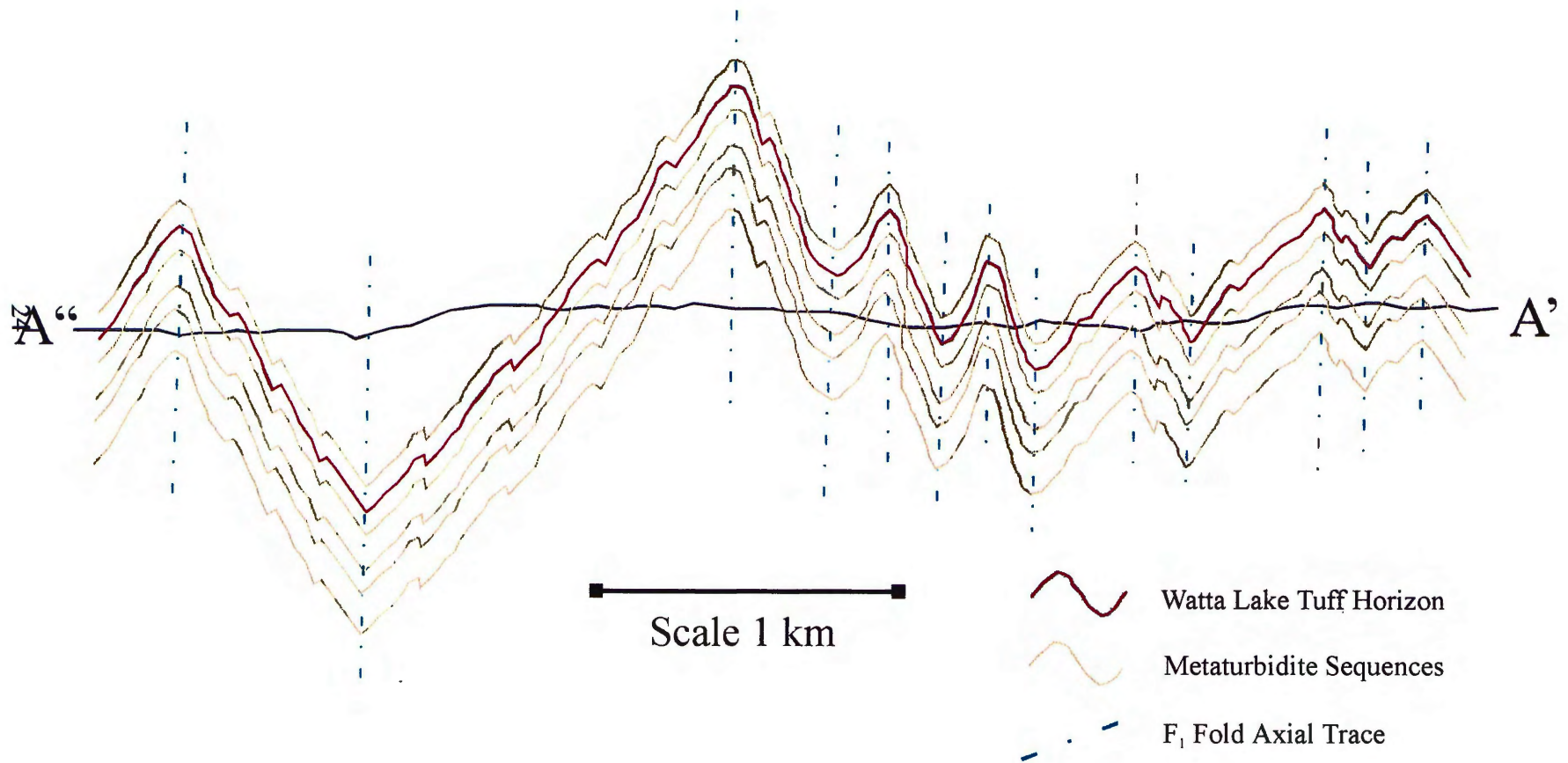


Figure 14: Stereoplot of bedding in Area 3 of map, along East side of Hearne Lake. Bedding plotted as poles, the great circle approximates the F_1 profile plane.

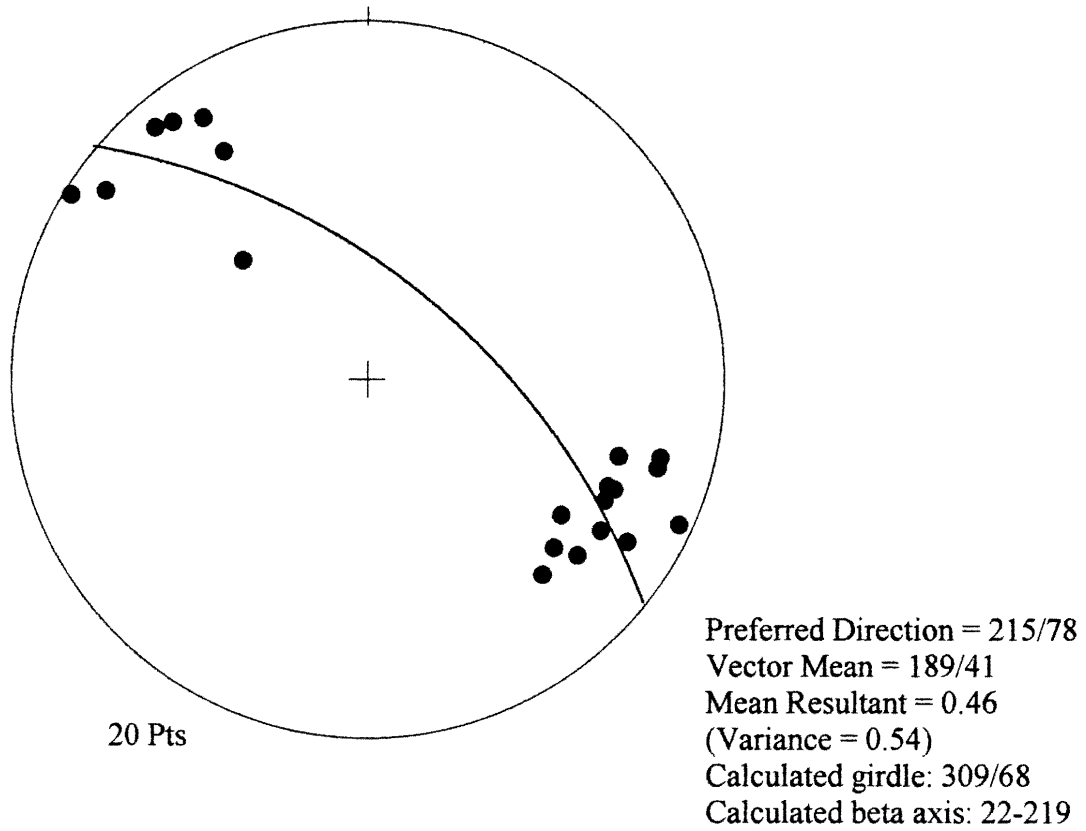


Figure 15: Stereoplot of bedding in Area 2 of map, along East side of Hearne Lake. Bedding plotted as poles, the great circle approximates the F₁ profile plane.

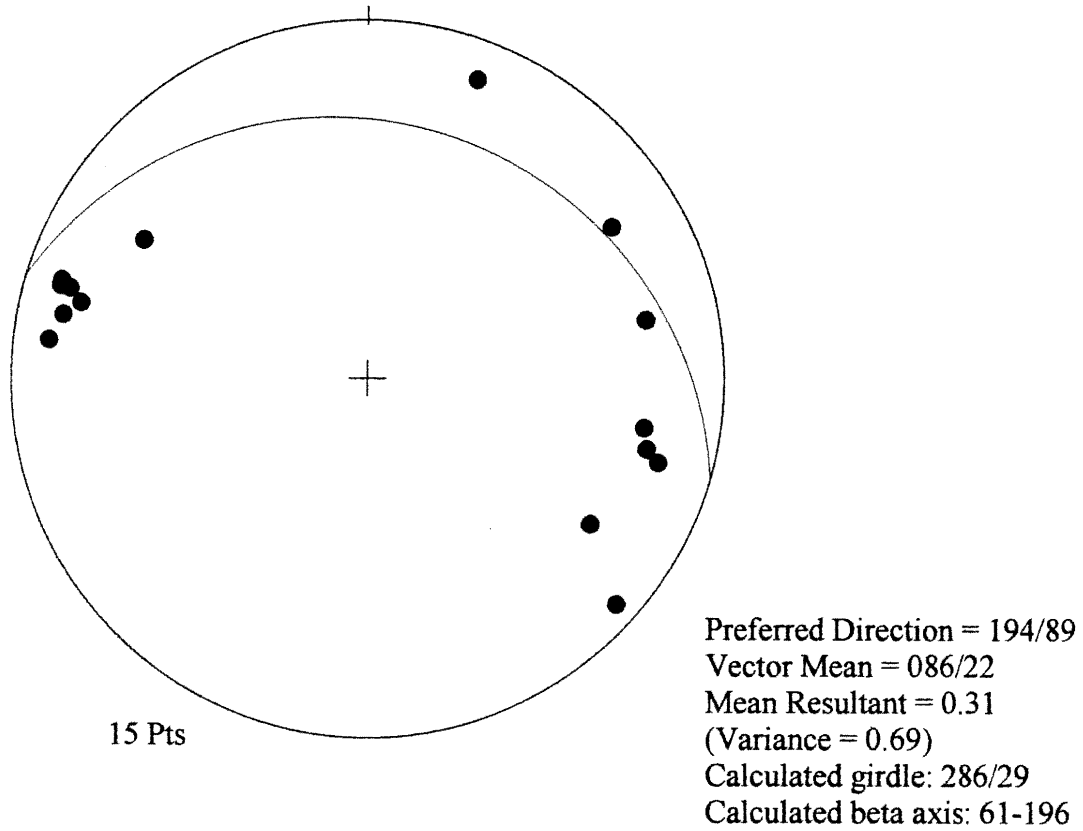
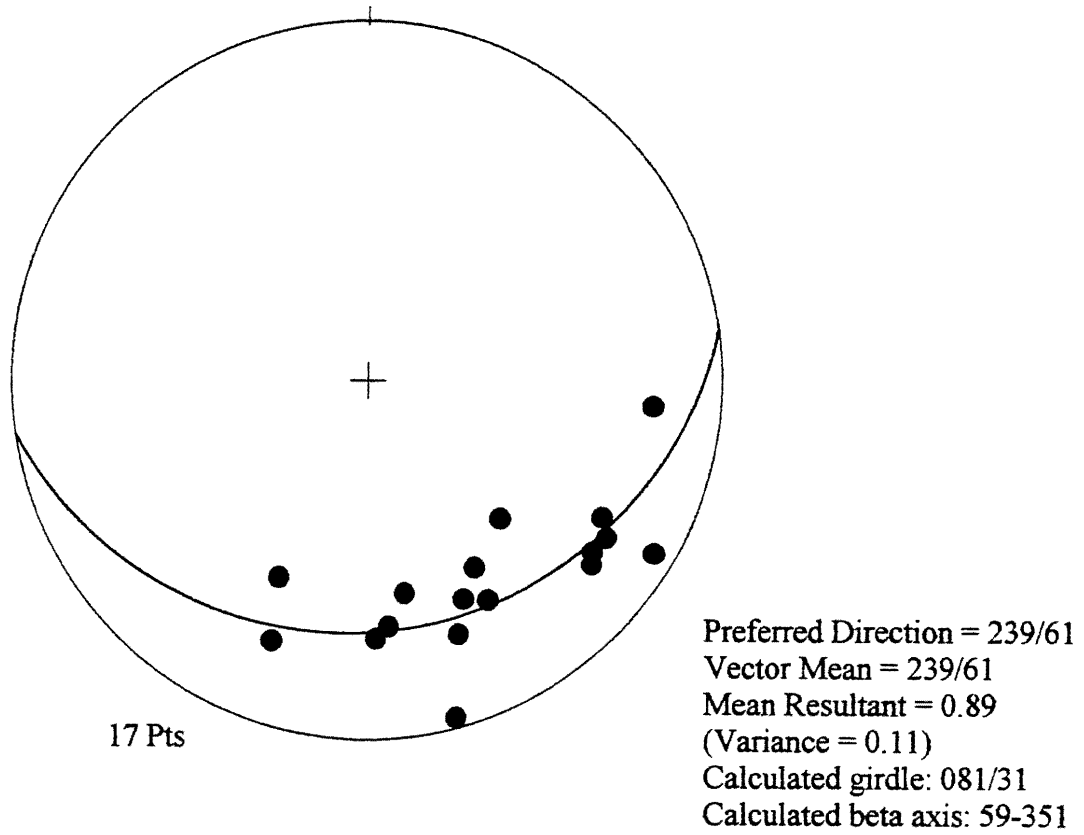


Figure 16: Stereoplot of bedding in Area 2 of map, along East side of Hearne Lake. Bedding plotted as poles, the great circle approximates the F₁ profile plane.



attitude of the F_2 hinge. The trend obtained for the hinges of the F_2 folds is approximately 351 degrees. The bedding forms a nearly closed dome shape pattern which is interpreted as a fold interference pattern. According to Ramsay's (1967) classification this interference pattern lies between Type 1 and Type 2 (Figure 17).

In a few locations, centimetre thick quartz veins, less than one meter in length, can be seen in outcrop. These veins form tight isoclinal, and sometimes ptgymatic folds. Field relations did not permit for relations to F_1 or F_2 folds

3.6 Cleavage

The majority of metasilstone contains a very closely spaced cleavage. Local fissile areas display a well defined slaty cleavage. Spaced cleavage was observed in the metasandstone units, although rare in outcrop. Cleavage was measured in the metasilstone beds when observed.

Cleavage poles for the whole map area are plotted on a stereonet (Figure 18). The average orientation of cleavage is 171/79. The strike is a close approximation for the axial trace of F_2 folds. The present orientation of the F_1 axial trace was determined to vary between 61-196, and 22-219. The cleavage cross-cuts the F_1 axial trace, and is therefore not axial planar to the F_1 folds. There is some variability in the cleavage measurements which can be attributed to: (i) the curved nature of the F_2 axial trace; or (ii) cleavage refraction; or (iii) as noted by Bleeker and Beaumont-Smith (1995), possible preservation of F_1 axial planar cleavage in low grade metamorphic zones.

3.7 Overprinting and Structural Interpretations

A number of the characteristics of the F_1 folds were modified by the F_2 deformation event. The fold amplitude decreases, with increasing distance from the fold interference pattern, thus suggesting the F_2 folds increased the amplitude of F_1 folds. The interlimb angles of F_1 folds are open to close, and the hinges vary from gently plunging in Area 3, to steeply plunging in the Area 2. The increase in plunge near the region of F_2

Figure 17: Expected outcrop patterns based on Ramsay fold interference classification.
 (Ramsay 1967)

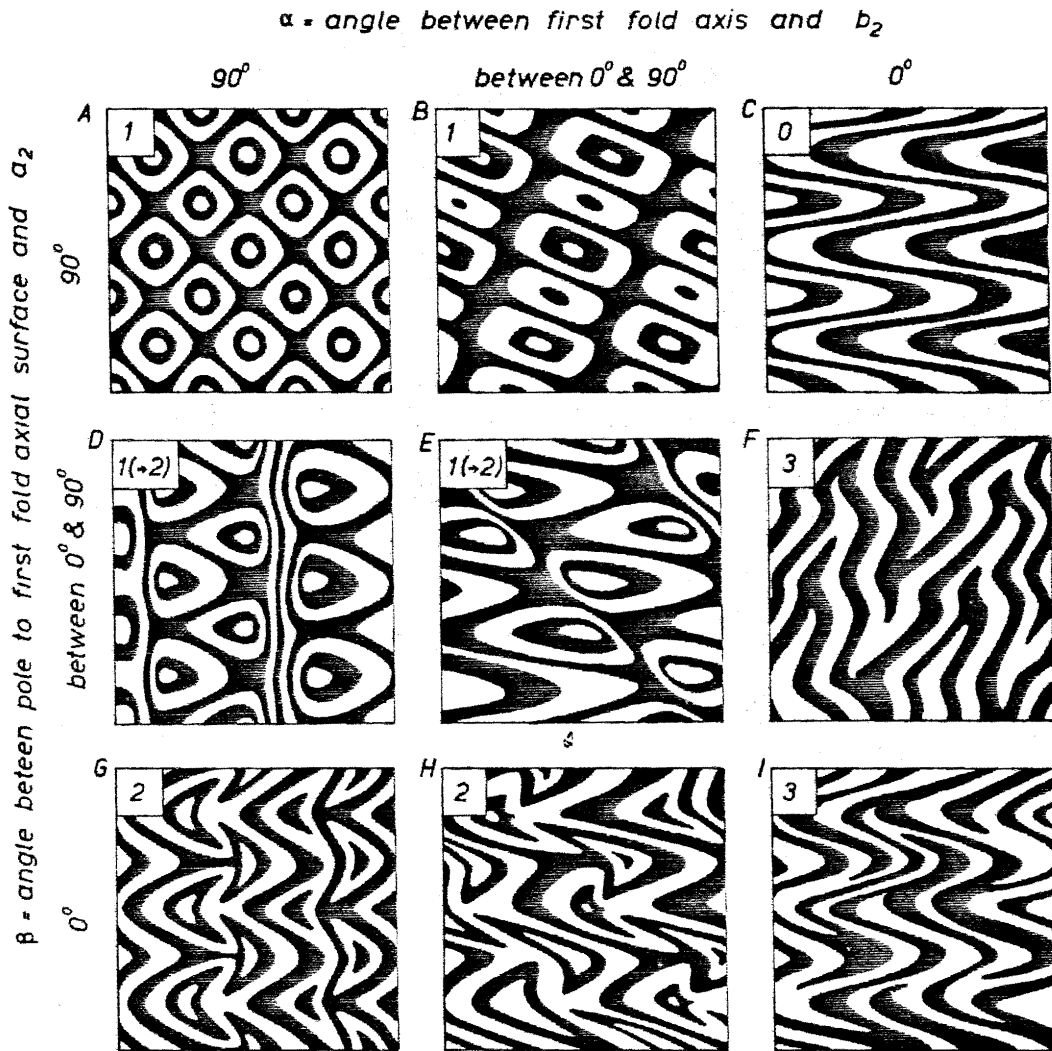
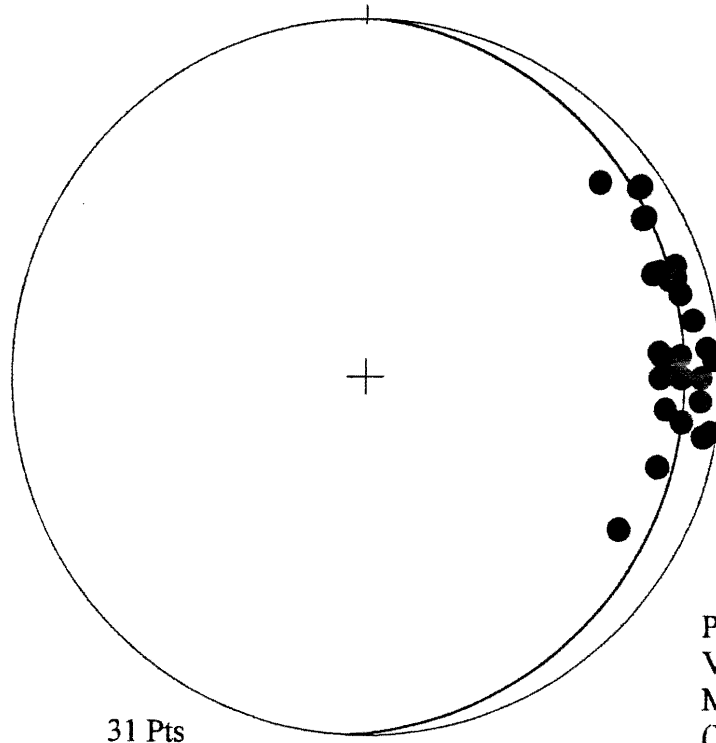


Figure 18: Stereoplot of S₂ cleavage for the map area.



Preferred Direction = 171/79
Vector Mean = 171/79
Mean Resultant = 0.96
(Variance = 0.04)
Calculated girdle: 003/11
Calculated beta axis: 79-273

deformation corresponds with Bleeker and Beaumont-Smith (1995) theory that the F_2 deformation increased the attitudes of plunges of F_1 folds. The domal shaped outcrop pattern was most likely generated when the F_2 deformation event refolded the F_1 bedding pattern. With reference to Ramsay's (1967) fold interference classification (Figure 17), the *alpha* and *beta* angles were estimated for this area. The *alpha* angle is close to 90 degrees, and the *beta* angle is close to 0 degrees. The outcrop pattern contains properties between a characteristic mushroom and dome shaped fold interference pattern. This pattern would be transitional between Type 1, and Type 2, although closer to Type 2. The outcrop map pattern lies between patterns "E" and "H" (Figure 17) of Ramsay's (1967) classification. Cleavage is approximately axial planar to the F_2 fold hinge. Observation based on the curvature of F_1 axial surface indicate that interlimb angles of F_2 folds are gentle to open (Fleuty 1964).

Chapter 4

Strain Analysis

4.1 Uses for Strain Analysis

A knowledge of the state of strain in the Burwash Formation is important for the reconstruction of the pre-tectonic turbidite sequences. Strain analysis provides the basic data required for the restoration of stratigraphic thicknesses (Lisle 1985).

4.2 Samples

Several samples of the Watta Lake Tuff were collected, during the 1998 and 99 summer field seasons. Sample locations are marked on the structural map (Figure 12). Sample number eK007 of the Watta Lake Tuff, was taken from the West side of Hearne Lake. The sample was oriented in the field and then removed with hammer and chisel. Sample eD076 was collected by Michelle DeYoung and Mark Ferguson, using a portable rock saw in the field. The WLT consists of several tuffaceous layers (Figure 08). The thick coarse grained layer contains grains that are visible to the naked eye and are obviously deformed.

The grains in the WLT are from a volcanic clasts. Some of the grains have an irregular shape, and are therefore assumed to initially have been non-spherical. Strained particles of all shapes have properties in common with the finite strain ellipse (Ramsay and Huber 1983). The relationship between clast shape before and after deformation is a very complicated function of original shape, and competence contrast between the clast, its matrix, and influence of neighbouring clasts (Ramsay and Huber 1983). A three dimensional ellipsoid can be calculated from three, two dimensional, sectional data sets. Calculations of the three dimensional strain ellipsoid are made less complicated by acquiring three strain ellipses on planes that are mutually perpendicular.

In the lab, samples were cut using a rock saw. The first plane (section c) was cut close to the plane of bedding, which could be observed in the sample. The other two planes (sections a, and b) were chosen to cut, at the greatest possible angle, across the principal planes of the visually estimated strain ellipsoid. Each of the cut planes was labeled (section a, b, and c), polished, and a thin section was made. It was decided that scanning of the rock surfaces at high resolution, and enhancement of the image using Adobe Photoshop 4.0, produced the most economical, and flexible method for making measurements. Two methods of estimating strain were employed, Rf/Phi and Fry plots.

4.3 Theoretical Basis of the Fry Method

The Fry (1979) method is ideal when a rock contains grains with locatable centers, but the object shape cannot be used to unambiguously determine strain. In such rocks it is common for objects to have a characteristic size, and therefore the center to center separation of nearest neighbours is controlled by the geometric constraints of the packing (Ramsay 1983). In order for the Fry method to produce results a series of redistributed originally uniform anti-clustered points is required.

The Fry plot produces a point vacancy or area of low concentration. This arises from the fact that any two original particles cannot come to lie closer than the sum of their radii. An elliptical vacancy field implies that the rock has suffered strain. The shape and orientation of the strain ellipse are directly recorded by the elliptical form of the field (Ramsay 1983). Around the vacancy field high concentrations of points will occur. This concentration relates to the commonest closest packing distance between particles. If the initial particles had a varied shape, or if the packing was not tight, this concentration will be weak (Ramsay 1983).

4.4 Methods using Fry Plot

The centers of grains for each of the sections (a, b, and c) from the sample eK007 were picked. Approximately 50 to 100 grains were required to produce a reasonable Fry plot. A dot was placed in the estimated grain centers which were in close contact with neighbouring grains using Adobe Photoshop 4.0. A copy of the grain centers was printed, and a Fry plot for each section was constructed. A Fry plot is constructed by placing a transparent overlay bearing graph axes, over the marked grain centers. The origin of the graph is centered over one of the grain centers. Each neighbouring grain center is marked on the graph. The graph must remain orthogonal and another grain center is placed under the origin. This process is repeated until all of the grain centers have been placed under the origin, and their neighbouring grains marked.

The Fry plots were scanned and imported into CorelDraw 7. Each of the sections had an elliptical vacancy field about the origin. Ellipses of known strain were drawn, and adjusted in size and rotated until they closely approximated the dense clustering of points. The results of the Fry plots are listed in Table 02.

4.5 Discussion of Fry Plots

The central vacancy fields of each of the sections were not uniform in point distribution. Section a (Figure 19, Appendix III), is the best constrained, with a dense cluster, around the vacancy field, which is surrounded by a lower density field. Section b (Figure 20, Appendix III), has a high density field at both ends of the interpreted major axis of the ellipse. The lack of point density along the minor axis, and the relatively low value of strain, allow for a significant amount of variability in estimated orientation. Section c (Figure 21, Appendix III) contains an elongated vacancy field. The orientation of the major axis of the resultant strain is well defined. An ellipse was fitted to the edges of the vacancy field for this section.

The Fry plots are dependent on spatial relationships between grain centers. The sample contains a matrix, which has a deflection in its foliation. I infer, from this, that

Table 02: Resultant strain and orientation, determined from sectional data of the samples eK007 and eD076. Fry and Rf/ Φ methods

	Fry Plot of Sample eK007	Rf/ Φ using DePaor Orientation net Sample eK007	Rf/ Φ using Ramsay method Sample eK007	Rf/ Φ using DePaor Orientation net Sample eD076
Section A	Rs= 1.70 $\Phi = -37^\circ$ wrt C	Rs= 1.30 $\Phi = -36^\circ$ wrt C	Rs= 1.35 $\Phi = -38^\circ$ wrt C	Rs= 1.48 $\Phi = 15^\circ$ wrt C
Section B	Rs= 1.50 $\Phi = -58^\circ$ wrt A	Rs= 1.02 $\Phi = -9^\circ$ wrt A	Rs= 1.10 $\Phi = -10^\circ$ wrt A	Rs= 1.97 $\Phi = -51^\circ$ wrt C
Section C	Rs= 2.00 $\Phi = 38^\circ$ wrt A	Rs= 1.90 $\Phi = 43^\circ$ wrt A	Rs= 2.00 $\Phi = 42^\circ$ wrt A	Rs= 3.30 $\Phi = -23^\circ$ wrt A

wrt = with respect to (section)

there is a competency contrast between the matrix and clasts. There may have been a minor amount of grain boundary movement between the grains.

4.6 Theoretical Basis of the Rf/phi Method

Ramsay (1967) devised a graphical method of strain analysis, Rf/Phi . He showed theoretically that a set of elliptical markers with identical ellipticity but variable orientation will show a characteristic pattern when their deformed axial ratios (Rf) and orientations (phi) are plotted (Figure 22). The Rf/phi plot forms a pattern, which is a function of the strain ellipse shape, and of the initial ellipticity of the markers. Ramsay's method allowed the effects of initial shape to be distinguished from those due to tectonic strain. The angle Phi is plotted along the x-axis, and the Rf ratio is plotted against a logarithmic y-axis. When all of the data are plotted, the pattern is compared with standard Marker Deformation Grids (Lisle 1985) (Figure 22), to determine the resultant strain and orientation.

DePaor (1988) developed a graphical method of Rf/Phi analysis with the use of a hyperbolic net, which he termed an orientation net (Figure 23). The north side of the orientation net is used for strain analysis. The R-axis runs through the center with 90 degree increments on each side. The strain contours are symmetrical non-orthogonal asymptotes with vertices on horizontal, and vertical axes. Points are plotted by rotating the R-axis, through the angle Phi (positive clockwise), and measuring Rf from the center, along the R-axis. The maximum principal stretch and orientation are located by dividing the points in half using the R-axis and the hyperbolas (strain contours) (DePaor 1988). DePaor's (1988) method gives Rs, by identifying the particular 50%-of-data curve that fits the deformation state.

4.7 Methods using Rf/Phi

Measurements were made on the three mutually perpendicular surfaces (a, b, and c) from each sample. Their geographical reference direction was determined from the

Figure 22: Standard Marker Deformation Grids, produced by Lisle 1985.

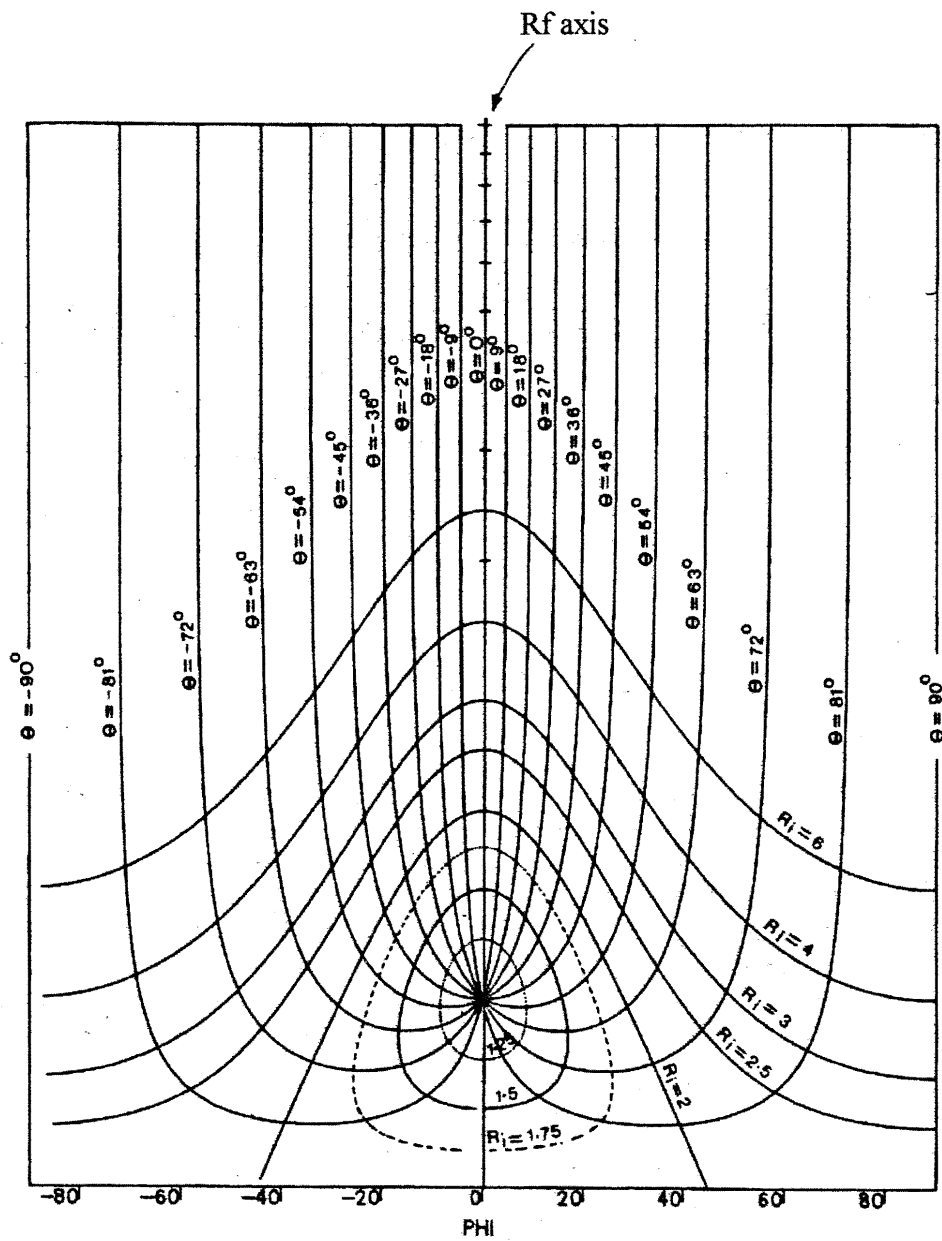


Figure 23: Orientation net produced by DePaor. Top half is used for strain analysis. The strain R_f is measured out from the origin, and the angle Φ is measured either direction of R (positive clockwise). (Reproduced from DePaor 1988)

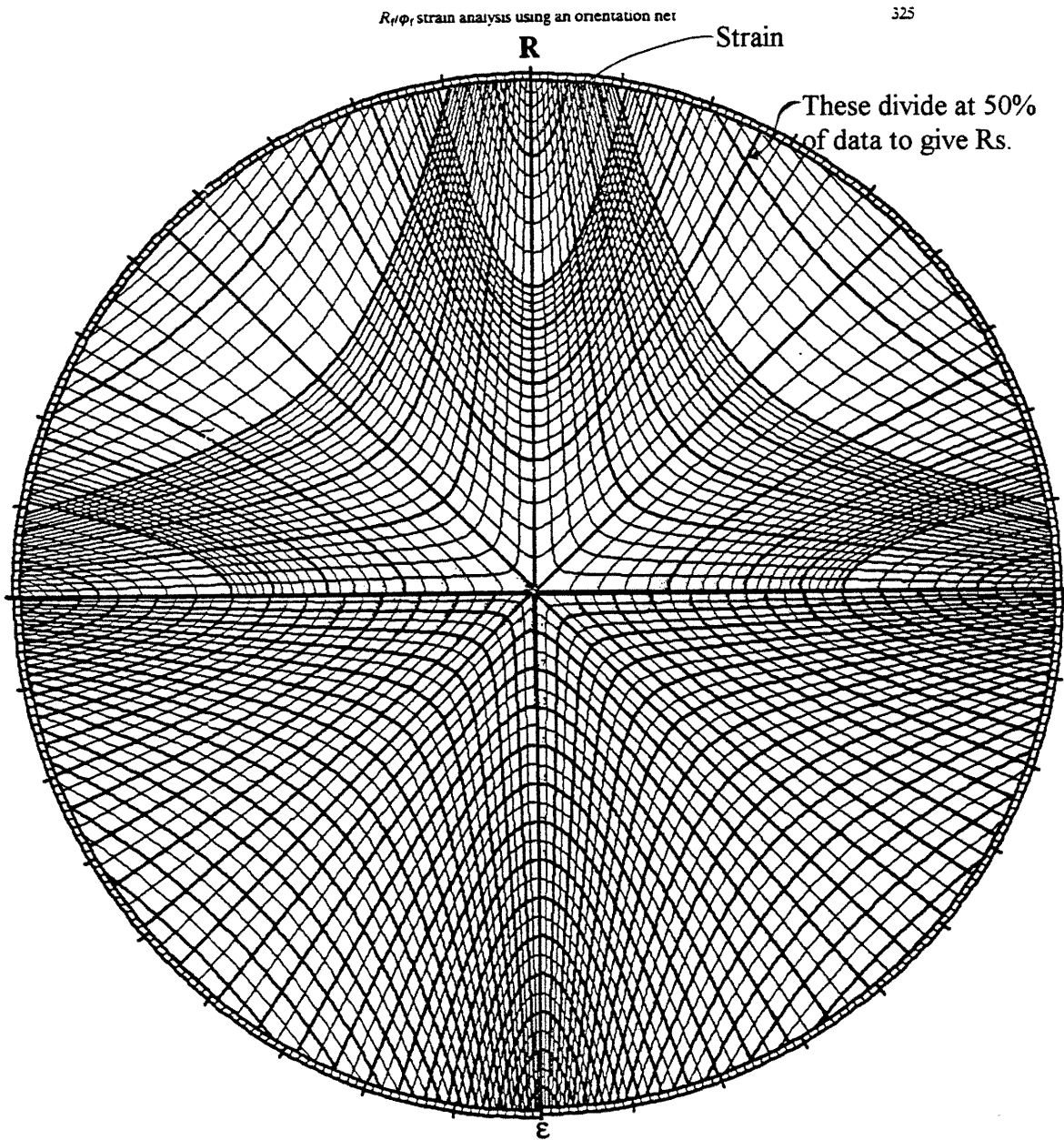


Fig. 1. The hyperbolic net.

oriented sample. Measurements of axial ratios were made from scanned images, enhanced using Adobe Photoshop 4.0. Clasts were outlined, and printed on paper. Generally a box was drawn around the grain, to closely approximate and facilitate measurement of the principal axes of the ellipse R_f . The longest dimension of the clast was measured as the major axis, and the longest dimension perpendicular to the major axis was taken as the minor axis. R_f was calculated from these axes. The angle ϕ was measured between the major axis, and a line parallel to one of the cut planes. The data for sections a, b, and c of sample eK007 are collected in Tables 03, 04 and 05 respectively, and located in Appendix III. The data for sections a, b, and c of sample eD076 are collected in Tables 06, 07 and 08 respectively, and located in Appendix III. The data from sample eK007 were plotted using Ramsay's (1967) method. Samples eK007, and eD076 were plotted on DePaor's (1988) orientation net. The R_f/ϕ plots are included in Appendix III (Figures 24-32). The results are listed in Table 02.

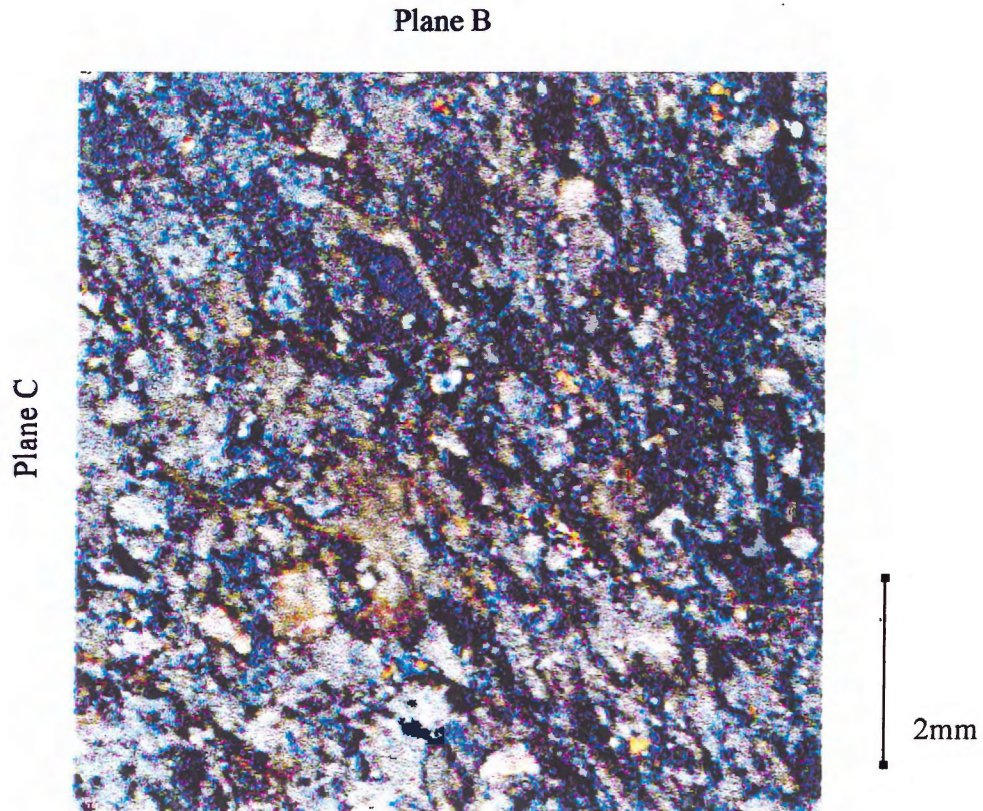
4.8 Discussion of the R_f/ϕ Method

A scan of each section with a strained, and oriented ellipse, representative of each method, is included in Figures 33 through 38 at the end of this chapter. The values produced using the DePaor (1988) orientation net, and the Ramsay (1967) R_f/ϕ method were very similar. The orientation net method produced values which were slightly lower, although the difference is statistically insignificant for this data. In sample eK007, section c appeared to have some asymmetry. The data points were tested using a symmetry test designed by Lisle (1985). The results validated the assumption of no initial fabric for this section. The grains analyzed in the R_f/ϕ method were larger than those used in the Fry approach. The effect of grain boundary sliding should be reduced in considering the larger grains. The issue of competence contrast between clasts and matrix has been studied by Gay (1968). Gay (1968) states that the effects of competence contrast becomes less significant when the grains are densely packed.

4.9 Discussion of Fry versus Rf/Phi plots

Figures 33 to 38 contain a scan of each section and a strained ellipse in the orientation produced by each plotting method. The resultant strain values from the Fry plots for sample eK007 are larger than those produced from either Rf/Phi method. Examination of the thin sections, revealed a platy matrix which was deflected around the clasts. This observation implies there were some inhomogeneity during deformation. The Rf/Phi plot concentrates on grain shape and orientation. The Rf/Phi plot will produce a bulk strain experienced by the clasts in the tuff layers. The Fry plot compares location of grain centers of nearest neighbours. The Fry method will account for grain movement and deformation of clasts. For this sample, the Fry plot gives a more representative value for the bulk strain experienced by the rock.

Figure 33: Scan of Sample eK007, section a

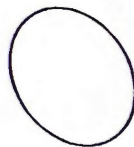


Strain ellipses produced using the following methods

Fry Plot



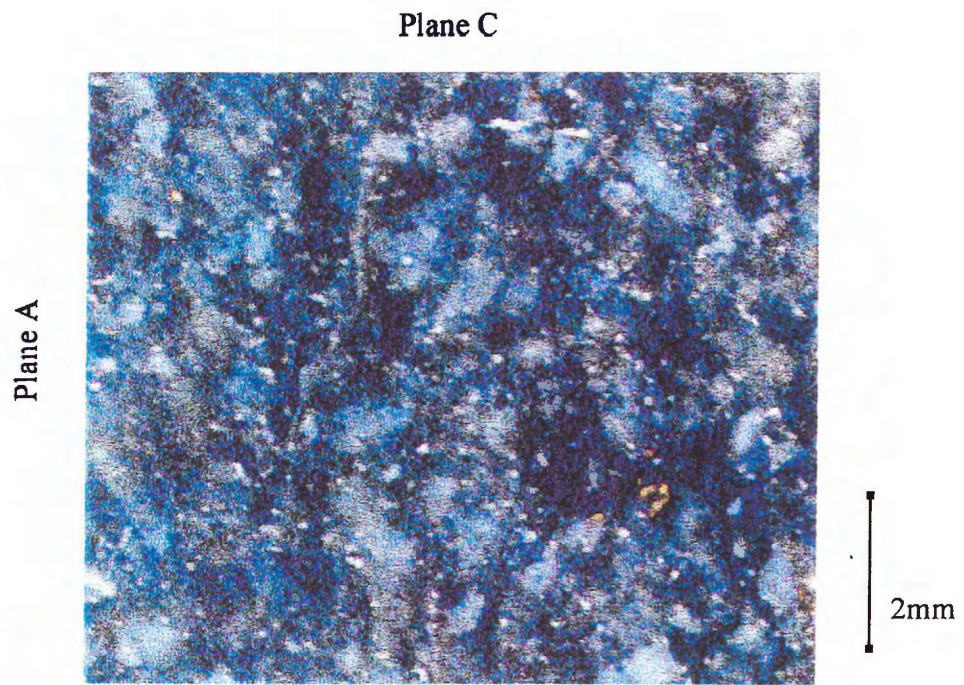
DePaor
Orientation net



Ramsay
Rf/Phi plot

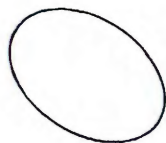


Figure 34: Scan of Sample eK007, section b

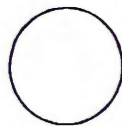


Strain ellipses produced using the following methods

Fry Plot



DePaor
Orientation net



Ramsay
Rf/Phi plot

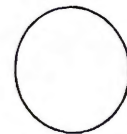
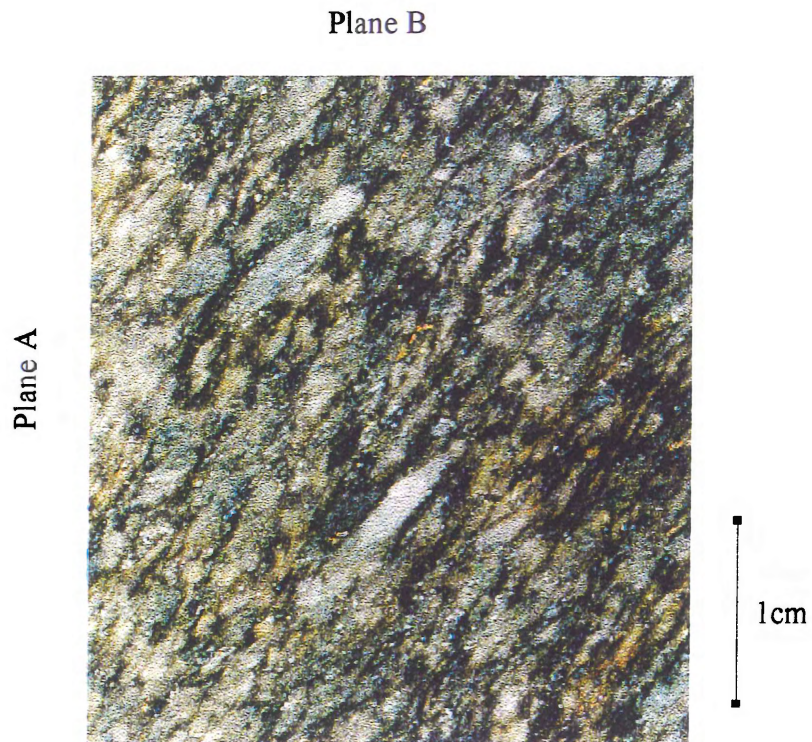


Figure 35: Scan of Sample eK007, section c



Strain ellipse produced using the following methods

Fry Plot



DePaor
Orientation net



Ramsay
Rf/Phi plot

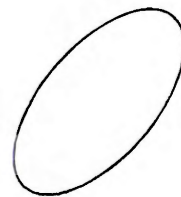
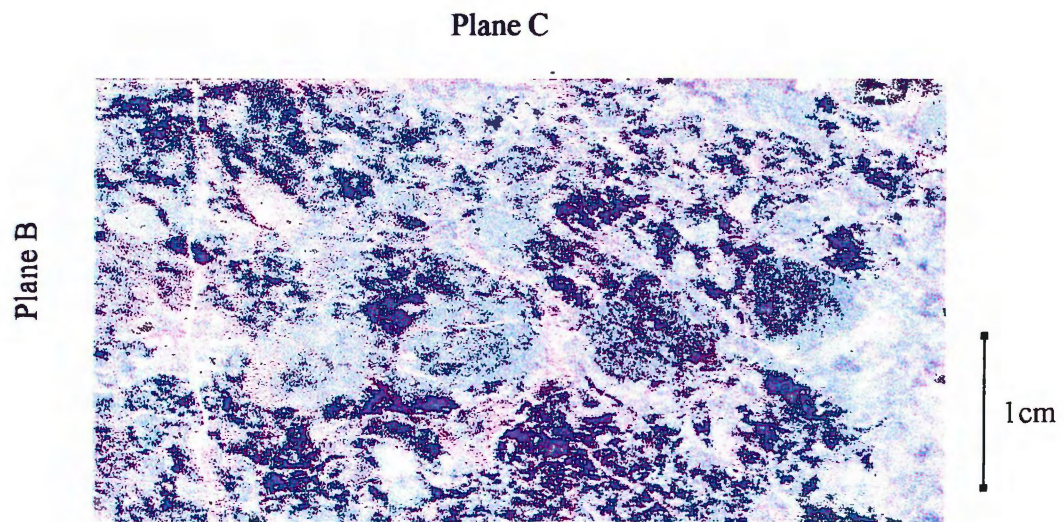


Figure 36: Scan of Sample eD076, section a



Strain ellipse produced with DePaor Orientation net

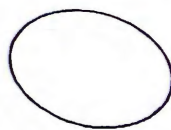
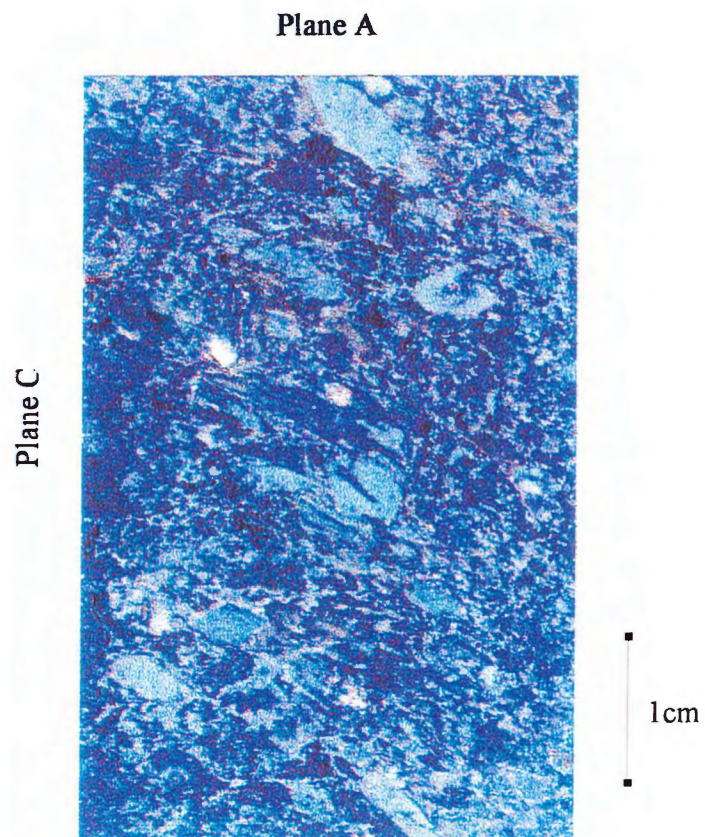


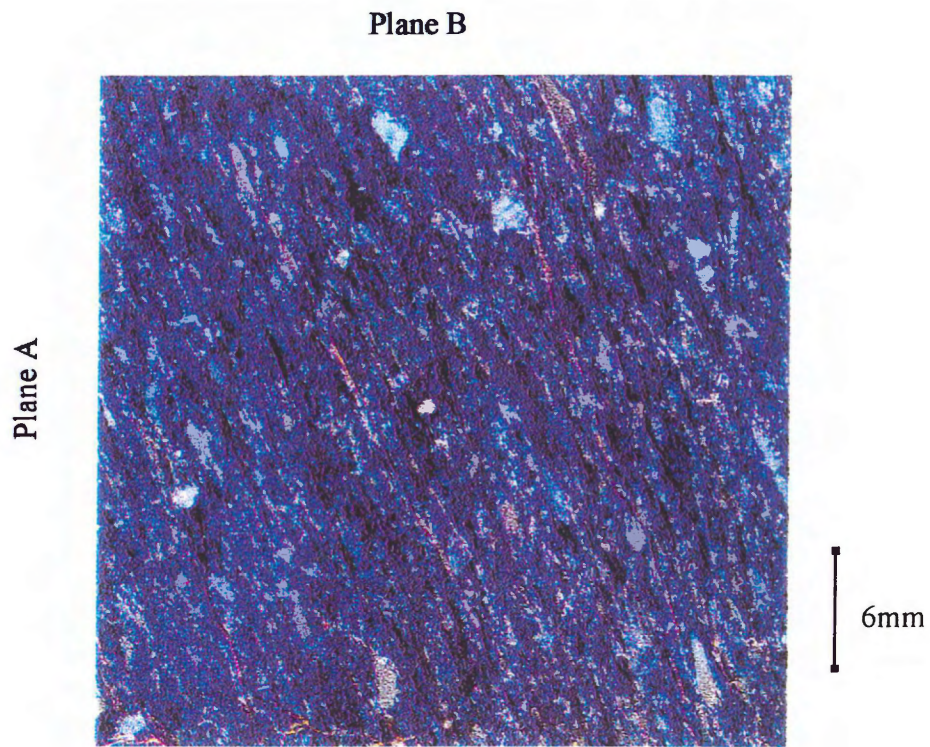
Figure 37: Scan of Sample eD076, section b



Strain ellipse produced with DePaor Orientation net



Figure 38: Scan of Sample eD076, section c



Strain ellipse produced with DePaor Orientation net



Chapter 5

3 Dimensional analysis and Conclusion

5.1 Producing the 3-Dimensional Strain Ellipsoid

The results from the sectional data for each sample were entered into the program E2E3, which was produced by Declan DePaor (Personal communication 2000). This program uses a graphical approach, in which the three sections can be adjusted. In order to minimize error, the areas of the ellipses must be adjusted so they intersect on the surface of a single ellipsoid. When an appropriate fit could not be achieved by only adjusting the area, the orientation of the resultant strain was adjusted for sections which were poorly constrained. The results of the data are included in Appendix III (Figure 39: Sample eK007 Fry plot data, Figure 40: Sample eK007 Rf/Phi data, and Figure 41: Sample eD076 Rf/Phi data).

The 3-dimensional strain ellipsoid can be determined using the data produced from the program E2E3. An Excel program was created by John Waldron to calculate an ellipsoid. The Excel program takes the adjusted ellipses from the three planes, and calculates the locations in 3-D, of 12 points on the surface of the strain ellipsoid (4 on each plane). It then applies a strain and a rotation to the locations of the points. The applied deformation is varied using the "Solver" in Excel until all 12 points lie on or close to the surface of a sphere. The inverse of this strain is then used as an estimate of the 3-D strain ellipsoid. A copy of this program and calculated data are included in Appendix III (Table 09: Sample eK007 Fry plot data, Table 10: Sample eK007 Rf/Phi data, and Table 11: Sample eD076 Rf/Phi data). The data is summarized in Table 12, which includes the principal axes of the 3-D ellipsoids, and their orientations.

Table 12: Summary of data produced by the Excel program. Table includes principal axes of 3-D ellipsoids, and their orientation.

Sample	Principal Axis	Stretch	Plunge	Trend
eK007	X	1.47	80	028
Fry plot	Y	0.89	09	192
Data	Z	0.76	03	283
eK007	X	1.5	74	054
Rf/Phi plot	Y	0.95	11	280
Data	Z	0.7	11	188
eD076	X	3.63	68	085
Rf/Phi plot	Y	0.7	21	253
Data	Z	0.4	04	345

Figure 42: Stereoplot of principal axes of the ellipsoid produced from sample eK007, plotted with the F_1 profile plane, F_2 axial trace, and cleavage from the sample.

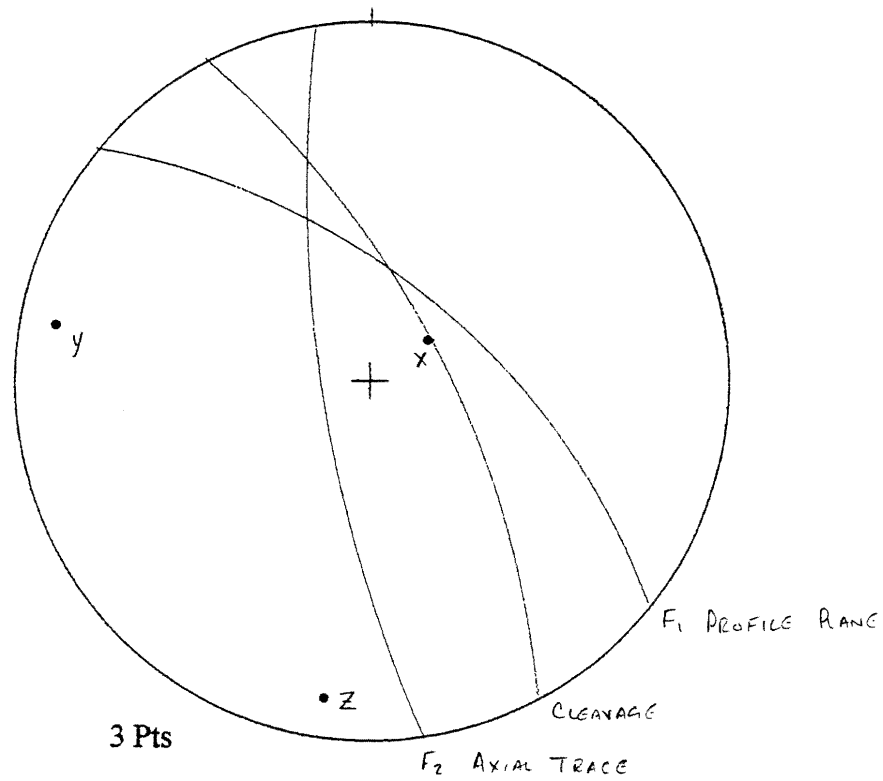
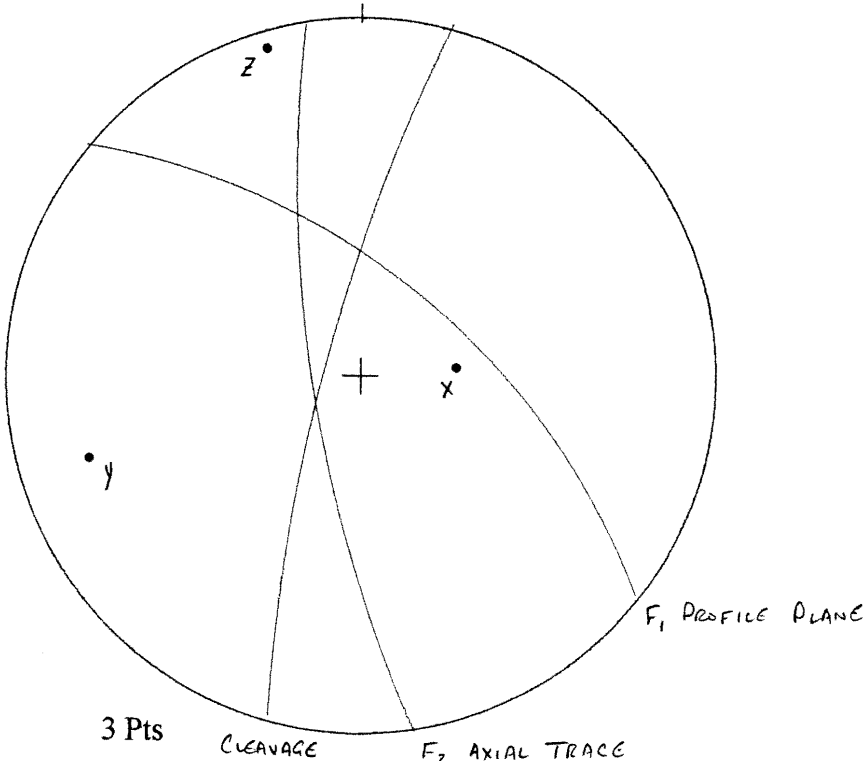


Figure 43: Stereoplot of principal axes of the ellipsoid produced from sample eD076, plotted with the F_1 profile plane, F_2 axial trace, and cleavage from the sample.



5.2 Discussion of 3-D Ellipsoid

The resultant strain calculated along the principal axes of the 3-D ellipsoid are recorded in table 12. The resultant ellipsoids have a prolate shape. The longest principal axis ranges from 1.47 in sample eK007 to 3.63 for sample eD076.

The three principal axes of the strain ellipsoid for samples eK007 and eD076 (Rf/Phi data) were plotted on a stereonet (Figures 42 and 43 respectively). The F_1 profile plane, F_2 axial trace, and cleavage from the sample were plotted as great circles. The long axis of the ellipsoid is steeply dipping. The shortening plane for the F_1 event is oriented NW-SE, and the F_2 shortening plane is oriented NE-SW. The prolate shape of the strain ellipse may have been formed by two episodes of plane strain related to the deformation events F_1 and F_2 .

5.3 Practical Application of the Calculated Ellipsoid

In order to restore a measured stratigraphic sections to its original depositional thickness, the inverse of the bulk strain must be applied. The Excel program designed by J. Waldron, includes calculations for the inverse for the strain along any arbitrary trend and plunge. The stratigraphic section, dY052, was measured through the WLT on the west side of Hearne Lake. The sample eK007 was collected at the same location of the section. The stretch required to restore the section was calculated using data produced from the Fry and Rf/Phi methods. The difference between the two results is less than 5%. A scale version of the measured section and restored section are displayed in Figure 44. Sample eD076 was used to restore section eD076 in the same manner (Figure 45).

Figure 44: Scale version of section dY052 on the left, restored version, on right. Section was scaled by 0.8



Section dY052

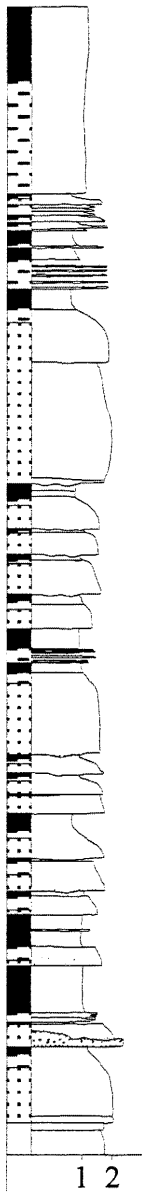
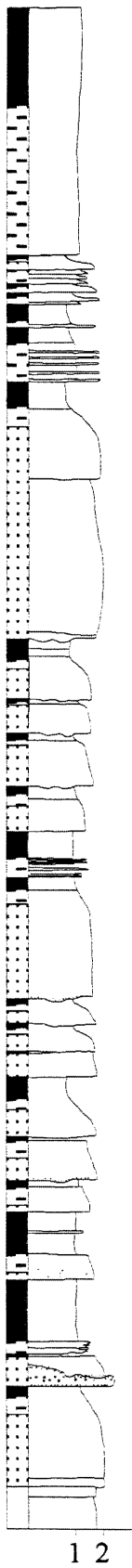
1m

Enlarged scale of grain size

m s vf M vc

M-mud
S-silt
VF, M, VC-sand

Figure 45: Scale version of section eD076 on the left, restored version, on right. Section was scaled by 0.7



1m

Section eD076

- 1: fine silty sand
- 2: fine sand

5.4 Conclusion

The Burwash formation has undergone two episodes of deformation related to folding. The structural map produced shows trace of bedding together with structural measurements and an interpretation of fold axial traces. The double plunging nature of the F_1 folds creates a complicated trace of the Watta Lake Tuff between outcrop locations. The fold interference pattern forms a nearly closed dome shape, in map pattern. The dome shaped, fold interference pattern is transitional between Type 1, and Type 2, and patterns "E" and "H" of Ramsay's (1967) classification. The F_2 folds may have produced an increase in amplitude, and plunge attitude of the F_1 folds. The cleavage is approximately axial planar to the F_2 fold hinge.

The coarse grained tuff layer is composed of elongate clasts surrounded by a platy matrix. The platy matrix is deflected about the clasts. Movement along grain boundaries is suspected; therefore the bulk strain would have had a component of inhomogeneity.

The Fry analysis is a good estimate of the bulk strain experienced by these rocks. The Fry analysis accounts for grain boundary movement and deformation of the clasts. The R_f/Φ method produces a good means for calculating strain experienced by the clasts in the tuff. The R_f/Φ results underestimated the bulk strain by approximately 5% when applied to actual stratigraphic columns in the area.

The 3-D ellipsoid can be determined from sectional data produced by the coarse grained tuff layer in the WLT. The ellipsoid was determined to have a prolate shape with the long axis steeply plunging. The prolate shape may have been the result of two nearly perpendicular plain strains, associated with the fold deformation events. The strain can be calculated for any arbitrary trend and plunge, and used to restore a stratigraphic section, to approximate its undeformed state.

5.5 Future Work

More work could be done to further understand the bulk strain in the area. More samples could be analyzed for strain from different parts of the folds. Samples from both limbs, and the hinge area, would help determine what type of strain was produced during the multiple stages of deformation. There are other samples with corresponding stratigraphic sections which could be analyzed and used to restore the sections.

References

- Bleeker, W. 1996. Thematic structural studies in the Slave Province, Northwest Territories: the Sleepy Dragon Complex. *In* Current Research, Part C. Geological Survey of Canada, Paper 1996-C, pp. 37-48.
- Bleeker, W. and Beaumont-Smith, C. 1995. Thematic structural studies in the Slave Province: preliminary results and implications for the Yellowknife Domain, Northwest Territories; in Current Research 1995-C; Geological Survey of Canada, pp. 87-96.
- Bleeker, W., Ketchum, J.W.F., and Davis, W.J. 1999a. The Central Slave Basement Complex, Part II: age and tectonic significance of high-strain zones along the basement-cover contact. *Canadian Journal of Earth Sciences*, **37**, 7: pp. 1111-1130.
- Bleeker, W., Ketchum, J.W.F., and Jackson, V.A. 1999b. The Central Slave Basement Complex, part I: its structural topology and autochthonous cover. *Canadian Journal of Earth Sciences*, **37**, 7: p 1083-1109.
- Bouma, A.H. 1962. *Sedimentology of some flysch deposits*: Amsterdam, Elsevier p. 168.
- DePaor, D.G. 1988. R_f/Φ Strain analysis using an orientation net. *Journal of structural Geology*. **10**: 4. pp. 323-333.
- Fluety, M.J. 1964. The description of folds, *Geological Association Proc.* **75**: pp. 461-492.
- Fry, N. 1979. Random point distributions and strain measurement in rocks. *Tectonophysics*. **60**: pp. 89-105.
- Fyson, W.K. 1975. Fabrics and deformation of Archean metasedimentary rocks, Ross lake Gordon lake area, Slave Province, Northwest Territories; *Canadian Journal of Earth Sciences*, **12**: pp. 765-776.
- Fyson, W.K., and Helmstaedt, H. 1988. Structural patterns and tectonic evolution of supercrustal domains in the Archean Slave Province. *Canadian Journal of Earth Sciences*, **25**: pp. 301-315.
- Gay, N.C. 1968. Pure shear and simple shear deformation in inhomogeneous viscous fluids. 1. Theory. *Tectonophysics*. **5**: pp. 211-234.

- Helmstaedt, H., Bell, R., Ellis, C.E., Howson, S., Jackson, V.A., and Relf, C. 1985. Geology of the Sito Lake area, NTS 85 J/16: NWT Geology Division, DIAND, Yellowknife, pp. 37-38.
- Henderson, J.B. 1972. Sedimentology of Archean turbidites at Yellowknife, Northwest Territories; *Canadian Journal of Earth Sciences*, **9**: p. 882
- Henderson, J.B. 1981. Archean basin evolution in the Slave Province Canada. *In* *Developments in Precambrian geology 4. Edited by. A. Kroner. Elsevier, Amsterdam*, pp. 213-235.
- Henderson, J.B. 1985. Geology of the Yellowknife - Hearne Lake area, District of MacKenzie, Northwest Territories. Geological Survey of Canada, Memoir 414.
- Hoffman, P.F. 1986. Crustal accretion in a 2.7-2.5 Ga "granite greenstone" terrane, Slave Province, NWT: a prograding trench-arc system? *Geological Association of Canada, Program with Abstracts*, **11**: pp. 82.
- Kusky, T.M. 1989. Accretion of the Archean Slave province: *Geology*, **17**: pp. 63-67.
- Lisle, R.J. 1985. Geological strain analysis, a manual for the Rf/ Φ technique. pp. 97. Pergamon Press, Oxford.
- McClay, K.R. 1987. The mapping of geological structures. pp. 161 *Geological Society of London Handbook*. John Wiley and Sons Ltd., England.
- McGlynn, J.C., and Henderson, J.B. 1970. Archean volcanism and sedimentation in the Slave Structural Province. *In* A.J. Baer, ed., *Symposium on Basins and Geocynclines of the Canadian Shield*. Geological Survey of Canada, Paper 70-40: pp. 31-44.
- McGlynn, J.C., and Henderson, J.B. 1972. The Slave Province: *In* *Variations in Tectonic styles in Canada. Edited by. R.A. Price and J.W. Douglas, Geological Association of Canada, Special Paper 11*, pp. 505-526.
- Padgham, W.A. 1987. The Yellowknife volcanic belt: setting and stratigraphy. *In* *Field guide Yellowknife mining district, The Yellowknife Geo-workshop Committee*. p.205.
- Padgham, W.A., 1990. The Slave Structural Province, an overview. *Mineral deposits of the Slave Province, Northwest Territories Field Trip 13. 8th IAGOD Symposium*.

Ramsay, J.G. 1967. Folding and fracturing of rocks. pp. 568 McGraw Hill Book Company, New York.

Ramsay, J.G. and Huber, M.I. 1983. The techniques of modern structural geology volume 1: strain analysis. pp. 302 Academic Press, London.

Yardley, B.W. 1989. An introduction to Metamorphic Petrology. pp. 248 . *Edited by* J. Zussman and W.S. MacKenzie. Longman Earth Science Series, England.

Appendix I

Field Data

Table 01: Bedding and cleavage measurements. "overturned" refers to bedding

Station	Strike	Dip	Cleavage	Strike	Dip
eE015	176	57		162	79
eE016	016	71			
eE017/019	208	85	overturned	360	90
eE018	220	67		178	75
eE020	197	74		175	86
eE021	275	85			
eE022	228	63			
eE023	205	86		176	73
eE024	213	67			
eE025	207	64		180	72
eE026	204	63			
eE027	212	75			
eE028	061	81			
eE030	106	62			
eE031	017	76		001	88
eE032	032	88			
eE033	195	74			
eE034	110	79			
eE036	073	80		211	72
eE037	265	59			
eE038	268	62		006	84
eE039	260	51			
eE040	294	51			
eE041	246	57			
eE042	247	64		184	84
eE043	214	69			
eE044	255	88	overturned		
eE053	240	60			
eE054	010	83			
eE055	241	54			
eE056	350	72		242	82
wb001	024	85			
wb002	298	49			
wb003	221	88	overturned		
wb004	250	57			
wb005	168	69		177	88
wb006	292	88	overturned	188	79
wb007	222	84	overturned		
wb008	018	79			
wb009	213	64			
wb010	194	70			
wb011	017	79			

wb012	007	79		
wb013	148	70		
wb014	190	68		
wb015	315	60		
wb016	268	48		
wb017	217	69		
wb018	045	78		
wb019	213	70		
wb020	130	81		
wb021	197	63		
wb022	053	80		
wb023	050	82		
wb024	204	65		
wb025	058	76		
wb026	220	66		
wb027	058	65	189	88
wb029	222	60		
wb215	215	56		
wb031	036	80		
wb032	044	40		
eK001	219	71	197	75
eK002	211	84	180	84
eK003	151	65	162	81
eK004	182	77	162	80
eK005	038	45		
eK006	031	79	010	80
eK007	266	61	332	74
eK008	245	57	002	84
eK009	290	67	330	89
eK010	349	64	176	78
eK011	210	66	190	86
eK012	110	79	145	84
eK013	226	45	351	80
eK014	025	86	180	78
eK015	130	84	150	79
eK016	056	81	160	82
eK017	240	51	340	86
eK018	356	82	356	82
eK019	207	74	001	78
eK020	270	53	325	65
eK021	103	74	145	83
eK022	241	60	359	83
eK023	250	65	335	78
eK024	185	70	150	80
eK025	095	80	140	75
eK026	090	75	160	75
eK027	184	55	162	79

eK028	196	61		165	81
eK029	000	66		165	81
eK030	180	63		175	72
eK031	043	84	overturned	199	89
eK032	012	76			
eK033	196	74		186	74
eK034	353	41		004	83
eK035	032	63		002	79
eK036	015	72			
eK037	290	56		320	84
eK038	172	73		160	77
eK039/040	265	72		170	83

Appendix II

Map

Refer to Pocket at back

Appendix III

Strain Calculations

Table 03: Sample eK007, section a, Rf/Phi data

Long Axis	Short Axis	Phi	RF
0.63	0.48	-70	1.31
0.5	0.3	-55	1.67
0.7	0.52	-13	1.35
0.71	0.29	-37	2.45
0.65	0.36	-9	1.81
0.72	0.41	-76	1.76
0.62	0.29	-88	2.14
0.62	0.18	-60	3.44
0.6	0.32	-61	1.88
0.92	0.4	-35	2.3
0.87	0.58	-76	1.5
0.72	0.4	74	1.8
1.12	0.52	-23	2.15
0.62	0.5	-28	1.24
0.6	0.21	-23	2.86
0.52	0.42	-63	1.24
1	0.4	-36	2.5
0.63	0.32	-34	1.97
0.64	0.31	-32	2.06
0.65	0.3	-51	2.17
0.62	0.42	-30	1.48
0.53	0.32	-54	1.66
0.35	0.3	-50	1.17
0.52	0.32	-22	1.63
0.98	0.36	-28	2.72
0.61	0.42	-38	1.45
0.52	0.43	66	1.21
0.7	0.29	-10	2.41
1	0.39	-49	2.56
0.72	0.39	3	1.85
0.72	0.42	17	1.71
0.82	0.45	-39	1.82
0.7	0.32	-57	2.19
0.62	0.42	-66	1.48
0.78	0.43	88	1.81
0.52	0.33	-8	1.58
0.82	0.42	-11	1.95
0.7	0.41	11	1.71
0.81	0.21	-56	3.86
1.1	0.52	-73	2.12

0.49	0.4	-72	1.23
0.97	0.45	-27	2.16
0.82	0.44	-35	1.86
0.5	0.3	-22	1.67
0.49	0.4	64	1.23
0.97	0.63	-11	1.54
0.71	0.6	-46	1.18
0.82	0.45	-77	1.82
0.58	0.45	46	1.29
0.58	0.29	12	2
0.8	0.48	-45	1.67
0.67	0.35	-81	1.91
0.71	0.44	-56	1.61
0.48	0.31	-15	1.55
0.72	0.45	-61	1.6
0.8	0.68	-18	1.18
0.83	0.7	-65	1.19
0.58	0.21	-2	2.76
0.96	0.61	-24	1.57
1.49	1.32	53	1.13
0.4	0.3	63	1.33
0.55	0.28	-52	1.96
0.57	0.3	-59	1.9
0.41	0.3	-62	1.37
1.4	1.04	3	1.35
0.93	0.41	-54	2.27
0.59	0.46	18	1.28
0.7	0.48	32	1.46
0.66	0.43	-61	1.53
0.48	0.42	-71	1.14
0.9	0.6	1	1.5
0.76	0.35	-30	2.17
0.44	0.32	-25	1.38
0.32	0.21	-70	1.52
1.09	0.51	-51	2.14
0.76	0.42	-74	1.81
0.58	0.39	-45	1.49
0.67	0.39	-1	1.72
0.62	0.28	-89	2.21
0.32	0.27	80	1.19
0.37	0.35	77	1.06
0.61	0.35	-36	1.74
0.7	0.3	-59	2.33
0.41	0.35	-48	1.17
0.45	0.32	79	1.41
0.8	0.39	-10	2.05
0.47	0.42	-50	1.12
0.58	0.26	-65	2.23
0.63	0.29	-25	2.17

Table 04: Sample eK007, section b, Rf/Phi data

Long Axis	Short Axis	Phi	RF
1.63	1.02	24	1.6
0.67	0.36	-49	1.86
0.76	0.32	-5	2.38
0.89	0.54	-58	1.65
0.72	0.4	-51	1.8
0.55	0.42	-2	1.31
0.8	0.5	-13	1.6
0.5	0.32	-43	1.56
0.69	0.49	37	1.41
0.54	0.4	71	1.35
0.88	0.63	3	1.4
0.92	0.62	-40	1.48
0.97	0.7	-42	1.39
1.21	0.63	-67	1.92
0.53	0.38	-20	1.39
1.4	0.62	-62	2.26
0.69	0.51	-68	1.35
0.62	0.38	-32	1.63
0.9	0.4	-21	2.25
0.62	0.32	-32	1.94
0.62	0.38	-83	1.63
0.62	0.39	23	1.59
0.6	0.4	84	1.5
0.61	0.41	-32	1.49
0.69	0.4	59	1.73
0.5	0.41	48	1.22
0.55	0.41	15	1.34
0.87	0.36	35	2.42
0.73	0.52	-36	1.4
0.61	0.44	55	1.39
0.61	0.37	-75	1.65
1.28	0.41	-43	3.12
0.62	0.58	50	1.07
0.56	0.5	50	1.12
0.8	0.4	-72	2
0.62	0.32	14	1.94
0.81	0.42	-70	1.93
0.72	0.41	45	1.76

0.69	0.44	-76	1.57
0.9	0.51	20	1.76
0.72	0.48	26	1.5
0.39	0.29	64	1.34
0.7	0.3	49	2.33
1	0.39	46	2.56
0.99	0.46	79	2.15
0.88	0.52	-2	1.69
0.59	0.39	49	1.51
0.62	0.35	-58	1.77
0.71	0.49	1	1.45
0.7	0.38	-37	1.84
0.62	0.3	-59	2.07
0.5	0.42	42	1.19
0.62	0.35	-76	1.77
0.71	0.62	-33	1.15
0.75	0.48	45	1.56
0.71	0.5	-86	1.42
0.52	0.44	-67	1.18
0.8	0.43	52	1.86
0.71	0.39	29	1.82
0.79	0.49	55	1.61
0.31	0.29	-37	1.07
0.61	0.4	11	1.53
0.72	0.3	5	2.4
0.97	0.72	-74	1.35

Table 05: Sample eK007, section c, Rf/Phi data, including calculations for asymmetry

Long Axis	Short Axis	Phi	RF	RF exp -1	deg to rad	Sin 2 Phi	Cos 2 Phi
0.8	0.24	39	3.33	0.3	0.6807	0.9782	0.2079
0.52	0.32	32	1.63	0.61	0.5585	0.8988	0.4384
0.38	0.13	68	2.92	0.34	1.1868	0.6947	-0.7193
0.44	0.31	59	1.42	0.7	1.0297	0.883	-0.4694
0.47	0.2	14	2.35	0.43	0.2443	0.4694	0.883
0.7	0.22	42	3.18	0.31	0.733	0.9945	0.1046
0.54	0.29	45	1.86	0.54	0.7854	1	0
0.53	0.3	39	1.77	0.56	0.6807	0.9782	0.2079
0.26	0.16	22	1.63	0.61	0.384	0.6947	0.7193
0.42	0.3	39	1.4	0.71	0.6807	0.9782	0.2079
0.3	0.13	32	2.31	0.43	0.5585	0.8988	0.4384
0.35	0.27	50	1.3	0.77	0.8727	0.9848	-0.1737
0.39	0.3	33	1.3	0.77	0.576	0.9136	0.4067
0.6	0.26	39	2.31	0.43	0.6807	0.9782	0.2079
1	0.37	44	2.7	0.37	0.7679	0.9994	0.035
0.2	0.13	0	1.54	0.65	0	0	1
0.74	0.34	40	2.18	0.46	0.6981	0.9848	0.1737
0.51	0.29	60	1.76	0.57	1.0472	0.866	-0.5
1.26	0.26	47	4.85	0.21	0.8203	0.9976	-0.0697
0.39	0.2	53	1.95	0.51	0.925	0.9613	-0.2756
0.8	0.33	59	2.42	0.41	1.0297	0.883	-0.4694
0.5	0.44	55	1.14	0.88	0.9599	0.9397	-0.342
0.36	0.3	48	1.2	0.83	0.8378	0.9945	-0.1046
0.76	0.4	50	1.9	0.53	0.8727	0.9848	-0.1737

0.46	0.22	61	2.09	0.48	1.0647	0.848	-0.53
0.54	0.21	56	2.57	0.39	0.9774	0.9272	-0.3746
0.48	0.24	43	2	0.5	0.7505	0.9976	0.0697
0.84	0.27	58	3.11	0.32	1.0123	0.8988	-0.4384
0.45	0.26	50	1.73	0.58	0.8727	0.9848	-0.1737
0.7	0.2	35	3.5	0.29	0.6109	0.9397	0.342
0.4	0.17	26	2.35	0.43	0.4538	0.788	0.6156
0.46	0.32	13	1.44	0.69	0.2269	0.4384	0.8988
0.8	0.23	53	3.48	0.29	0.925	0.9613	-0.2756
0.3	0.18	38	1.67	0.6	0.6632	0.9703	0.242
0.32	0.18	22	1.78	0.56	0.384	0.6947	0.7193
0.42	0.24	35	1.75	0.57	0.6109	0.9397	0.342
0.31	0.29	-43	1.07	0.93	-0.7505	-0.9976	0.0697
0.2	0.15	42	1.33	0.75	0.733	0.9945	0.1046
0.25	0.09	52	2.78	0.36	0.9076	0.9703	-0.242
0.72	0.19	52	3.79	0.26	0.9076	0.9703	-0.242
0.19	0.11	10	1.73	0.58	0.1745	0.342	0.9397
0.47	0.24	27	1.96	0.51	0.4712	0.809	0.5878
0.4	0.21	38	1.9	0.53	0.6632	0.9703	0.242
0.63	0.12	55	5.25	0.19	0.9599	0.9397	-0.342
0.53	0.12	64	4.42	0.23	1.117	0.788	-0.6156
0.4	0.13	45	3.08	0.32	0.7854	1	0
0.42	0.3	23	1.4	0.71	0.4014	0.7193	0.6947
2.13	0.5	44	4.26	0.23	0.7679	0.9994	0.035
1.01	0.21	47	4.81	0.21	0.8203	0.9976	-0.0697
0.98	0.3	60	3.27	0.31	1.0472	0.866	-0.5
0.7	0.24	40	2.92	0.34	0.6981	0.9848	0.1737
0.76	0.2	75	3.8	0.26	1.309	0.5	-0.866
0.59	0.2	38	2.95	0.34	0.6632	0.9703	0.242
0.7	0.31	45	2.26	0.44	0.7854	1	0
0.59	0.35	60	1.69	0.59	1.0472	0.866	-0.5
0.67	0.3	39	2.23	0.45	0.6807	0.9782	0.2079

0.81	0.29	40	2.79	0.36	0.6981	0.9848	0.1737
0.57	0.21	41	2.71	0.37	0.7156	0.9903	0.1391
0.77	0.28	43	2.75	0.36	0.7505	0.9976	0.0697
0.5	0.31	41	1.61	0.62	0.7156	0.9903	0.1391
0.4	0.25	44	1.6	0.63	0.7679	0.9994	0.035
0.4	0.33	21	1.21	0.83	0.3665	0.6691	0.7432
0.32	0.2	37	1.6	0.63	0.6458	0.9613	0.2756
0.63	0.22	51	2.86	0.35	0.8901	0.9782	-0.2079
0.52	0.22	39	2.36	0.42	0.6807	0.9782	0.2079
0.8	0.26	43	3.08	0.32	0.7505	0.9976	0.0697
0.48	0.28	41	1.71	0.58	0.7156	0.9903	0.1391
0.4	0.24	44	1.67	0.6	0.7679	0.9994	0.035
0.84	0.42	59	2	0.5	1.0297	0.883	-0.4694
0.37	0.19	41	1.95	0.51	0.7156	0.9903	0.1391
0.29	0.16	40	1.81	0.55	0.6981	0.9848	0.1737
1.09	0.6	42	1.82	0.55	0.733	0.9945	0.1046
0.5	0.25	43	2	0.5	0.7505	0.9976	0.0697
0.78	0.21	25	3.71	0.27	0.4363	0.766	0.6428
0.98	0.4	44	2.45	0.41	0.7679	0.9994	0.035
0.49	0.26	50	1.88	0.53	0.8727	0.9848	-0.1737
0.31	0.28	-32	1.11	0.9	-0.5585	-0.8988	0.4384
1.29	0.4	35	3.23	0.31	0.6109	0.9397	0.342
0.4	0.33	20	1.21	0.83	0.3491	0.6428	0.766
0.34	0.21	56	1.62	0.62	0.9774	0.9272	-0.3746
0.4	0.24	-47	1.67	0.6	-0.8203	-0.9976	-0.0697
0.54	0.48	-87	1.13	0.88	-1.5184	-0.1046	-0.9945
0.81	0.3	60	2.7	0.37	1.0472	0.866	-0.5
0.36	0.23	20	1.57	0.64	0.3491	0.6428	0.766
0.48	0.47	51	1.02	0.98	0.8901	0.9782	-0.2079
0.97	0.32	38	3.03	0.33	0.6632	0.9703	0.242
0.48	0.35	42	1.37	0.73	0.733	0.9945	0.1046
0.62	0.4	53	1.55	0.65	0.925	0.9613	-0.2756

A3-9

0.66	0.23	61	2.87	0.35	1.0647	0.848	-0.53
0.97	0.4	45	2.43	0.41	0.7854	1	0
0.8	0.22	47	3.64	0.27	0.8203	0.9976	-0.0697
0.44	0.28	44	1.57	0.64	0.7679	0.9994	0.035
0.45	0.2	51	2.25	0.44	0.8901	0.9782	-0.2079
0.7	0.38	41	1.84	0.54	0.7156	0.9903	0.1391
0.41	0.32	10	1.28	0.78	0.1745	0.342	0.9397
0.79	0.4	19	1.98	0.51	0.3316	0.6156	0.788
0.98	0.48	49	2.04	0.49	0.8552	0.9903	-0.1392
0.93	0.49	63	1.9	0.53	1.0996	0.809	-0.5879
0.6	0.29	57	2.07	0.48	0.9948	0.9136	-0.4067
0.71	0.44	61	1.61	0.62	1.0647	0.848	-0.53
0.82	0.26	42	3.15	0.32	0.733	0.9945	0.1046
0.5	0.3	20	1.67	0.6	0.3491	0.6428	0.766
0.42	0.2	37	2.1	0.48	0.6458	0.9613	0.2756
0.51	0.41	30	1.24	0.81	0.5236	0.866	0.5
0.35	0.32	56	1.09	0.92	0.9774	0.9272	-0.3746
Sums				54.09		86.7953	6.3699
Harmonic Mean H					sum of sin/cos		13.6258
1.96					vector mean Phi		0.75
					in degrees=		42.97

Table 06: Sample eD076, section a, Rf/Phi data

Long Axis	Short Axis	Phi	RF
3.02	1.74	15	1.74
7.63	4.41	4	1.73
5.32	3.31	35	1.61
8.1	4.96	5	1.63
5.86	3.97	20	1.48
3.22	1.81	0	1.78
2.74	1.8	20	1.52
3.95	2.31	21	1.71
2.44	1.21	9	2.02
5.37	3.29	26	1.63
4.9	2.67	29	1.84
2.19	1.42	28	1.54
2.87	1.57	-1	1.83
4.66	2.87	28	1.62
1.78	0.89	-15	2
2.74	1.8	32	1.52
4.6	1.97	22	2.34
3.73	3.43	-1	1.09
2.31	1.17	15	1.97
2.72	1.75	88	1.55
9.65	4.94	-24	1.95
2	1.37	75	1.46
3.99	2.02	18	1.98
9.72	6.32	21	1.54
7.08	4.46	4	1.59
3.38	2.01	24	1.68
5.13	1.76	29	2.91
4.92	3.42	-18	1.44
2.3	1.81	8	1.27
5.55	3.66	-59	1.52
3.78	3.38	12	1.12
4.46	1.49	28	2.99
2.59	0.94	-3	2.76
3.08	1.52	-28	2.03
7.34	3.06	-13	2.4
3.37	1.67	80	2.02
3.97	1.93	13	2.06
19.6	12.68	-8	1.55

15.01	5.09	-24	2.95
5.9	4.54	70	1.3
6.02	5.19	45	1.16
8.1	3.86	44	2.1
6.13	3.49	23	1.76
17.74	11.95	18	1.48
2.84	2	6	1.42
5.3	3.06	-21	1.73
5.68	3.49	-35	1.63
2.68	2.06	-23	1.3
5.16	3.81	-44	1.35
6.28	4.49	-8	1.4
3.32	2.84	-27	1.17
2.59	1.75	21	1.48
4.48	2.53	23	1.77

Table 07: Sample eD076, section b, Rf/Phi data

Long Axis	Short Axis	Phi	RF
16.56	7.27	-44	2.28
4.07	2.71	-50	1.5
5.26	2.51	-69	2.1
1.82	1.07	-21	1.7
8.67	4.17	-75	2.08
4.32	1.44	-41	3
6.96	2.32	-79	3
9.9	3.29	-72	3.01
5.75	4.06	-47	1.42
6.41	3.25	-76	1.97
5.4	1.96	-54	2.76
4.36	2.32	-83	1.88
5.87	2.15	-58	2.73
3.23	1.89	-38	1.71
2.76	1.4	-17	1.97
4.52	2.65	-37	1.71
3.05	2.06	-83	1.48
4.31	3.38	-48	1.28
2.39	1.67	1	1.43
11.36	7.27	-81	1.56
4.14	1.87	-48	2.21
4.82	2.73	-48	1.77
3.44	2.4	-19	1.43
3.25	1.08	10	3.01
3.81	2.25	-60	1.69
4.45	1.39	-54	3.2
7.36	2.69	-56	2.74
3.55	3.02	-30	1.18
4.56	2.71	-46	1.68
4.41	0.96	-65	4.59
2.82	1.2	-34	2.35
9.85	3.98	-36	2.47
10.94	3.99	-50	2.74
11.17	3.21	-64	3.48
9.15	2.15	-57	4.26
3.38	1.2	-50	2.82
4.76	2.04	-62	2.33
4.07	1.31	-87	3.11

8.03	3.73	-54	2.15
2.62	1.13	-34	2.32
1.48	0.93	-87	1.59
2.03	1.27	-47	1.6
4.67	1.36	-57	3.43
2.99	1.7	53	1.76
3.48	0.86	-60	4.05
3.32	0.96	-27	3.46
10.53	5.62	87	1.87
9.49	5.21	-53	1.82
5.45	1.79	-52	3.04
5.9	1.7	-54	3.47
4.73	1.27	-45	3.72
8.66	3.81	-51	2.27
7.86	2.82	-54	2.79
4.82	1.35	-49	3.57
7.39	3.26	-67	2.27
4.49	3.23	-48	1.39
4.95	2.39	-55	2.07
4.17	1.82	-66	2.29

Table 08: Sample eD076, section c, Rf/Phi data

Long Axis	Short Axis	Phi	RF
7.1	2.33	-15	3.05
6.26	1.42	-24	4.41
3.82	1.3	-17	2.94
6.91	2.27	-19	3.04
4.06	1.5	-23	2.71
3.44	1.78	-25	1.93
9.18	1.09	-21	8.42
7.38	1.85	-21	3.99
2.07	1.04	-13	1.99
3.72	1.59	-20	2.34
4.95	0.86	-26	5.76
3.42	0.65	-25	5.26
2.52	0.71	-30	3.55
2.29	0.6	-18	3.82
7.44	2.27	-11	3.28
7.21	3.94	-19	1.83
6.13	2	-25	3.07
4.6	1.32	-23	3.48
6.64	1.15	-31	5.77
18.73	2.62	-25	7.15
7.01	1.07	-15	6.55
3.2	1.09	-21	2.94
4.59	1.38	-26	3.33
9.39	4.1	-48	2.29
5.04	3.93	-35	1.28
4.49	1.46	-22	3.08
5.67	1.28	-29	4.43
6.71	1.53	-32	4.39
11.2	1.85	-18	6.05
2.95	0.75	-28	3.93
5	1.18	-21	4.24
5.77	1.51	-26	3.82
6.2	2.46	-32	2.52
3.28	0.98	-25	3.35
5.3	1.66	-43	3.19
6.54	2.27	-20	2.88
4.79	1.42	-23	3.37
4.4	0.7	-23	6.29

2.61	0.86	-37	3.03
3.64	1.64	-29	2.22
3.39	0.76	-28	4.46
5.04	1.09	-32	4.62
6.7	2.13	-32	3.15
5.03	2.01	-33	2.5
6.78	1.65	-17	4.11
6.09	1.74	-19	3.5
6.72	2.3	-30	2.92
5.53	2.54	-6	2.18
7.07	2.03	-24	3.48
8.6	1.96	-22	4.39
7.47	2.74	-6	2.73
4.28	1.13	-28	3.79
4.93	2.18	-13	2.26
6.55	1.89	-33	3.47
9.41	2.79	-17	3.37
5.08	2.22	-21	2.29
9.75	2.04	-18	4.78
5.83	1.52	-8	3.84

Figure 19: Fry plot of Sample eK007, section a

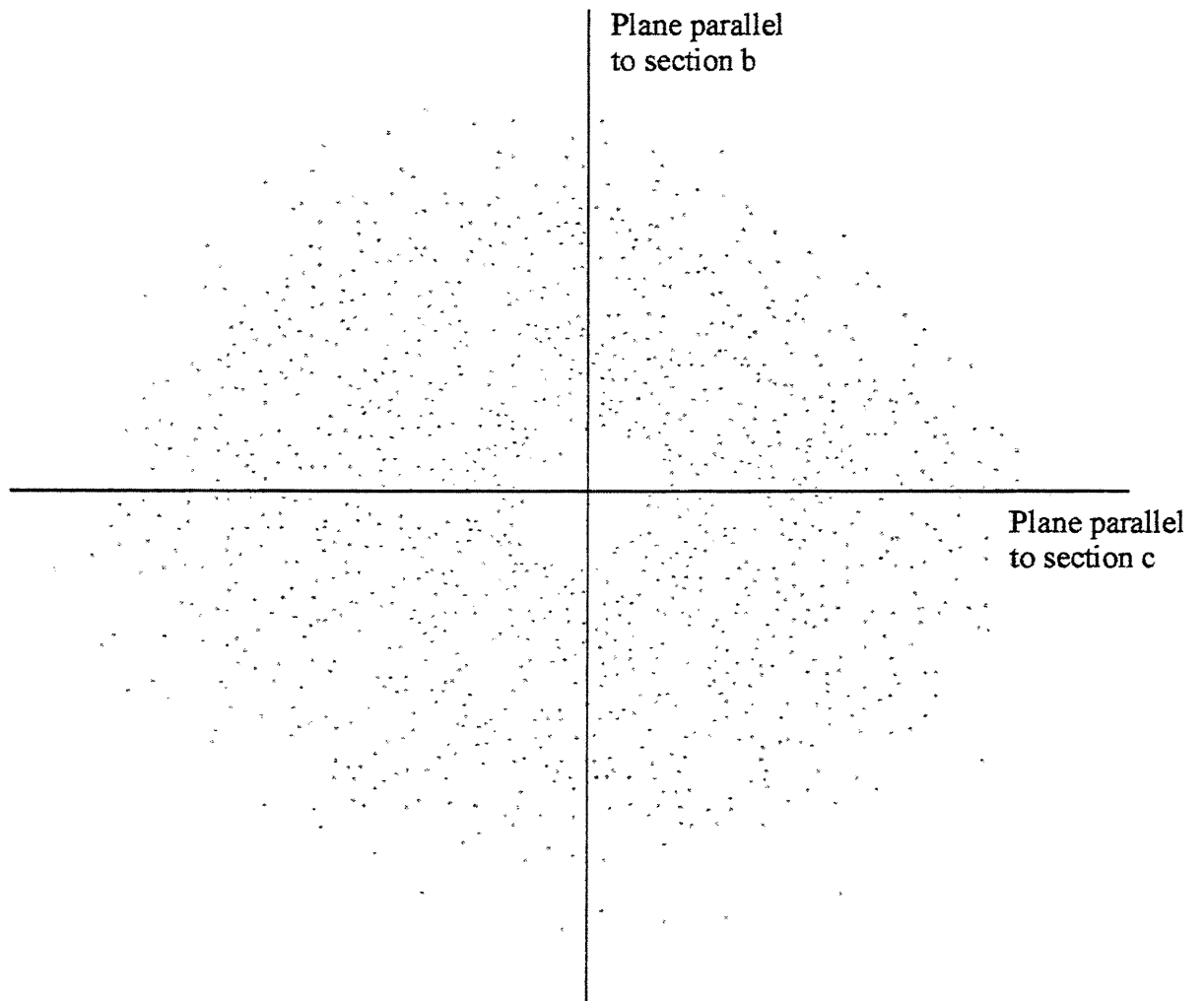


Figure 20: Fry plot of Sample eK007, section b

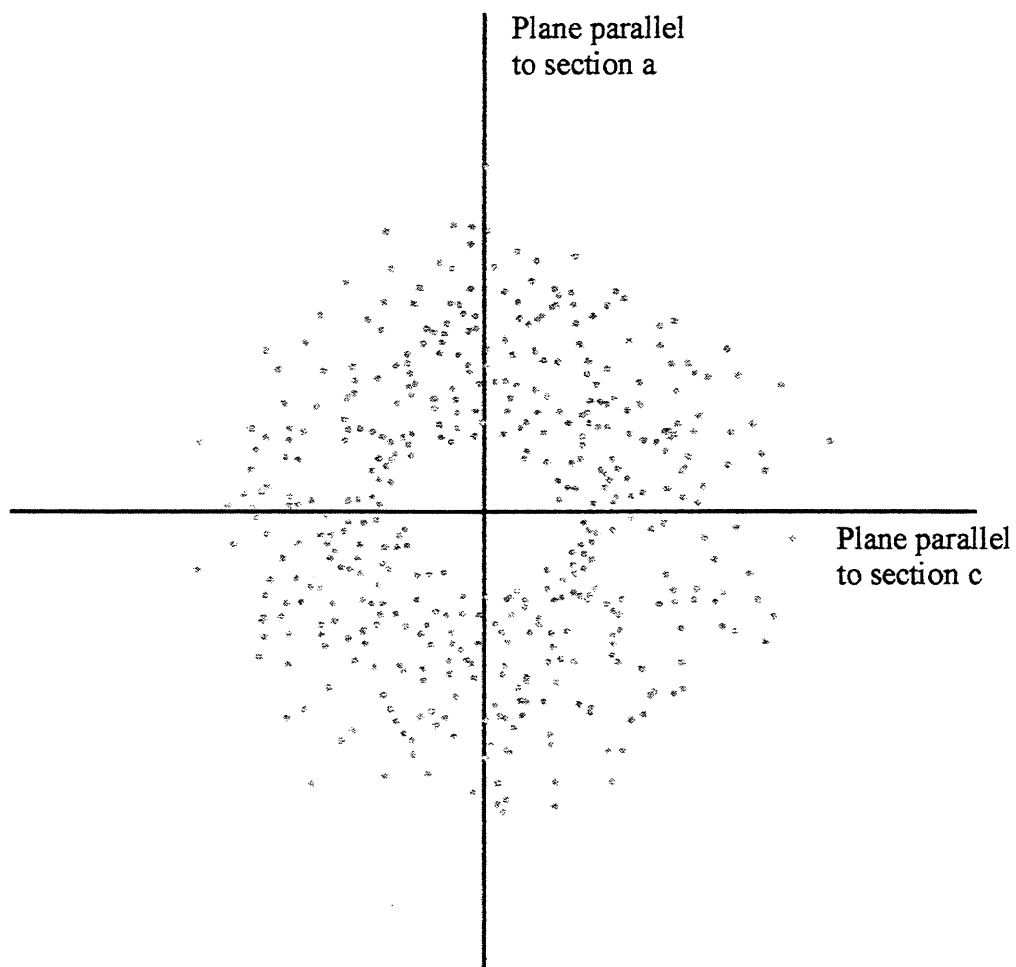


Figure 21: Fry plot of Sample eK007, section c

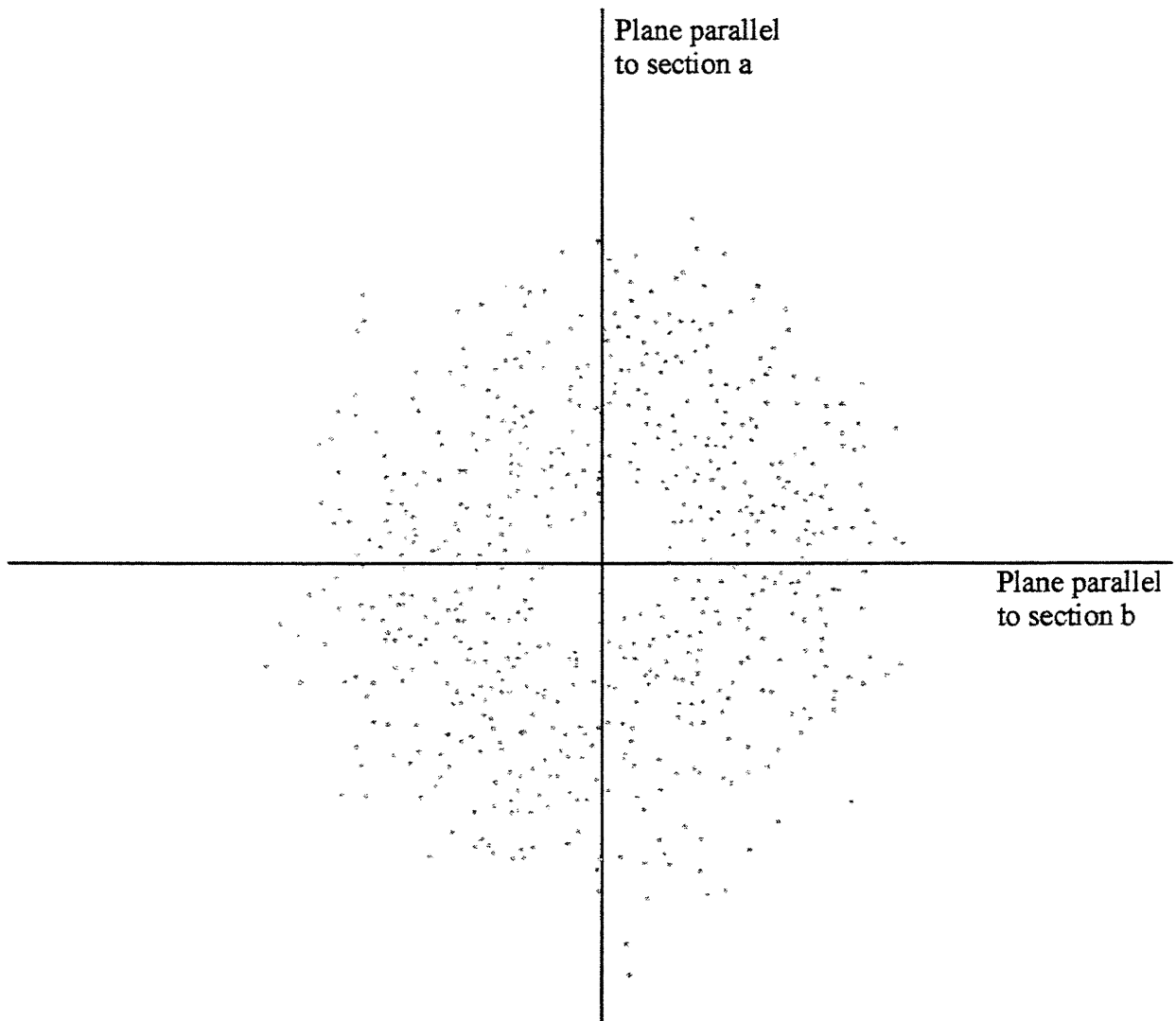


Figure 24: Sample eK007, section a. Plot of Rf/Phi data on logarithmic graph paper, used for comparison with Marker Deformation Grids produced by Lisle(1985).

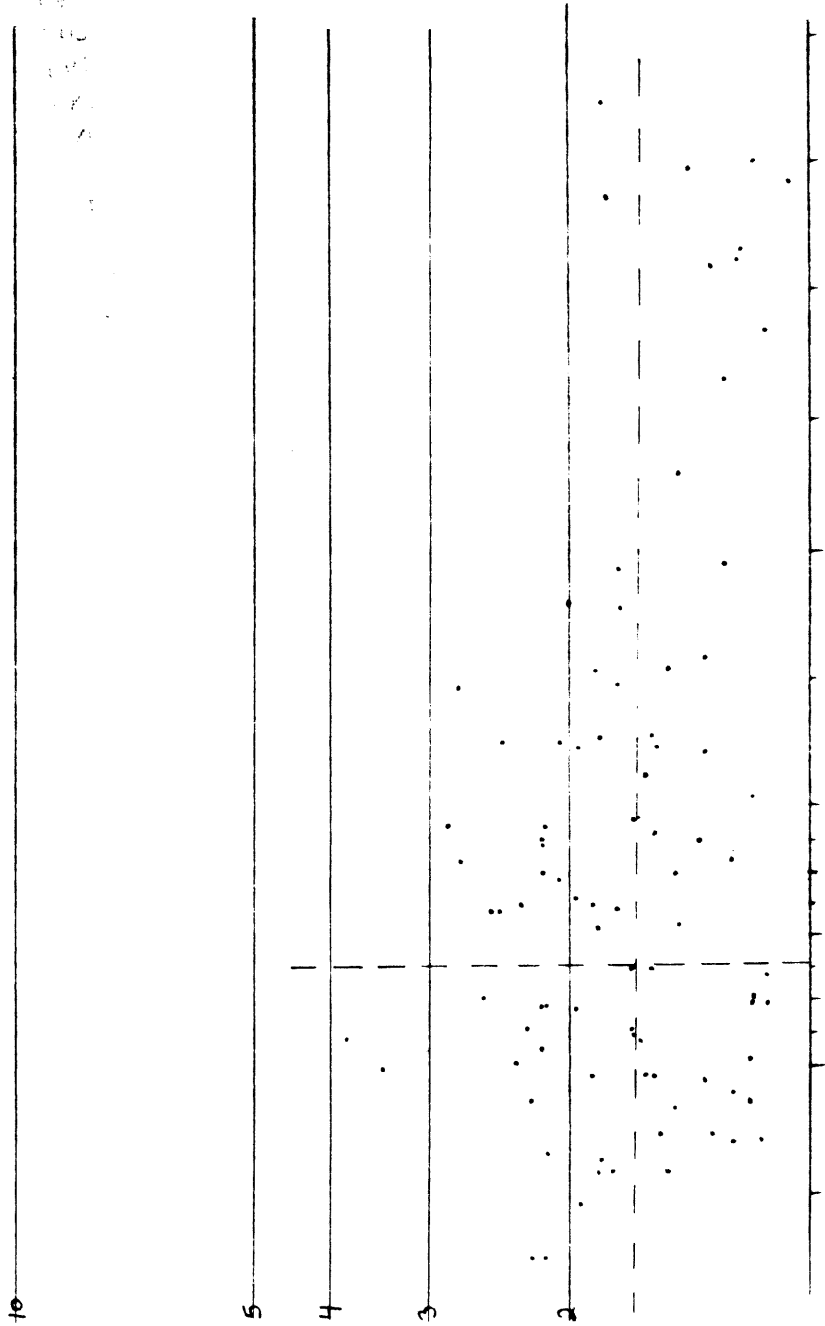


Figure 25: Sample eK007, section b. Plot of Rf/Φ data on logarithmic graph paper, used for comparison with Marker Deformation Grids produced by Lisle(1985).

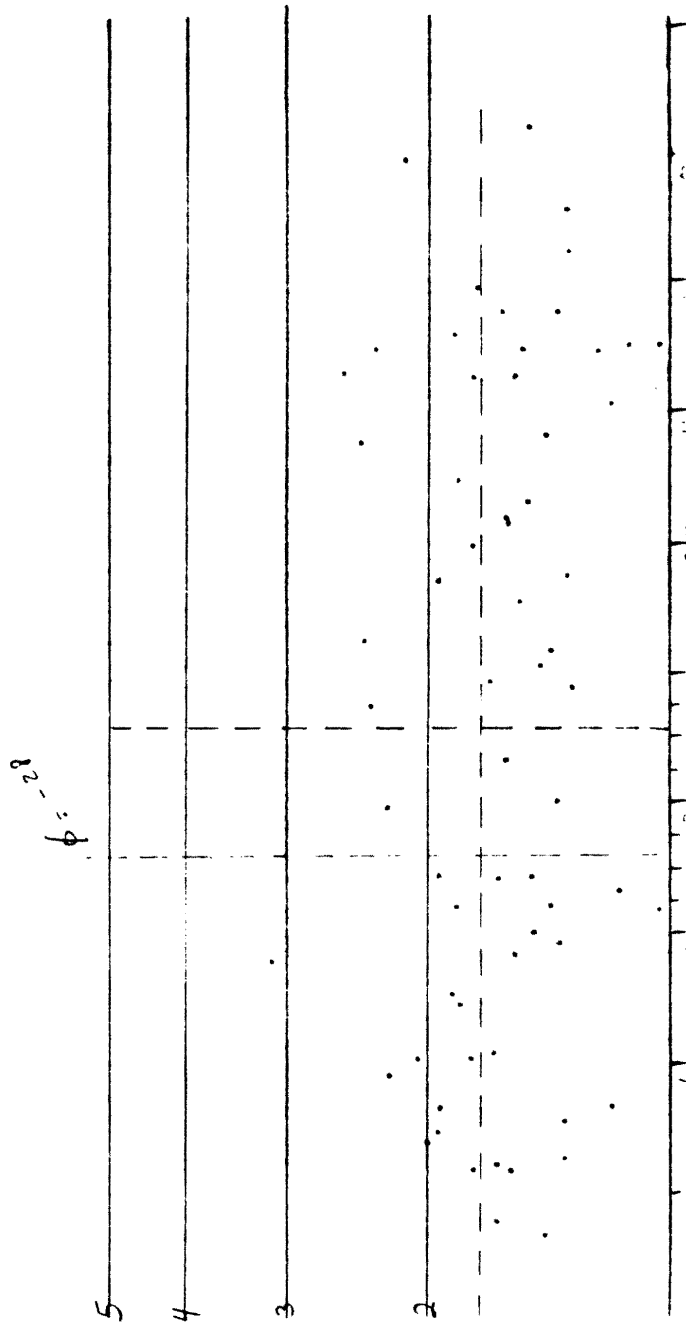


Figure 26: Sample eK007, section c. Plot of Rf/Phi data on logarithmic graph paper, used for comparison with Marker Deformation Grids produced by Lisle(1985).

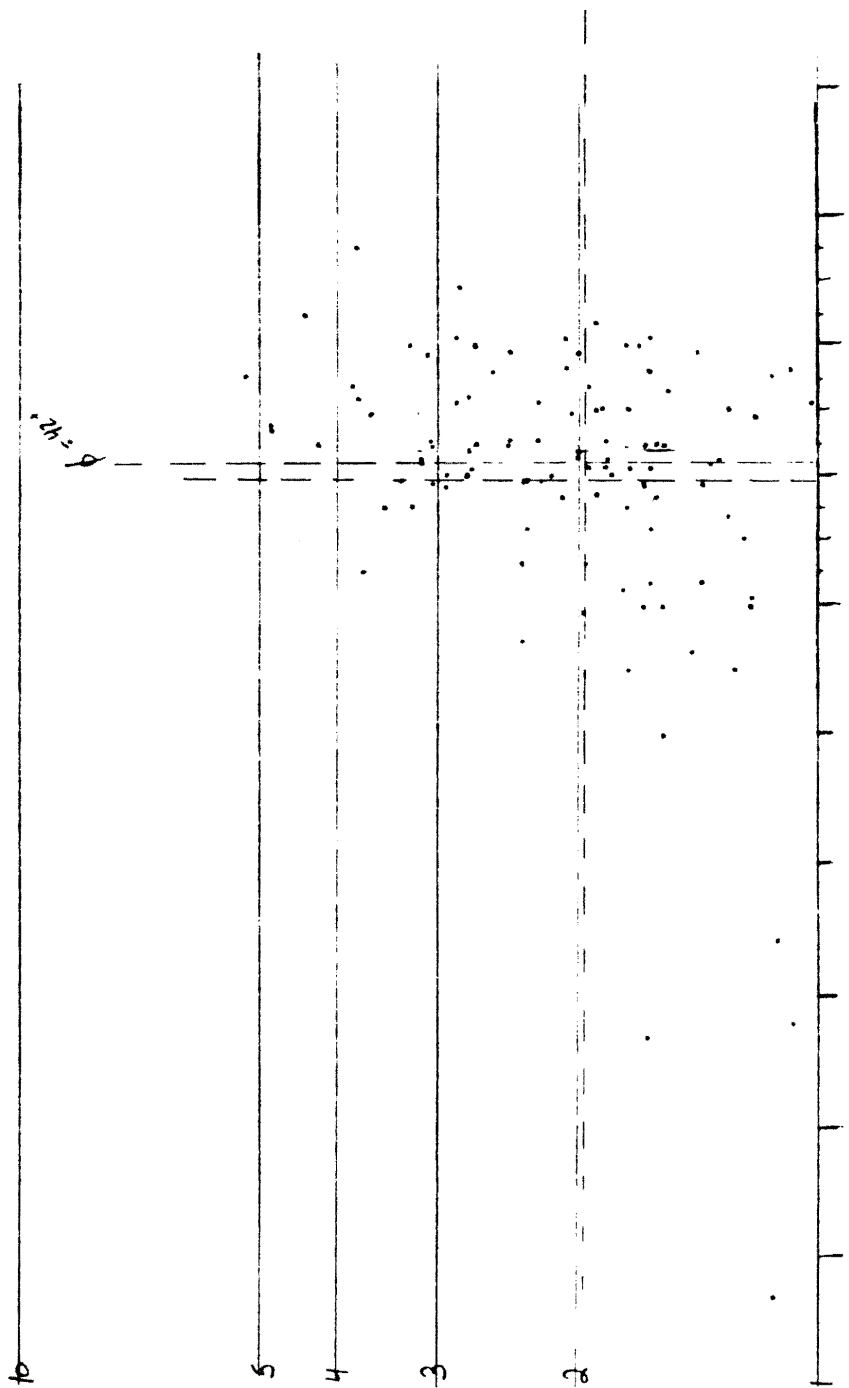


Figure 27: Sample eK007, section a. Plot of Rf/Phi data on DePaor's orientation net

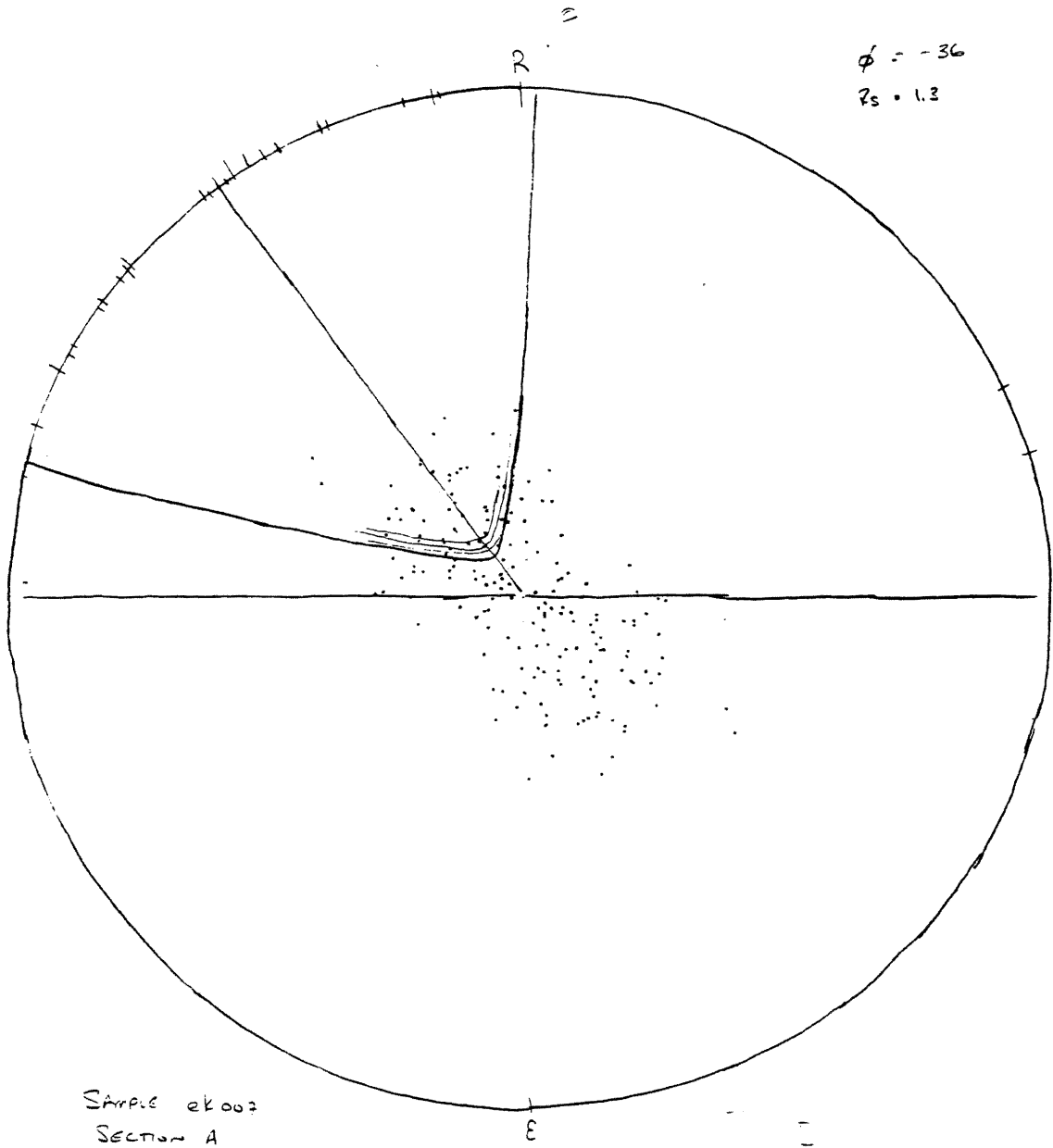


Figure 28: Sample eK007, section b. Plot of Rf/Phi data on DePaor's orientation net

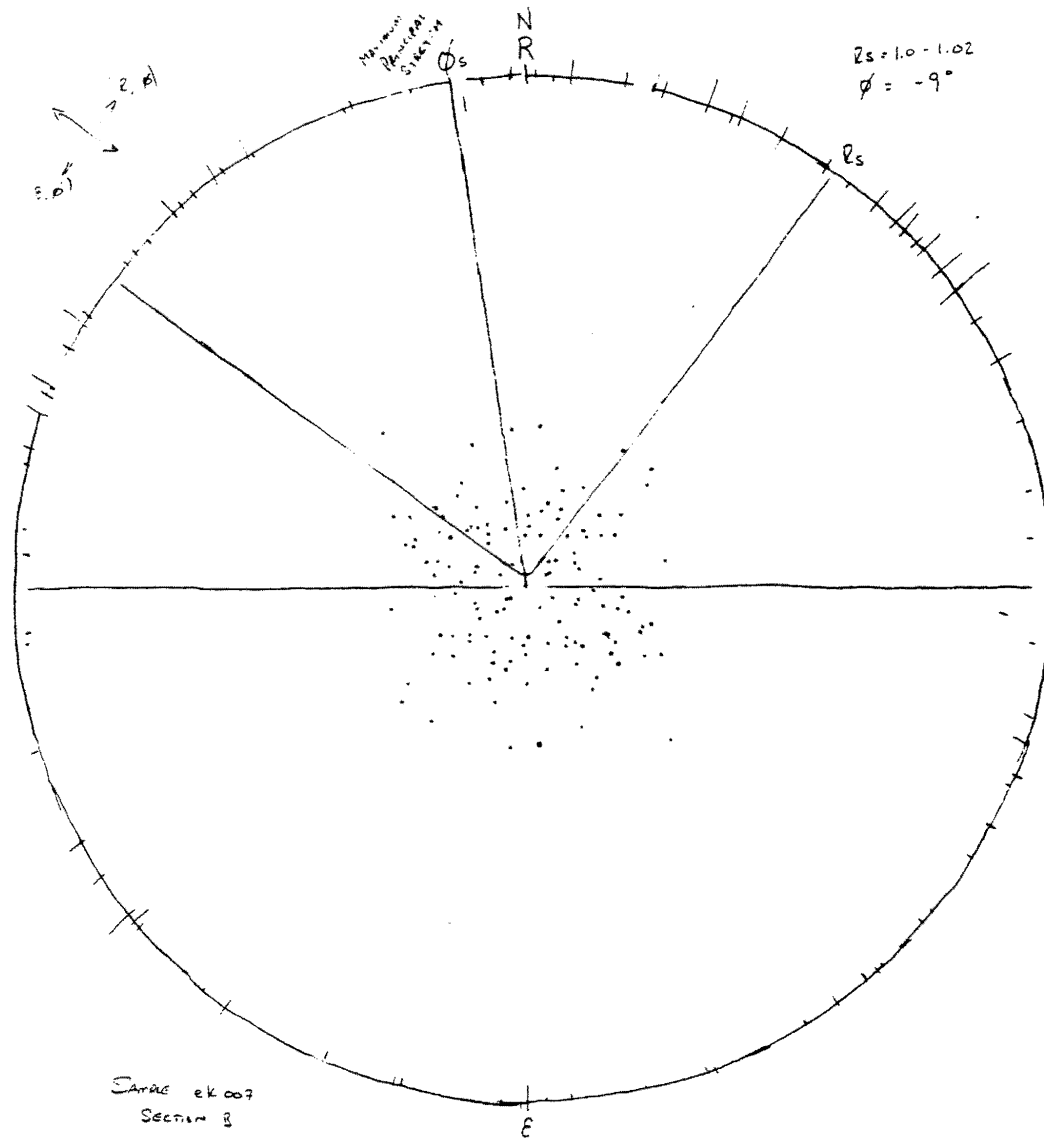
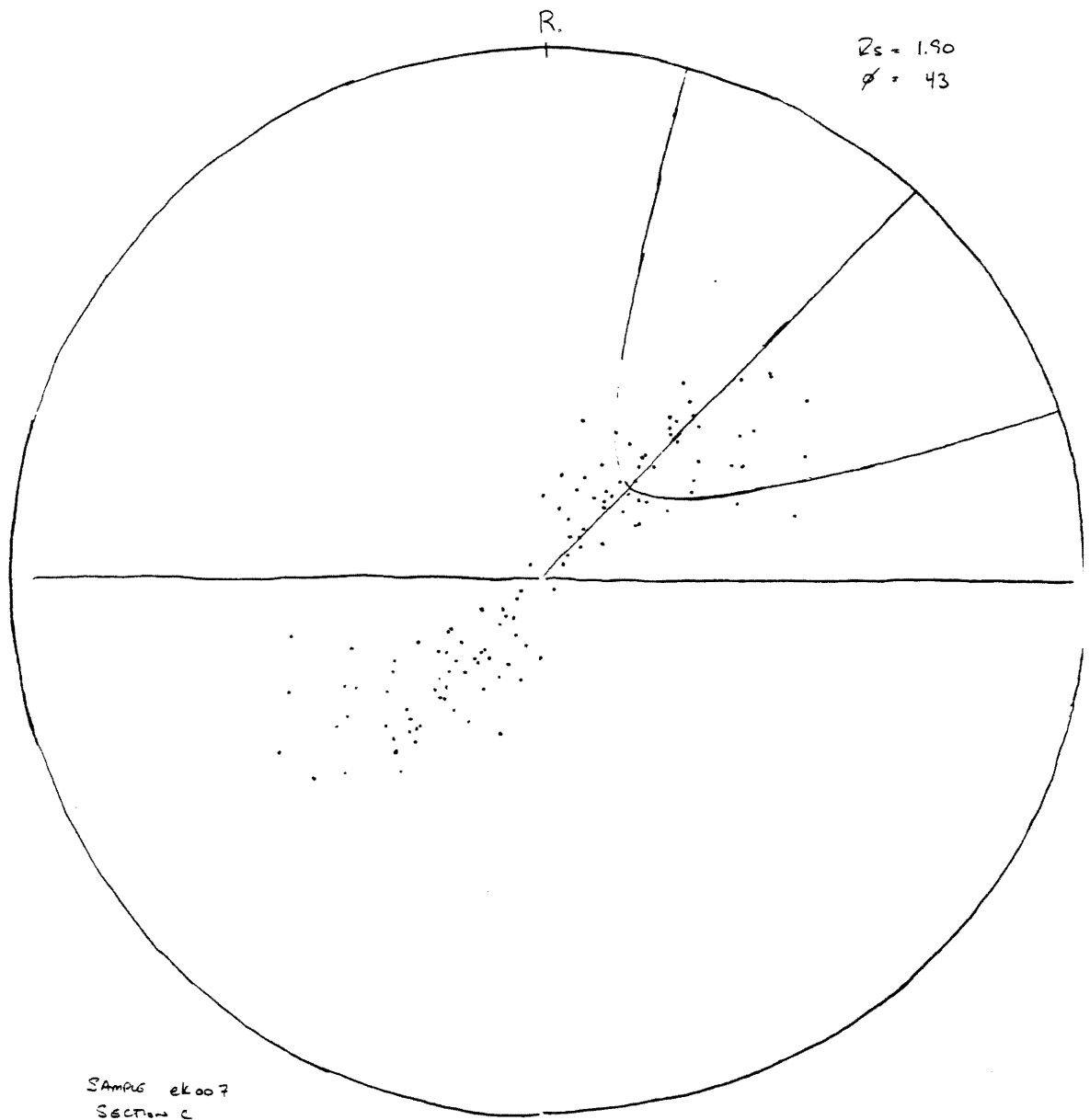


Figure 29: Sample eK007, section c. Plot of Rf/Phi data on DePaor's orientation net



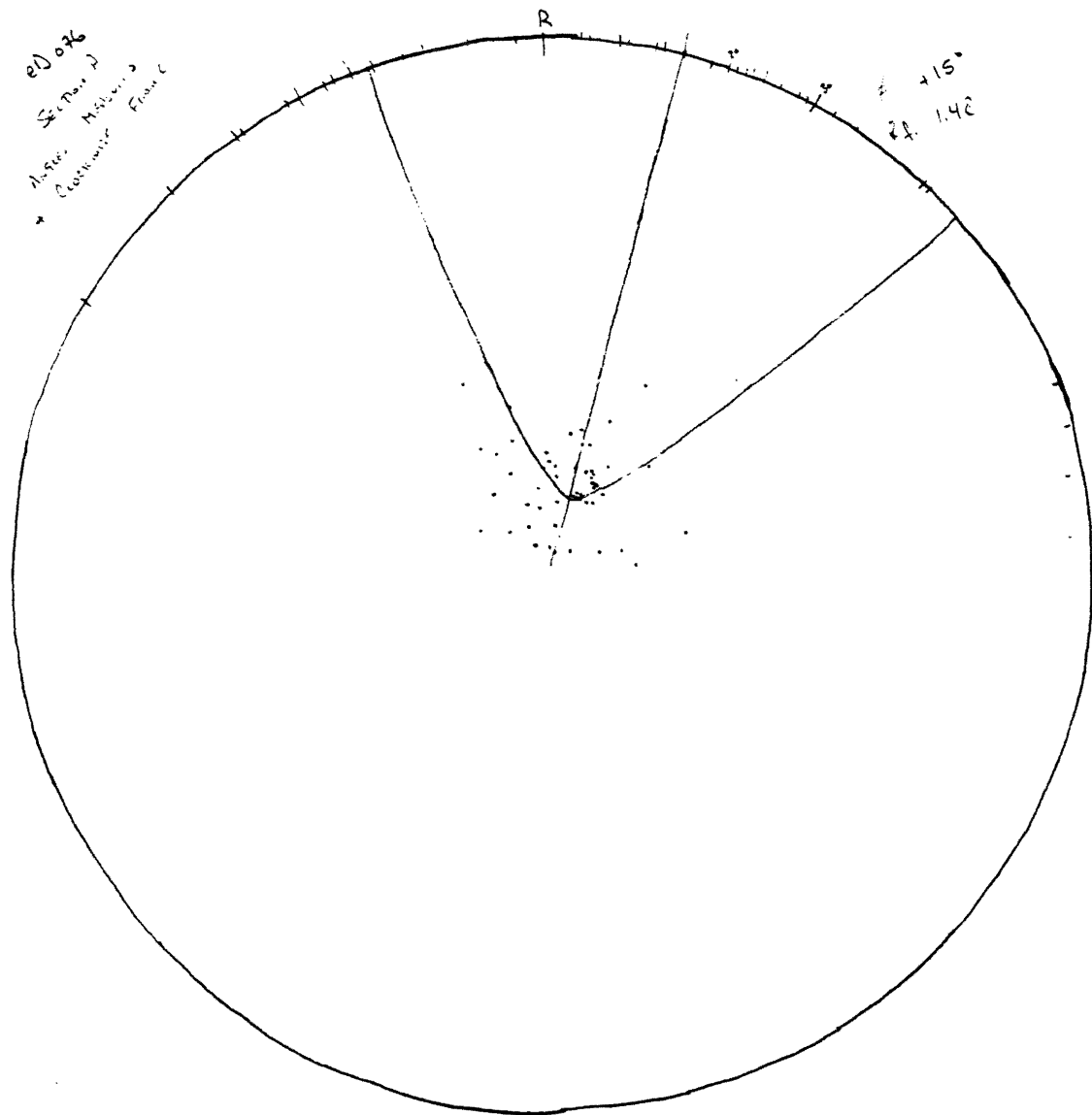


Figure 30: Sample eD076, section a. Plot of Rf/Phi data on DePaor's orientation net

Figure 31: Sample eD076, section b. Plot of Rf/Phi data on DePaor's orientation net

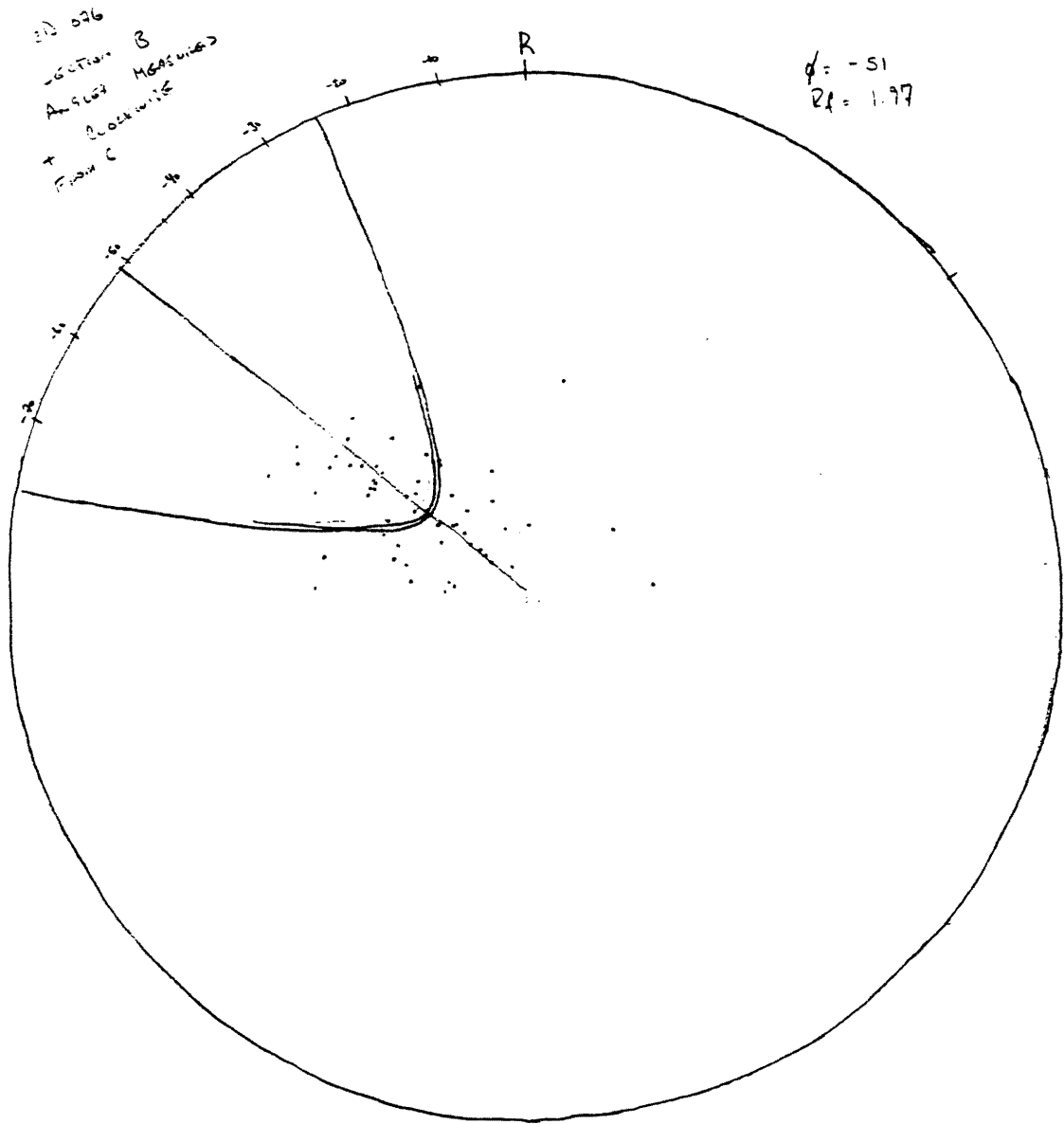


Figure 32: Sample eD076, section c. Plot of Rf/Phi data on DePaor's orientation net

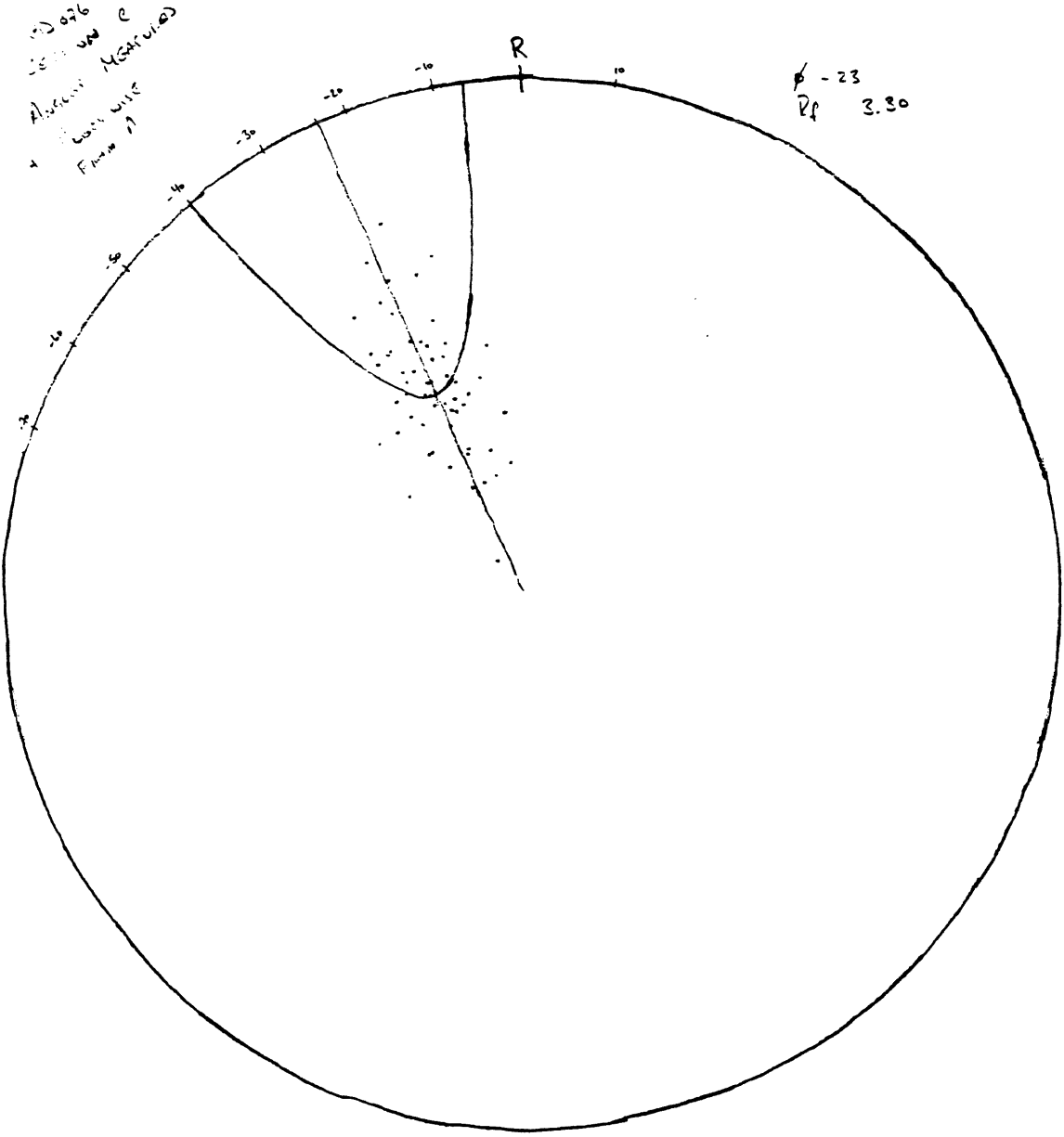
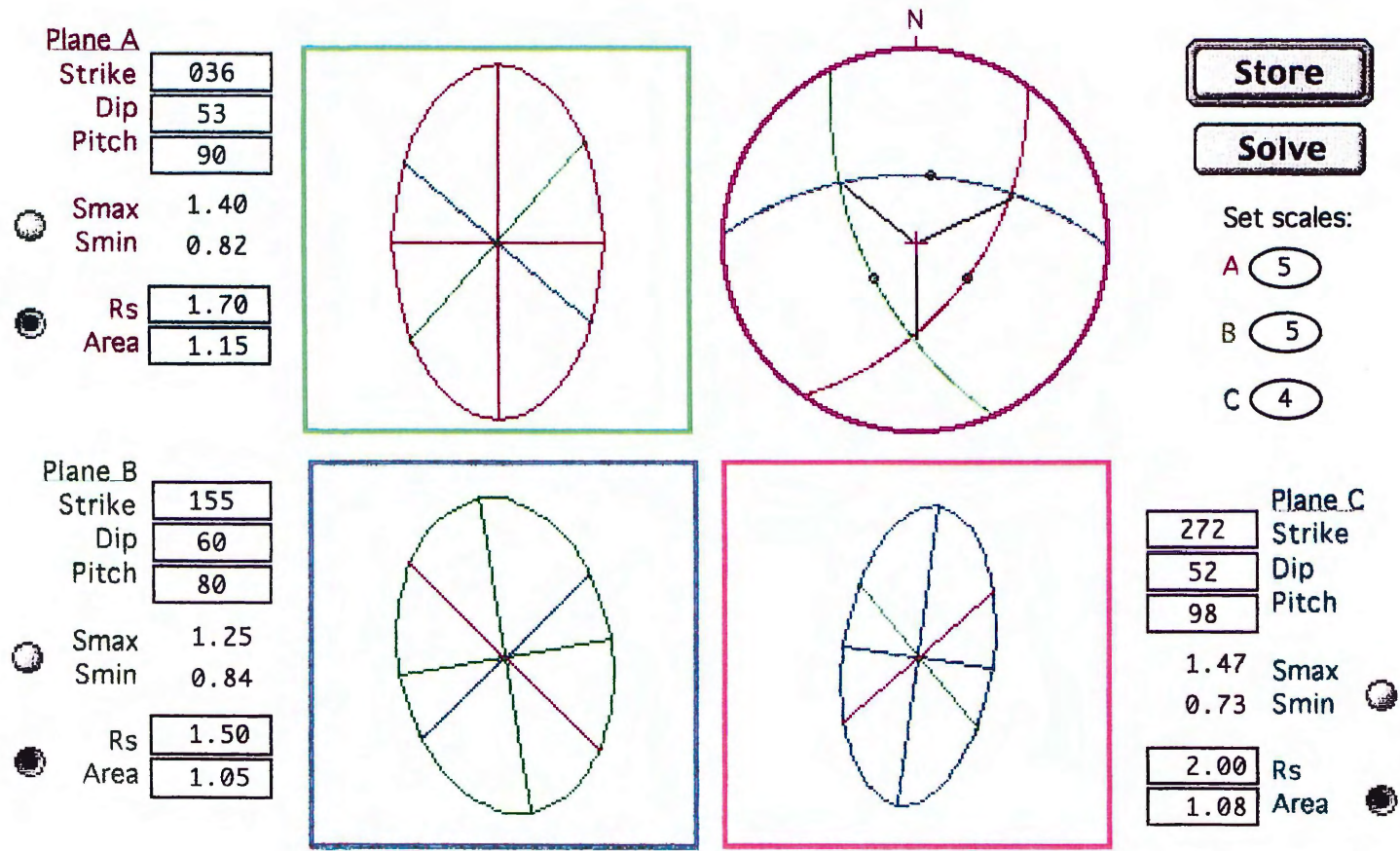
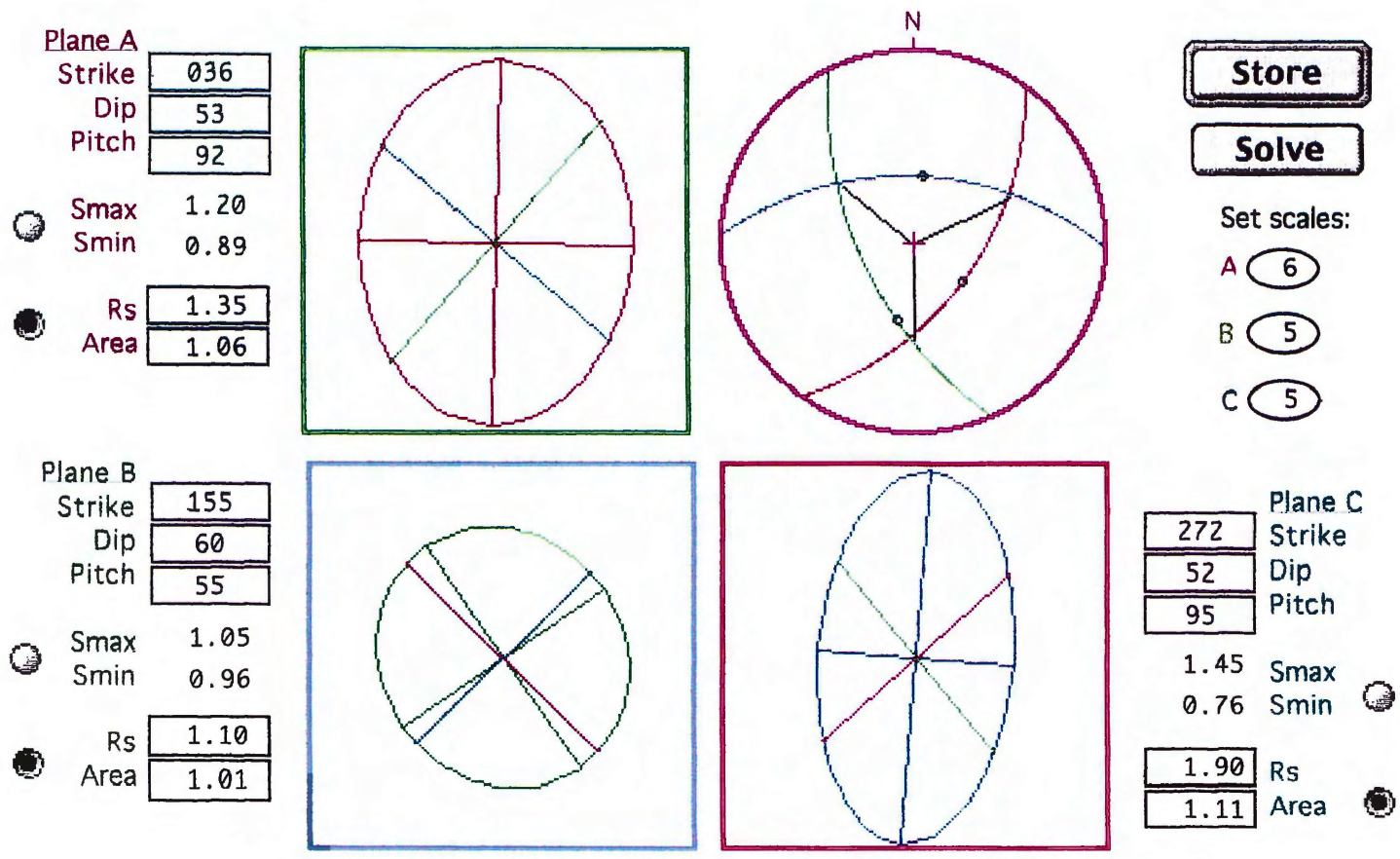


Figure 39: Sample eK007 (Fry data) Results of adjusting the three ellipses using the program E2E3 (DePaor 1988)



A3-28

Figure 40: Sample eK007 (Rf/Phi data) Results of adjusting the three ellipses using the program E2E3 (DePaor 1988)



A3-29

Figure 41: Sample eD076 (Rf/Phi data) Results of adjusting the three ellipses using the program E2E3 (DePaor 1988)

A3-30

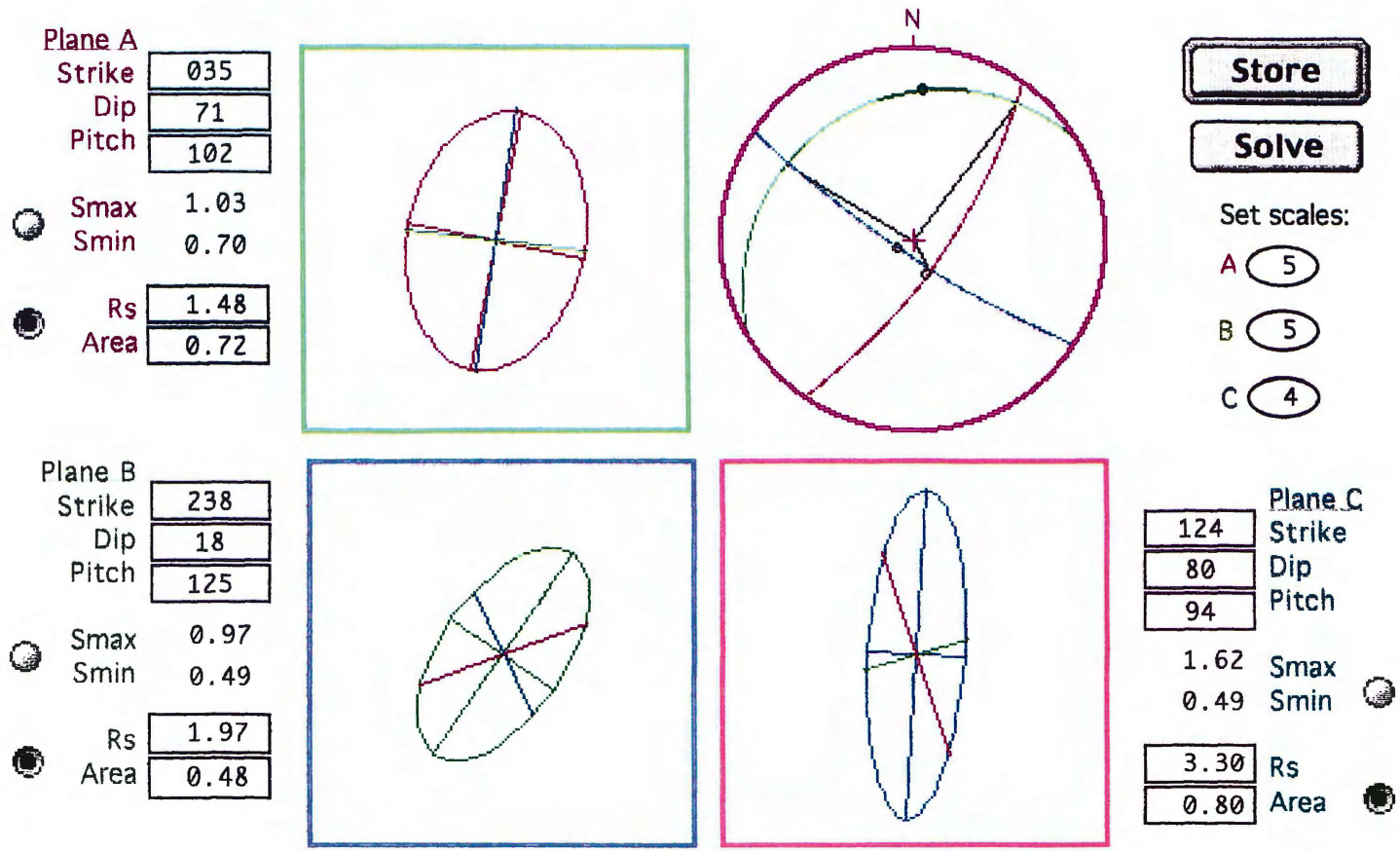


Table 09: Sample eK007 (Fry plot data) Calculated 3-D ellipsoid (Excel program by J. Waldron)

Sample eK007 (Fry) 3-D strain from 3 strain ellipses

reading	Enter two axes		Intercalated		Enter two axes		Intercalated		Enter two axes		Intercalated		test data	
	1	2			3	4			5	6				
plunge	52.00	37.00			58.00	32.00			52.00	38.00			trend	19.1
trend	125.00	305.00			217.00	306.00			15.00	305.00			plunge	56
stretch	1.40	0.82			1.25	0.84			1.47	0.73			1 LEAVE THIS AT 1.0	
x	0.7060	-0.5364	0.1199	0.8786	-0.3986	-0.5763	-0.6894	0.1256	0.2342	-0.4712	-0.1676	0.4988		-0.8138
y	-0.4944	0.3756	-0.0840	-0.6152	-0.5290	0.4187	-0.0780	-0.6701	0.8742	0.3299	0.8515	0.3848		-0.5489
z	1.1032	0.4935	1.1290	0.4311	1.0601	0.4451	1.0643	0.4348	1.1584	0.4494	1.1369	0.5013		-0.1908

Trial values to restore to sphere			
degrees		radians	
rotationx	-92.65	rotationx	-1.62
rotationy	-12.72	rotationy	-0.22
rotationz	98.82	rotationz	1.72
stretchx	0.63		
stretchy	1.21		
stretchz	1.03		

Results				
axis	S	plunge	trend	Stretches at const. Vol.
a	1.59	80.25	27.97	1.47
b	0.82	9.39	192.30	0.76
c	0.97	2.59	282.73	0.89
DeltaV	1.27			1.00
sum	0.4590	0.0382	mean square error	

Calculate inverse of restoring strain ellipsoid

stretches			rotate z			rotate y			rotate x			raw plunge	raw trend	pos plunge	trend
x	y	z	x	y	z	x	y	z	x	y	z				
1.59	0.00	0.00	-0.24	1.58	0.00	-0.24	1.58	-0.05	-0.24	-0.13	-1.5715	-80.25	-152.03	80.253	27.9696
0.00	0.82	0.00	-0.81	-0.13	0.00	-0.79	-0.13	-0.18	-0.79	-0.17	0.13448	9.39	-167.70	9.3913	-167.7
0.00	0.00	0.97	0.00	0.00	0.97	-0.21	0.00	0.95	-0.21	0.95	-0.0438	-2.59	102.73	2.5854	282.729

Calculations for strain removal

rotatedx																
x	0.7060	-0.5364	0.1199	0.8786	-0.3986	-0.5763	-0.6894	0.1256	0.2342	-0.4712	-0.1676	0.4988				-0.8138
y	-1.0792	-0.5103	-1.1239	-0.4022	-1.0345	-0.4640	-1.0596	-0.4034	-1.1976	-0.4642	-1.1751	-0.5186				0.2160
z	-0.5449	0.3524	-0.1361	-0.6345	-0.5775	0.3977	-0.1271	-0.6895	0.8197	0.3088	0.7980	0.3612				-0.5395
rotatedy																
x	0.5688	-0.4457	0.0870	0.7174	-0.5160	-0.4746	-0.7005	-0.0292	0.4089	-0.3917	0.0122	0.5661				-0.9126
y	-1.0792	-0.5103	-1.1239	-0.4022	-1.0345	-0.4640	-1.0596	-0.4034	-1.1976	-0.4642	-1.1751	-0.5186				0.2160
z	-0.6869	0.4618	-0.1592	-0.8123	-0.4756	0.5148	0.0277	-0.7003	0.7480	0.4050	0.8153	0.2426				-0.3471
rotatedz																
x	-1.1536	-0.4360	-1.1240	-0.5074	-0.9431	-0.3858	-0.9397	-0.3941	-1.2461	-0.3987	-1.1630	-0.5992				0.3533
y	-0.3967	0.5187	0.0863	-0.6472	0.6684	0.5402	0.8546	0.0907	-0.2205	0.4582	0.1681	-0.4799				0.8687
z	-0.6869	0.4618	-0.1592	-0.8123	-0.4756	0.5148	0.0277	-0.7003	0.7480	0.4050	0.8153	0.2426				-0.3471
stretched																
x	-0.7235	-0.2734	-0.7049	-0.3182	-0.5915	-0.2419	-0.5893	-0.2472	-0.7815	-0.2500	-0.7294	-0.3758				0.2216
y	-0.4813	0.6294	0.1047	-0.7854	0.8111	0.6554	1.0370	0.1101	-0.2676	0.5560	0.2039	-0.5823				1.0541
z	-0.7082	0.4761	-0.1641	-0.8374	-0.4903	0.5307	0.0286	-0.7219	0.7711	0.4175	0.8405	0.2501				-0.3579
lengthsq	1.1210	0.8352	0.7313	1.1913	1.1172	0.8774	1.1931	0.7710	1.1300	0.7389	1.1314	0.7368				1.1350
deviation	0.0146	0.0272	0.0722	0.0366	0.0137	0.0150	0.0373	0.0525	0.0169	0.0682	0.0173	0.0693				0.0182

0.81257618 stretch along test line

A3-31

Table 10: Sample eK007 (Rf/Phi plot data) Calculated 3-D ellipsoid (Excel program by J. Waldron)

Sample eK007 3-D strain from 3 strain ellipses

reading	Enter two axes		Intercalated		Enter two axes		Intercalated		Enter two axes		Intercalated	
	1	2	3	4	5	6	7	8	9	10	11	12
plunge	52.00	2.00	44.00	28.00	52.00	4.00						
trend	130.00	38.00	190.00	315.00	12.00	275.00						
stretch	1.20	0.89	1.05	0.96	1.45	0.76						
x	0.5659	0.5476	0.7874	0.0130	-0.1312	-0.5994	-0.5166	0.3311	0.1856	-0.7553	-0.4028	0.6653
y	-0.4749	0.7009	0.1598	-0.8314	-0.7438	0.5994	-0.1022	-0.9498	0.8732	0.0661	0.6642	0.5707
z	0.9456	0.0311	0.6906	0.6467	0.7294	0.4507	0.8344	0.1971	1.1426	0.0530	0.8454	0.7705

test data

trend	191
plunge	56
	1 LEAVE THIS AT 1.0
	-0.8138
	-0.5489
	-0.1908

Trial values to restore to sphere			
degrees		radians	
rotationx	-101.22	rotationx	-1.77
rotationy	-10.20	rotationy	-0.18
rotationz	99.28	rotationz	1.73
stretchx	0.62		
stretchy	1.32		
stretchz	0.97		

Results				Stretches at const. Vol.			
axis	S	plunge	trend				
a	1.62	74.26	54.22	1.50			
b	0.76	11.08	188.21	0.70			
c	1.03	11.04	280.40	0.95			
DeltaV	1.25			1.00			
sum	0.0343	0.0029	mean square error				

Calculate inverse of restoring strain ellipsoid

Calculate inverse of restoring strain ellipsoid															
stretches			rotate z			rotate y			rotate x						
x	y	z	x	y	z	x	y	z	x	y	z	raw plunge	raw trend	pos plunge	trend
1.62	0.00	0.00	-0.26	1.60	0.00	-0.26	1.60	-0.05	-0.26	-0.36	-1.5559	-74.26	-125.78	74.259	54.2154
0.00	0.76	0.00	-0.75	-0.12	0.00	-0.73	-0.12	-0.13	-0.73	-0.11	0.14512	11.08	-171.79	11.076	-171.79
0.00	0.00	1.03	0.00	0.00	1.03	-0.18	0.00	1.01	-0.18	0.99	-0.1966	-11.04	100.40	11.043	280.395

Calculations for strain removal

rotatedx													
x	0.5659	0.5476	0.7874	0.0130	-0.1312	-0.5994	-0.5166	0.3311	0.1856	-0.7553	-0.4028	0.6653	-0.8138
y	-0.8351	-0.1669	-0.7085	-0.4725	-0.5707	-0.5587	-0.7986	-0.0085	-1.2907	-0.0649	-0.9585	-0.8668	0.2940
z	-0.6498	0.6815	0.0224	-0.9414	-0.8716	0.5002	-0.2626	-0.9700	0.6341	0.0545	0.4869	0.4099	-0.5013
rotatedy													
x	0.4419	0.6596	0.7789	-0.1539	-0.2834	-0.5013	-0.5549	0.1541	0.2950	-0.7337	-0.3102	0.7274	-0.8897
y	-0.8351	-0.1669	-0.7085	-0.4725	-0.5707	-0.5587	-0.7986	-0.0085	-1.2907	-0.0649	-0.9585	-0.8668	0.2940
z	-0.7398	0.5737	-0.1174	-0.9288	-0.8346	0.5984	-0.1670	-1.0133	0.5912	0.1874	0.5506	0.2856	-0.3492
rotatedz													
x	-0.8954	-0.2710	-0.8248	-0.4415	-0.5175	-0.4706	-0.6987	-0.0332	-1.3214	0.0542	-0.8960	-0.9727	0.4335
y	-0.3015	-0.6241	-0.6545	0.2281	0.3717	0.5848	0.6764	-0.1507	-0.0831	0.7345	0.4606	-0.5781	0.8307
z	-0.7398	0.5737	-0.1174	-0.9288	-0.8346	0.5984	-0.1670	-1.0133	0.5912	0.1874	0.5506	0.2856	-0.3492
stretched													
x	-0.5539	-0.1676	-0.5102	-0.2731	-0.3201	-0.2911	-0.4322	-0.0205	-0.8174	0.0336	-0.5543	-0.6017	0.2682
y	-0.3992	-0.8262	-0.8665	0.3019	0.4921	0.7742	0.8954	-0.1995	-0.1100	0.9724	0.6098	-0.7653	1.0997
z	-0.7209	0.5590	-0.1144	-0.9050	-0.8132	0.5831	-0.1627	-0.9873	0.5761	0.1826	0.5365	0.2783	-0.3403
lengthsq	0.9929	1.0115	1.0120	0.9924	1.0029	1.0120	1.0075	1.0075	1.0060	0.9899	0.9833	1.0125	1.1820
deviation	0.0001	0.0001	0.0001	0.0001	0.0000	0.0001	0.0001	0.0001	0.0000	0.0001	0.0003	0.0002	0.0331

0.78472934 stretch along test line

A3-32

Table 11: Sample eD076 (Rf/Phi plot data) Calculated 3-D ellipsoid (Excel program by J. Waldron)

Sample eD076 3-D strain from 3 strain ellipses

reading	Enter two axes		Intercalated		Enter two axes		Intercalated		Enter two axes		Intercalated	
	1	2	3	4	5	6	7	8	9	10	11	12
plunge	68.00	10.00	15.00	10.00	80.00	3.00						
trend	160.00	39.00	5.00	270.00	232.00	125.00						
stretch	1.03	0.73	0.97	0.49	1.62	0.49						
x	0.1320	0.4524	0.4132	-0.2266	0.0817	-0.4826	-0.2835	0.3990	-0.2217	0.4008	0.1267	-0.4402
y	-0.3626	0.5587	0.1387	-0.6514	0.9334	0.0000	0.6600	0.6600	-0.1732	-0.2807	-0.3209	0.0760
z	0.9550	0.1268	0.7649	0.5857	0.2511	0.0851	0.2377	0.1174	1.5954	0.0256	1.1462	1.1100

test data

trend	144
plunge	11
	1 LEAVE THIS AT 1.0
	-0.1544
	-0.7942
	0.5878

Trial values to restore to sphere			
degrees		radians	
rotationx	-112.18	rotationx	-1.96
rotationy	15.76	rotationy	0.28
rotationz	92.09	rotationz	1.61
stretchx	0.23		
stretchy	2.11		
stretchz	1.20		

Results					
axis	S	plunge	trend	Stretches at const. Vol.	
a	4.36	68.30	84.54	3.63	
b	0.47	3.94	344.59	0.40	
c	0.83	21.31	253.05	0.70	
DeltaV	1.72			1.00	
sum	0.0608	0.0051	mean square error		

Calculate inverse of restoring strain ellipsoid

stretches		rotate z			rotate y			rotate x			raw plunge	raw trend	pos plung	trend	
x	y	z	x	y	z	x	y	z	x	y	z				
4.36	0.00	0.00	-0.16	4.36	0.00	-0.15	4.36	0.04	-0.15	-1.60	-4.0496	-68.30	-95.46	68.297	84.5435
0.00	0.47	0.00	-0.47	-0.02	0.00	-0.46	-0.02	0.13	-0.46	0.13	-0.0326	-3.94	164.59	3.9354	344.59
0.00	0.00	0.83	0.00	0.00	0.83	0.23	0.00	0.80	0.23	0.74	-0.303	-21.31	73.05	21.307	253.053

Calculations for strain removal

rotatedx																
x	0.1320	0.4524	0.4132	-0.2266	0.0817	-0.4826	-0.2835	0.3990	-0.2217	0.4008	0.1267	-0.4402				-0.1544
y	-0.7474	-0.3283	-0.7607	-0.2963	-0.5849	-0.0788	-0.4693	-0.3579	-1.4119	0.0822	-0.9402	-1.0565				-0.2444
z	-0.6963	0.4695	-0.1604	-0.8243	0.7695	-0.0321	0.5214	0.5668	-0.7627	-0.2696	-0.7299	-0.3487				-0.9573
rotatedy																
x	0.3161	0.3079	0.4413	0.0058	-0.1304	-0.4557	-0.4144	0.2300	-0.0062	0.4590	0.3202	-0.3289				0.1114
y	-0.7474	-0.3283	-0.7607	-0.2963	-0.5849	-0.0788	-0.4693	-0.3579	-1.4119	0.0822	-0.9402	-1.0565				-0.2444
z	-0.6343	0.5747	-0.0421	-0.8549	0.7628	-0.1620	0.4248	0.6539	-0.7943	-0.1506	-0.6681	-0.4551				-0.9632
rotatedz																
x	-0.7585	-0.3394	-0.7763	-0.2964	-0.5797	-0.0621	-0.4538	-0.3660	-1.4107	0.0654	-0.9513	-1.0438				-0.2483
y	-0.2886	-0.2957	-0.4132	0.0050	0.1517	0.4583	0.4313	-0.2168	0.0578	-0.4617	-0.2856	0.3673				-0.1024
z	-0.6343	0.5747	-0.0421	-0.8549	0.7628	-0.1620	0.4248	0.6539	-0.7943	-0.1506	-0.6681	-0.4551				-0.9632
stretched																
x	-0.1740	-0.0779	-0.1781	-0.0680	-0.1330	-0.0142	-0.1041	-0.0840	-0.3237	0.0150	-0.2183	-0.2395				-0.0570
y	-0.6083	-0.6234	-0.8709	0.0106	0.3197	0.9660	0.9091	-0.4570	0.1218	-0.9732	-0.6020	0.7743				-0.2158
z	-0.7606	0.6892	-0.0505	-1.0252	0.9147	-0.1942	0.5094	0.7841	-0.9524	-0.1806	-0.8012	-0.5458				-1.1551
lengthsq	0.9894	0.9325	0.8904	1.0275	0.9780	0.9854	1.0473	0.9114	1.0133	0.9899	1.0256	0.9771				1.1765
deviation	0.0001	0.0046	0.0120	0.0008	0.0005	0.0002	0.0022	0.0078	0.0002	0.0001	0.0007	0.0005				0.0311

0.70884827 stretch along test line

A3-33

